Analysis of the Effect of Bending, Fatigue, Erosion-Corrosion and Tensile Stresses on HVOF Coating of Metallic Surfaces

by

Hussain Al Fadhli B.Sc M.Sc

A thesis submitted in fulfillment of the requirement for the degree of

Doctor of Philosophy

Supervisor:

Dr. Joseph Stokes

Dublin City University
School of Mechanical and Manufacturing Engineering

March 2006

DECLARATION

I herby certify that this material, which I now submit for assessment on the programme of study leading to the award of Doctor of Philosophy, is entirely my own work and has not been taken from the work of others save and to the extent that such work has been cited and acknowledged within the text of my work.

Signed: _____ I.D. Number: 53147278

Date: March 2006.

ACKNOWLEDGMENTS

First of all I thank ALLAH, who bestowed me with the strength to complete this work.

I shall always remain indebted to my supervisor Dr. Joseph Stokes, who helped me throughout my thesis by his invaluable inspiration, encouragement and continuous guidance. He was always there to help me in the difficult times during this work. I am also extremely thankful to Professor Bekir Sami Yilbas for his valuable suggestions and guidance during the startup plan and the execution of this work. I am deeply grateful to Professor Saleem Hashmi (Head of School) and Dr. Malika Ardhaoui for their help, support and enhancement of this work.

I am grateful for the support of the Mechanical Services Shops Department in the Saudi Oil Company (Saudi Aramco) represented by Mr. Alaaeldeen Mustafa, Mr. Sulaiman Al Rasheed, Mr. Abdullah Al-Jameel, Mr. Mohammed Al-Sultan, Mr. Abdulrahman Al-Dkhail and Mr. Naser Al-Naimi (Head of Department). I am also grateful for the support of Martial Testing and Metallographic Group/CSD, Corrosion Testing Unit/R&DC at Saudi Aramco and Mechanical Engineering Department at King Fahd University of Petroleum and Minerals for supporting this research work. This research would not have occurred without utilizing their laboratory facilities, their support is acknowledged.

Finally, I would like to thank my parents and my wife who prayed and provided me the moral support that I needed the most throughout my study.

ABSTRACT

Analysis of the Effect of Bending, Fatigue, Erosion-Corrosion, and Tensile Stresses on HVOF Coating of Metallic Surfaces

By

Hussain Al-Fadhli BSc, MSc

The aim of the present study was to evaluate the bending, fatigue, tensile stresses and erosion-corrosion characteristics of HVOF thermally sprayed Inconel-625 powder coatings when deposited on three different metallic surfaces: (a) plain stainless steel (SS), (b) spot-welded stainless steel (SW-SS), and (c) a composite surface of stainless steel and carbon steel welded together (C-SS-CS) under three conditions: (i) surface as-coated, (ii) surface as-coated and subjected to aqueous static corrosion for two weeks, and (iii) surface as-coated and subjected to aqueous static corrosion for four weeks.

The predictions of the residual stresses generated during the deposition of the coating over the different metallic surfaces were also performed using analytical and numerical model studies. Validation of the models was carried out by comparing the results to experimental data. The surface morphology and the elemental composition of the coatings before and after each test were examined using SEM and EDS techniques.

The results indicate that the presence of weld or having a composite substrate formed by two different materials does affect the residual stresses at the interface, as it lowers bending, tensile, fatigue strength and enhancing corrosion effect, as observed by the analytical and experimental analyses carried out in this research. Microscopic observation of the fractured surfaces showed that the cracks were formed at the interface between the coating and substrate material as well as within the coating. Presence of non-melted particles in the coating enhanced crack propagation and erosion rates. The presence of oxides, namely Al_2O_3 at the interface between the coating and the substrate material left over from the surface preparation process also had an effect. Hence careful control is required when applying welds beneath surface coatings.

TABLE OF CONTENTS

LIST OF FIGURES

LIST OF TABLES

1

INTRODUCTION

In many industrial applications, including oil and gas production and in the petrochemical fields, the behaviour of material surfaces is of major importance. The appropriate selection of bulk materials and the coating of equipment components is an important consideration for the economic success of these industries. Moreover, the need to minimise cost and enhance the reliability of rotating and stationary fluid machinery equipment that is subjected to highly erosive and corrosive environments is mandatory. In many cases, surfaces are exposed to multiple deterioration mechanisms, such as wear and corrosion, at the same time, thus the probability of material failure is increased. It is estimated that the cost of unwanted wear and corrosion in the USA alone is in excess of US$ 3 billion per year. This alone provides significant impetus for research in the area of protective coatings [1, 2].

Thermal spraying is one of the most useful techniques used to produce coatings to protect components from the effects of wear and corrosion. Today, increasing use is being made of thermal spray deposits in technologies developed in industrial fields such as oil and gas, the marine, medicine, the petroleum, steel, textiles and printing industries [3]. Thermal spray technology has developed rapidly over the past twenty years, in line especially with progress in aircraft engines and the chemical industries [4]. New materials and surfacing contact has led to the development of engineering coatings that provide protection from wear, corrosion, and elevated temperatures, and allow for reliable performance in increasingly hostile environments [5, 6].

The high velocity oxygen fuel (HVOF) thermal spraying technique has been widely adapted in many industries due to its high flexibility and cost effectiveness [7]. This technique's wide applications include component repair involving either rebuilding worn out parts or enhancing the surface properties by using coatings material with better characteristics. The superior characteristics of HVOF coatings, which include high bonding strength and lower porosity and oxidation, have increased the efficacy of this process when compared to other coating techniques [8, 9, 10]. However, despite huge progress in the development of this technology, practical applications in the repair field still present many research challenges, and problems such as detected coating failures which occur in day to day operation still require solutions. The coating material used in this investigation, Inconel-625 powder, manufactured by Sulzer Metco (Diamalloy 1005), has various applications in several industries due to its superior corrosion resistance [10]. The application of this coating material is very common; however, the application of this material over welded and dissimilar materials has not yet been widely researched [11, 12, 13].

The report initially describes the coating characterisation of the Inconel-625 deposit. Following this, the material's resistance to several mechanical tests - including bending, fatigue, erosion-corrosion, and tensile testing, where the coating material is applied over plain, welded and dissimilar substrate materials - will be investigated. The substrate materials which were selected are SS 316 and Carbon Steel 4140, and the welding material chosen is SS 309.

The remainder of the report is divided into three chapters. Chapter Two gives a summary of relevant literature concerning HVOF spraying processing and design, equipment and theory, and applications focusing on the Inconel-625 material. The literature will also present previous research on coating bending, fatigue, erosion corrosion, and tensile tests. Various research sources were considered, including conference proceedings, with more focus on the annual thermal spray conference

proceedings as it is dedicated to thermal spray coating processes. Relevant journals supported by industry data were also considered. It was noted that the testing of HVOF sprayed coating materials was increasing and that most of the related research was relatively new; this assisted in selecting the latest, most up-to-date research in this regard [14, 15].

The experimental procedure is described in Chapter Three. This chapter is divided into six main sections, which include full descriptions of the spray system used, powder material morphology, substrate surface preparation, coating characterisation techniques, mechanical tests sample preparation as well as the spray process modelling technique. The mechanical tests sample preparation, which is the core of this work, is divided into four parts, where each part is concerned with the experimental procedure and set-up for the specific tests, including bending, fatigue, erosion-corrosion, and tensile tests. Modifications added to each experimental set-up are explained separately in each part and the ASTM standard used is addressed. Spray process finite element modelling (residual stress development during the cooling process of the coating) is presented in the final section of Chapter Three. This section describes the finite element analysis technique and procedures used in the research.

The experimental results and discussion are presented in Chapter Four. The results show a detailed characterisation of the Inconel-625 powder including Scanning Electron Microcopy (SEM) and Energy Dispersive Spectroscopy (EDS) analysis. Mechanical properties such as porosity, microhardness of the tested coating that had been studied in the previous research [16] are also discussed. The mechanical test results are shown separately in four parts to indicate the effect of each individual test. The mechanical tests results as a whole are correlated with the microstructural analysis and discussed to conclude the chapter.

Finally, Chapter Five presents the overall conclusions drawn from the results and provides recommendations for future work in this area. Such future research might

include expanding the current study to include other powders such as WC-Co as this is on one of the most widely used powders, especially in the areas of high temperature application and the aerospace industries [17]. Eight different articles were published out of this work: two journal papers, three conference papers and three posters, a list of which may be consulted in the "Publications Arising from This Work" section at the end of this thesis.

2

LITERATURE SURVEY

2.1 INTRODUCTION

Surface engineering is defined as a multidisciplinary activity which aims to tailor the properties of the surface of an engineering component so that its function and serviceability can be improved [18]. Surface treatment can be used in many different ways to improve the component's mechanical properties such as hardness, strength and toughness, which results in improvements in the component's fatigue, wear and corrosion resistance [19]. Similarly, environmental properties such as resistance to high temperature oxidation, aqueous corrosion and solidification can be improved by selecting a surface treatment technique such as the thermal spray process [20].

Although for most applications the surface is not made totally independent from its bulk material, the demands on surface and bulk properties are often quite different. For example, in the case of a sea-water pump shaft exposed to high slurry fluid flow, the bulk of the material must have sufficient bending and fatigue strength at the surface to provide an acceptably safe service life under repetitive cyclic loading on the shaft. Conversely, the surface of the material must also possess sufficient resistance to oxidation and erosion-corrosion under the conditions of service fluid impingement and corrosion attack to achieve that same component life.

In many instances, it is either more economical or absolutely necessary to select a proper coating material with the required properties to enhance the component surface [21, 22]. However, in some practical cases the surface of the bulk material

under the same working condition may not be uniform. In other words, either it has some weld spots randomly distributed over the surface or it is joined to another material with different properties. Hence, applying a coating over these different surfaces requires further investigation in order to achieve optimum results and minimise costs and potential safety hazards resulting from catastrophic equipment failures.

The literature survey of this report focuses on several points, including surface science, thermal spray coating technique, feedstock materials, and a detailed literature on the HVOF process theory and application. This will lead to a section describing the HVOF thermally sprayed Inconel-625 coating, focusing on the testing and characterisation of this material. Finally, a background of the literature in the area of the spray process modeling will be addressed.

2.2 SURFACE SCIENCE

The first step in the process of understanding thermal spray coating technology is to understand the surface to which the coating is applied. The concept of defining surfaces as the exterior phase of an object has now been expanded to being defined as the interface between solid objects and their surroundings [23]. The reason for expanding this concept is that coatings are applied not only to enhance surfaces and restore worn out parts, but also to protect these surfaces from their in-service harsh environments [24]. The components' interfaces encounter physical, chemical, electrical and other factors during performance. These forces can degrade the components and cause them to fail [25]. Surface coatings, such as thermal spray coatings, can help deal with these circumstances and reduce their effect. Before one can decide on the coating processes to be used to provide the best solutions, one needs to further explain in detail the mechanisms that cause these materials to fail. Three of the most significant problems that need to be addressed are; corrosion, fatigue and erosion-corrosion.

2.2.1 Wear

Wear can be defined as the physical removal of a material from a solid surface by another solid material [26]. The interaction is characterised by load and relative motion where both can produce several kinds of wear, including the modes of sliding wear, impact wear and rolling contact wear or any combination of these types. A summary of the characteristics of the different wear types is shown in Figure 1.

Multibody impact wear can be further broken down into erosive wear and cavitation wear (or cavitation erosion) [26, 27]. Erosive wear involves the cumulative effects of many particles striking a surface.

These particles can be solids, liquid droplets, collapsing bubbles, or solid-liquid mixtures called slurries [28]. Slurry is defined as a mixture of solid particles in liquid, with a consistency as to be capable of being pumped like a liquid [29]. One major part of this research is dealing with the multibody impact wear resulted from jet impingement fluid (slurry) tests, the effect of which causes the damage shown in Figure 2. Hence, the following section will discuss the theory of erosion-corrosion separately. A list of ASTM wear test methods, organised by type of wear and surface damage, is given in Table 1.

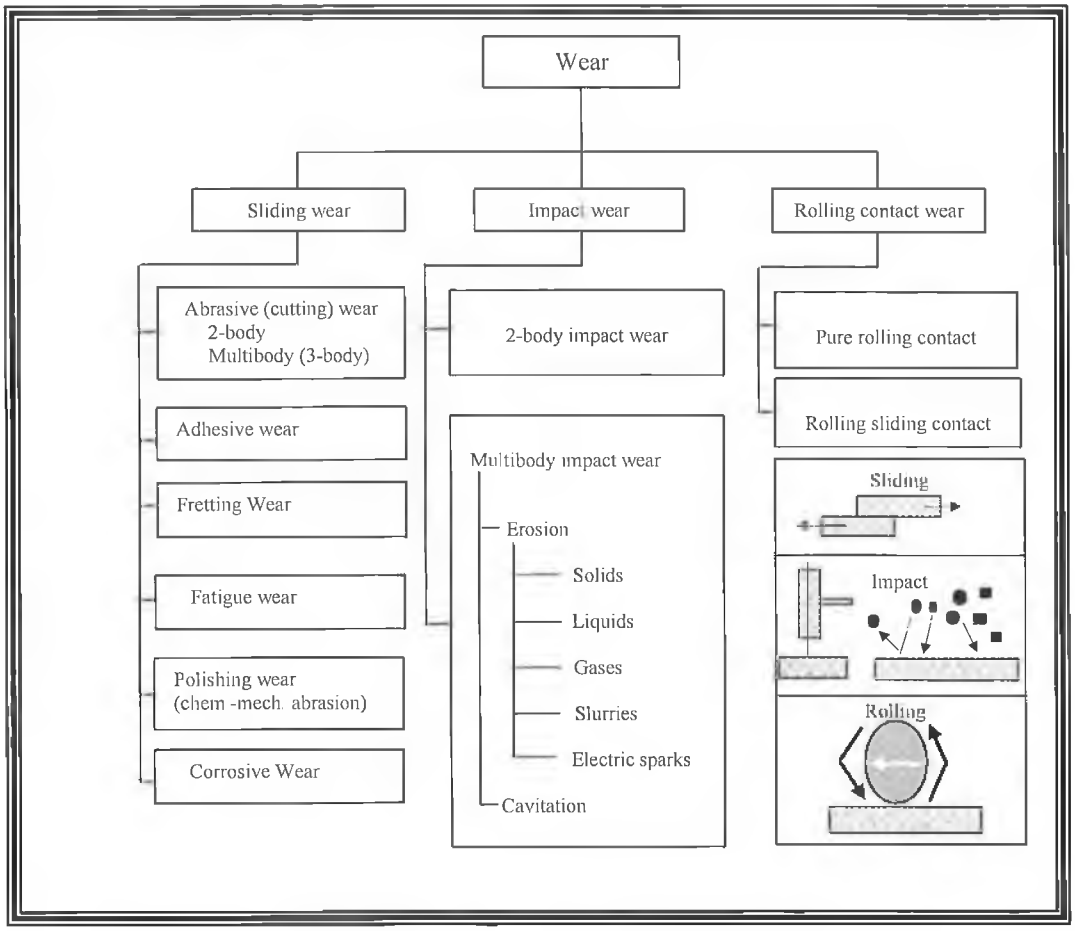

Figure 1 Major categories of wear, [30].

Table 1 ASTM: Wear test methods grouped by form of wear, [30].

Form of wear	Designation	Title	Means of wear measurement
Abrasive wear, 2-body	G 56	Test Method for Abrasiveness of Ink-Impregnated Fabric Printer Ribbon	Surface profiling or other method
	G 132	Test Method for Pin Abrasion Testing	Mass loss
	G 119	Guide for Determining Synergism between Wear and Corrosion	Mass loss and corrosion-related measurements
Erosive wear, cavitation fluid	G 32	Test Method for Cavitation Erosion Using Vibratory Apparatus	Mass loss
Erosive wear, liquid droplets	G 73	Practice for Liquid Impingement Erosion Testing	Mass loss
Erosive wear, slurry	G 75	Test Method for Determination of Slurry Abrasivity (Miller Number) and Slurry Abrasion Resistance Response of Materials (SAR Number)	Mass loss
Erosive wear, solid particles	G 76	Test Method for Conducting Erosion Tests by Solid Particle Impingement Using Gas Jets	Mass loss
Fretting wear	D 4170	Test Method for Fretting Wear Protection of Lubricating Greases	Mass loss ratio
Sliding wear	D 2266	Test Method for Wear Preventative Characteristics of Lubricating Grease (Four-Ball Method)	Wear scar diameter
Surface damage, galling	G 98	Test Method for Galling Resistance of Materials	Visual inspection, critical load for galling
Surface damage, scoring	D 2782	Test Method for Extreme-Pressure Properties of Lubricating Fluids	"OK" value of maximum mass (weight) for load just below critical scoring condition

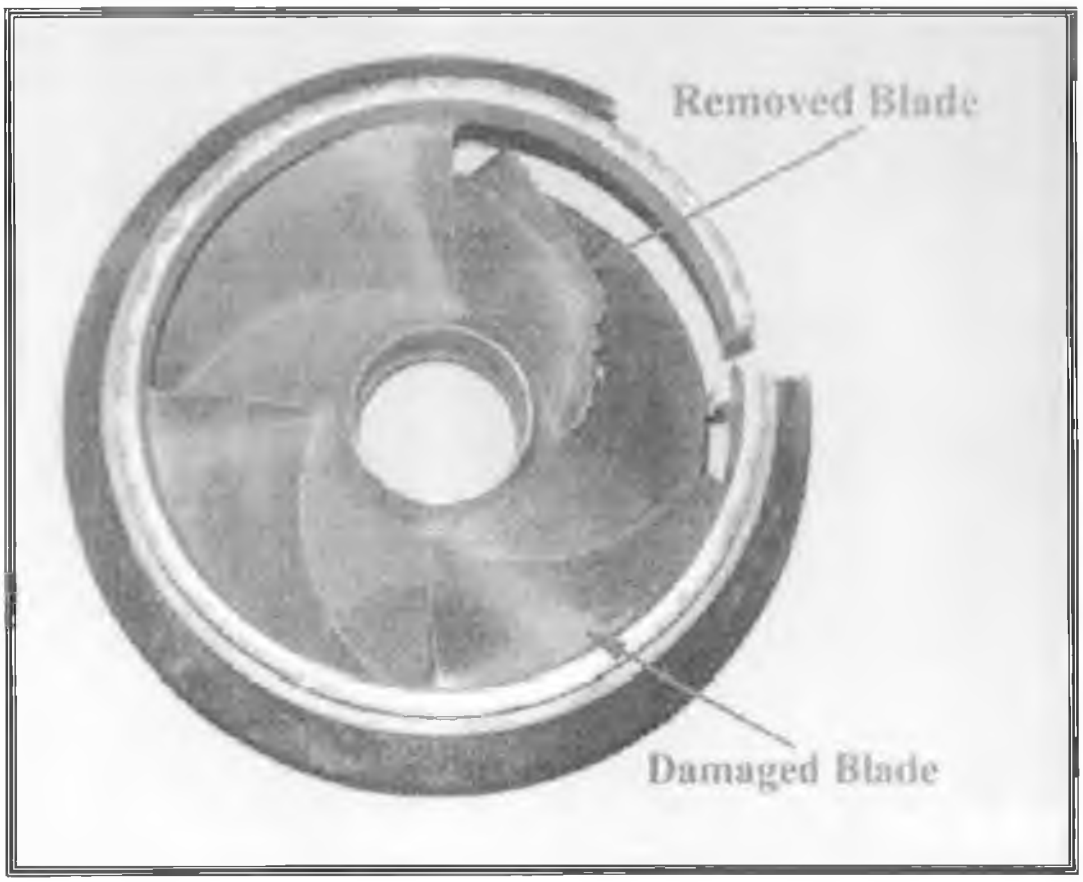

Figure 2 Industrial pump impeller subjected to impact (erosion-corrosion) wear, [31].

2.2.2 Corrosion

Corrosion is the result of the undesirable chemical interaction of a surface with its environment [32]. There are several factors that contribute to corrosion failure, including condensation of the containing water-soluble ionic species such as chlorides and sulfites, the degree of exposure to wind and sun, the shape of the structure, the presence of crevices, joints, improperly applied welds, vibrations, and design stresses (Figure 3), [33]. In general, corrosion might be classified into several basic categories: uniform, pitting, intergranular, crevice, and galvanic [34]. Various types of testing techniques can be used to investigate corrosion failures or

to evaluate the resistance to corrosion of metals and alloys. These include accelerated tests, electrochemical tests and simulated-service tests [35, 36, 37].

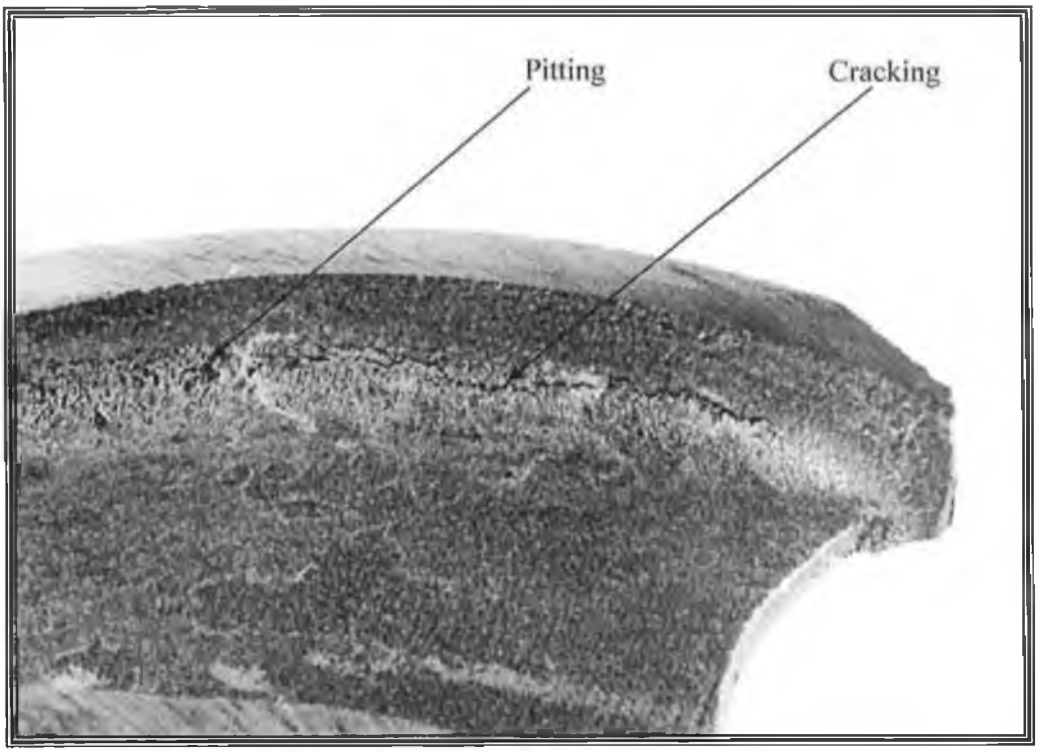

Figure 3 Pitting and cracking at the junction between web and flange of a cast 316 type stainless steel impeller as a result of flow of sea water, [33].

2.2.3 Erosion-Corrosion

Erosion-corrosion is a form of material degradation that involves electrochemical corrosion and mechanical wear processes resulting from fluid motion [38]. For most materials, there are critical velocities beyond which protective films are swept away and this accelerates corrosion. The critical velocity differs greatly from one material to another and may be as low as 0.6 to 0.9 m/s (2 to 3 ft/s) for soft metal alloys to more than 27 m/s (90 ft/s) for some hard metals such as titanium [39]. During the erosion-corrosion mechanism, the total material loss is mainly

composed of the sum of the separate pure electrochemical corrosion and the surface wear process [40]. Moreover, the deterioration mechanism is dependent on a wide range of variables that include the properties of the erodent particles (for example kinetic energy, flux, hardness, shape and size), the targeted material (for example hardness and strain hardening coefficient), and the environment (salinity, temperature, and pH), as well as the complex hydrodynamic effect such as impact velocity and impact angle [41]. In practical applications the erosion-corrosion phenomena can damage surfaces in a variety of ways. One of the most common in the oil and gas industries occurs in sub sea pump internals, where impeller wear rings and valve stems handle rapidly flowing or impinging liquid streams (Figure 2). This kind of damage is accentuated when the flowing slurries contain highly corrosive (for example sea water) mixtures and especially when contaminated with solid particles [42]. Obviously, this can lead to substantial operating breakdown maintenance, and increased production costs in a wide variety of offshore oil and gas industries.

Recent studies of erosion-corrosion have been focused on metallic materials, ranging from low-grade cast iron and carbon steel to the higher grade of austenitic and duplex stainless steels and high grade nickel alloys [42]. As these materials suffer from aggressive erosion-corrosion conditions, there is always a strong incentive for alternative surface engineering options to be developed, one of which is thermal spray coatings [30, 42].

2.2.4 Fatigue

Fatigue can be defined as the failure that occurs in structures when subjected to dynamic and fluctuating stresses having a maximum stress value less than the ultimate tensile strength of the material [43]. It is estimated that 90% of all metallic failures are a result of fatigue [44]. The process of fatigue usually starts with the initiation of cracks that propagated at a certain time and become long enough to cause failure (Figure 4), [45]. However, this mechanism of failure is

catastrophic and insidious, and can occur suddenly without warning. In practice, except for a few relatively brittle materials, the prediction of the fatigue life of a material is complicated because fatigue life is very sensitive to small changes in loading conditions, local stresses, and the local characteristics of the material [46]. As it is difficult to account for these minor changes in either the dynamic stress-prediction techniques or the fatigue-failure criteria, this results in a large degree of uncertainty, inherent in analytical predictions of fatigue life. Therefore, the designer must rely on experience with similar parts and eventually on qualification testing of prototypes or production parts.

In general, factors that influence fatigue life include [47, 48]:

- Type of loading (uniaxial, bending, torsional)
- Shape of loading curve
- Frequency of load cycling
- Magnitude of stresses
- Part size
- Fabrication method and surface roughness
- Operating temperature
- Operating atmosphere.

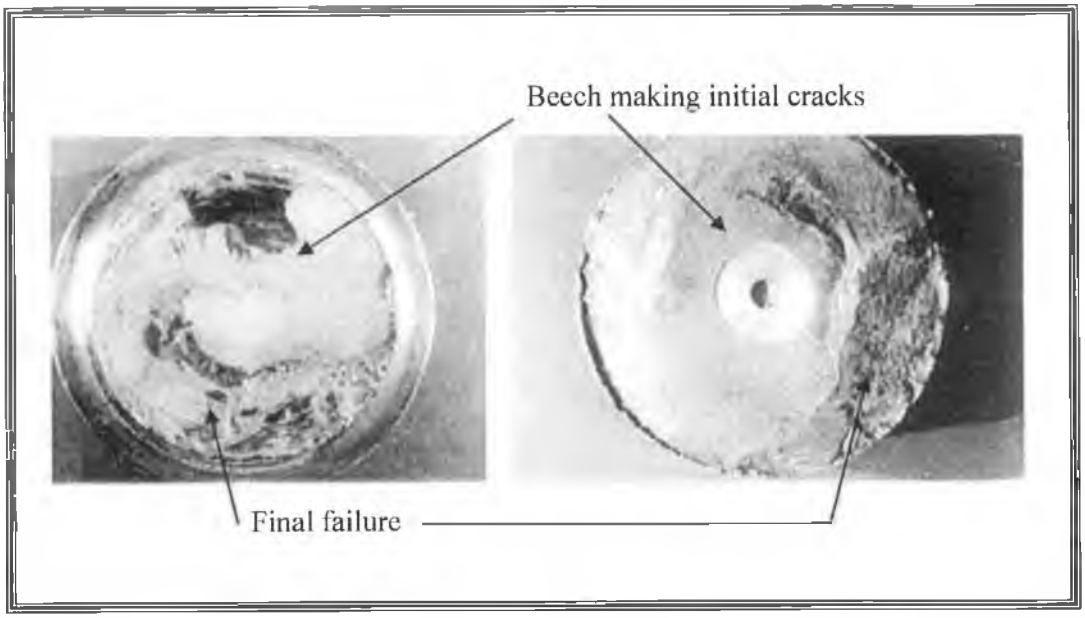

Figure 4 Photograph of pump shaft failure due to cyclic fatigue, [45].

2.3 THERMAL SPRAY COATING TECHNIQUE

2.3.1 Initiation of Thermal Spray Coating

Thermal spraying was first discovered and used at the state of last century and research in this field has progressed ever since (Figure 5). The recognised beginning of thermal spraying is believed to have been in 1911, with a flame spray process (metallizing) developed by Schoop and Guenther [49]. In the 1950s, the broad application of new refractory materials (mostly related to the aerospace industry) commenced and this saw the birth of the detonation gun deposition spraying process (invented by R. M. Poorman, H. P. Sargent, and H. Lamprey and patented in 1955) [49]. The 1970s witnessed the development of vacuum plasma spraying (VPS) and the atmospheric plasma spraying (APS) [50]. Finally, during the 1980's, with the development of High Velocity Oxy-Fuel (HVOF), thermal spraying became widely recognised as an industrial technology [50].

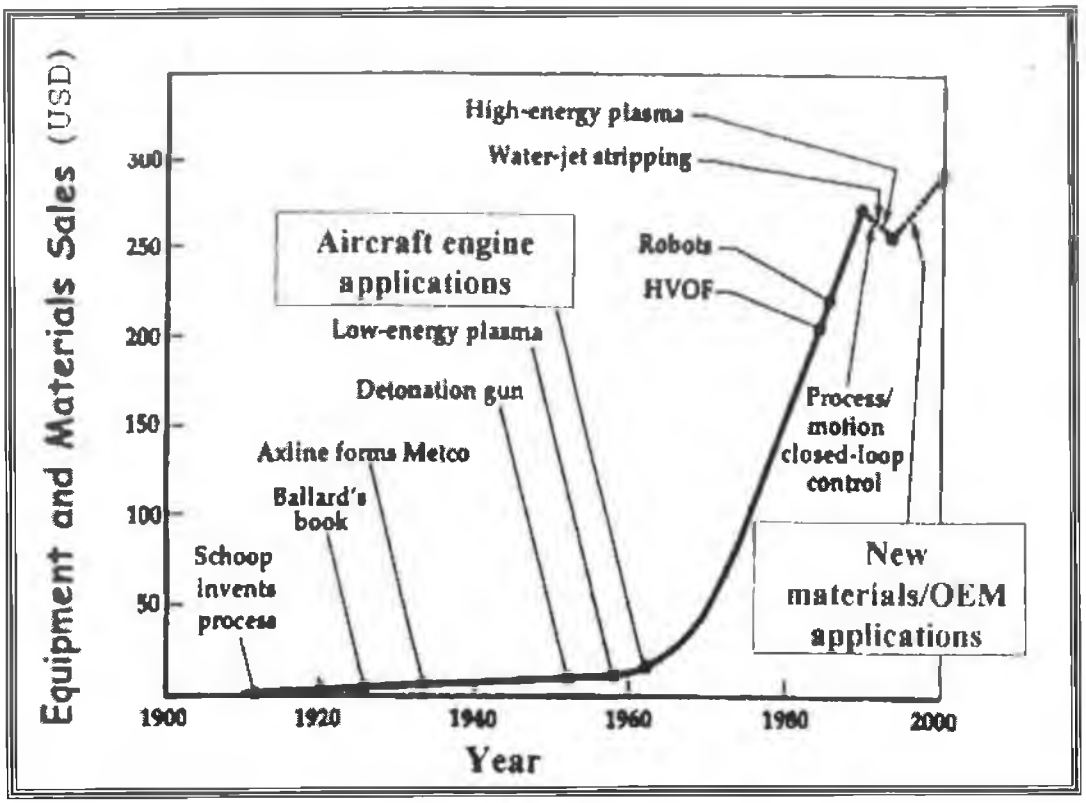

Figure 5 Timeline development of the thermal spray industry, [49].

2.3.2 Thermal Spray Coating Types and Characteristics

The thermal spray technique can be grouped into a number of different processes: flame spraying, arc spraying, plasma spraying, detonation gun spraying, and HVOF spraying. The next section will briefly cover each of these processes, but will focus chiefly on HVOF as this was the process used in this research.

(1) Flame Spray Process

The flame spray process uses a combustible gas as a heat source to melt the coating material (Figure 6). The coating material can either be powder or wire form on deposition. The heat source is a mix of fuel gas–oxygen flame. Different fuel gases may be used including acetylene (C_2H_2) and propane (C_3H_8) where acetylene produces the highest combustion temperature. The Jet gas speeds are typically low, below 100 m/s (330 ft/s) and particle velocities around 80 m/s (260 ft/s), due to the process having relatively low pressure and low flow rate [50]. The combustion temperature is usually above 2600°C (4700°F) [50]. High levels of porosity and oxidation are considered a major disadvantage in the flame spray process [51].

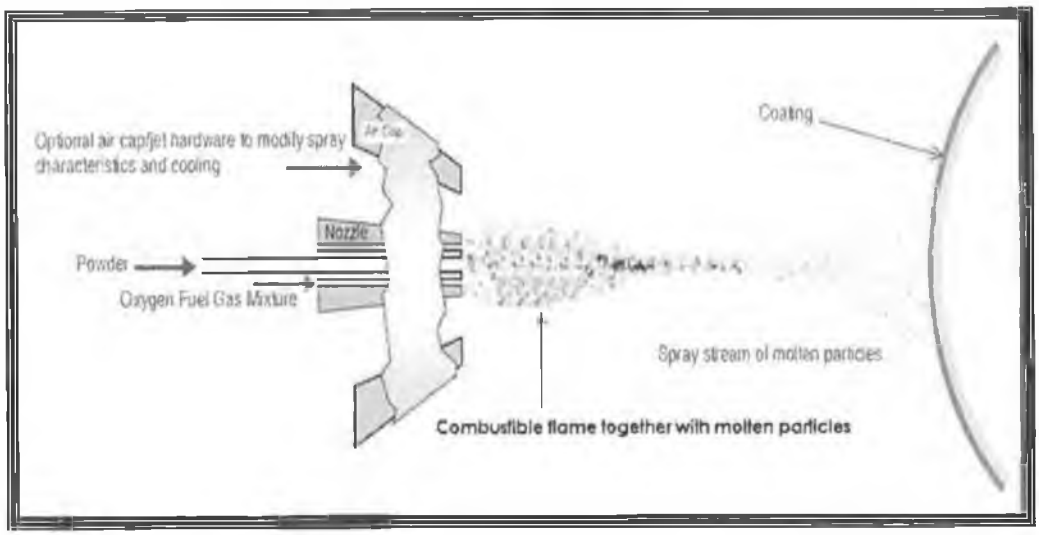

Figure 6 Schematic diagram of the flame spray process, [51].

(2) Arc Spray Process

In the arc spray process, a pair of electrically conductive wires (which will atomise the final deposit) are melted by means of an electric arc (Figure 7). The molten

material is atomized by compressed air and propelled towards the substrate surface. Electric arc spray coatings are normally denser and stronger than their equivalent combustion spray coatings. Low running costs, high spray rates and efficiency make it a good tool for spraying large areas and at high production rates. The disadvantages of the electric arc spray process are that only electrically conductive wires can be sprayed and if substrate preheating is required, a separate heating source is needed. The main applications of the arc spray process are anti-corrosion coatings of zinc and aluminum and machine element work on large components [49, 50].

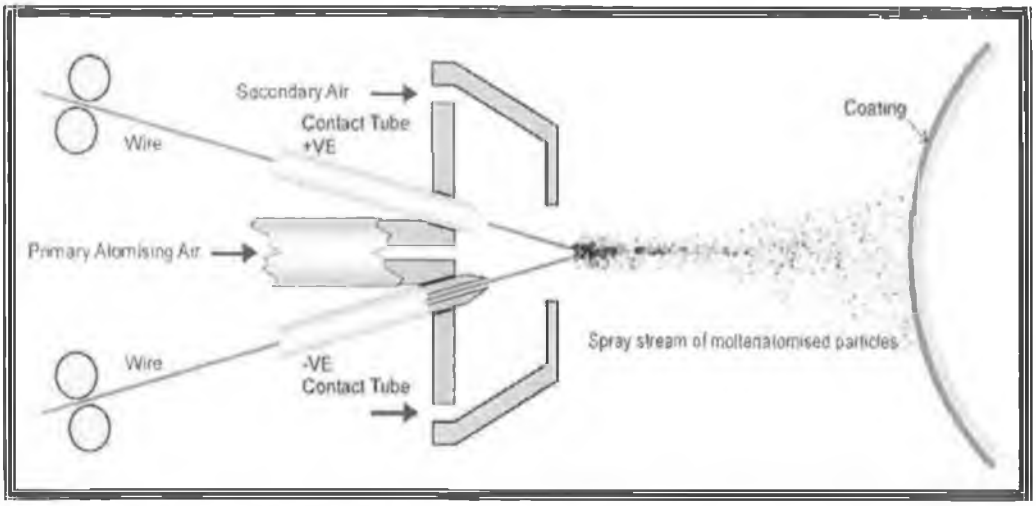

Figure 7 Schematic diagram of the electric arc spray [49].

(3) Detonation Gun Process

The detonation gun basically consists of a long, water cooled barrel with inlet valves for the gases and powder (Figure 8). Oxygen and fuel (acetylene most commonly) are fed into the barrel along with a charge of powder. A spark is used to ignite the gas mixture and the resulting detonation heats and accelerates the powder to supersonic speeds down the barrel. A pulse of nitrogen is used to purge

the barrel after each detonation. This process is repeated many times a second. The operation frequency is typically four to eight cycles per second, giving a relatively low spray rate of 0.3 to 0.9 kg/hr. The high kinetic energy of the hot powder particles on impact with the substrate results in a build up of a very dense and strong coating [52].

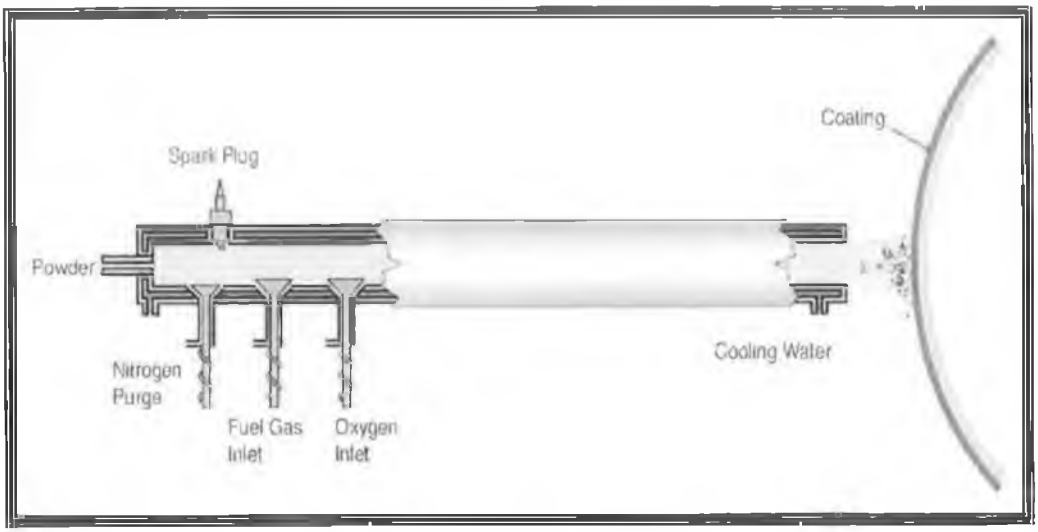

Figure 8 Schematic diagram of the detonation gun spray system, [52].

(4) Plasma Spray Process

In the plasma spray process, material in the form of powder is injected into a very high temperature plasma flame, where it is rapidly heated and accelerated to a high velocity (Figure 9). Plasma is initiated by a high current discharge, produced from electric current, which causes localised ionization for the gas (argon, nitrogen, hydrogen, or helium). The resistance heating from the arc causes the gas to be ionized and reach extreme temperatures, forming a plasma [50]. The temperature of the gas can be as high as 15,000-20,000°C, depending on the gas used, and the operating energy often reaches 720 MJ (682,800 BTU) [51]. Therefore, plasma spraying has the advantage of spraying very high melting point materials such as

refractory metals like tungsten and ceramics like zirconia, unlike combustion processes. Plasma spray coatings probably account for the widest range of thermal spray coatings and applications, which therefore makes this process the most versatile. The disadvantages of the plasma spray process are relative high cost and the complexity of the process [49, 50].

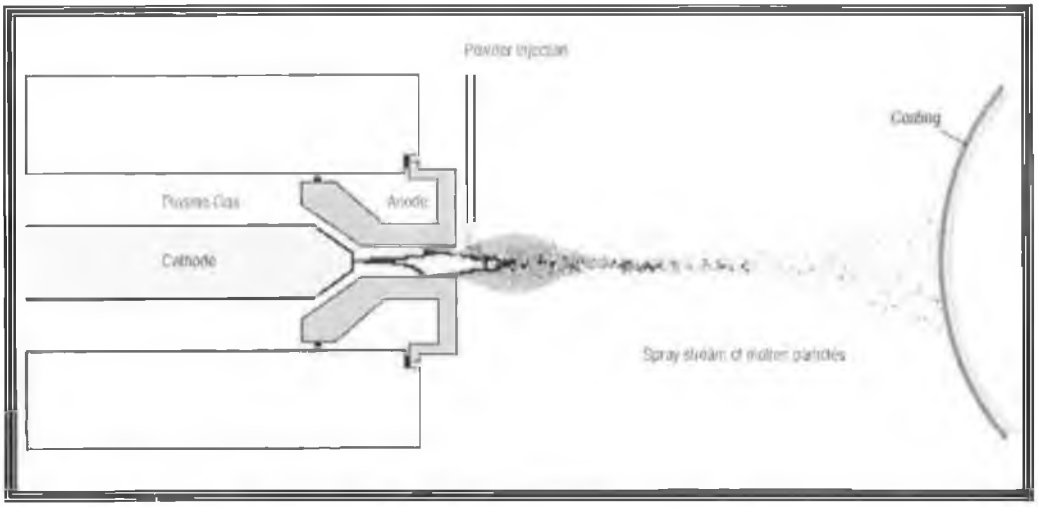

Figure 9 Schematic diagram of the plasma spray system, [52].

(5) The High Velocity Oxy-Fuel (HVOF)

The High Velocity Oxy-Fuel (HVOF) thermal spray process is basically the same as the powder flame spray process except that this process has been developed to produce extremely high spray velocities. This is achieved by using a nozzle arrangement to acquire the velocities together with high flow rates of gases (Figure 10). This process is relatively new compared to other thermal spray methods [52]. A detailed explanation of this process will be introduced in Section 2.5 as this is the process that was used in the current work.

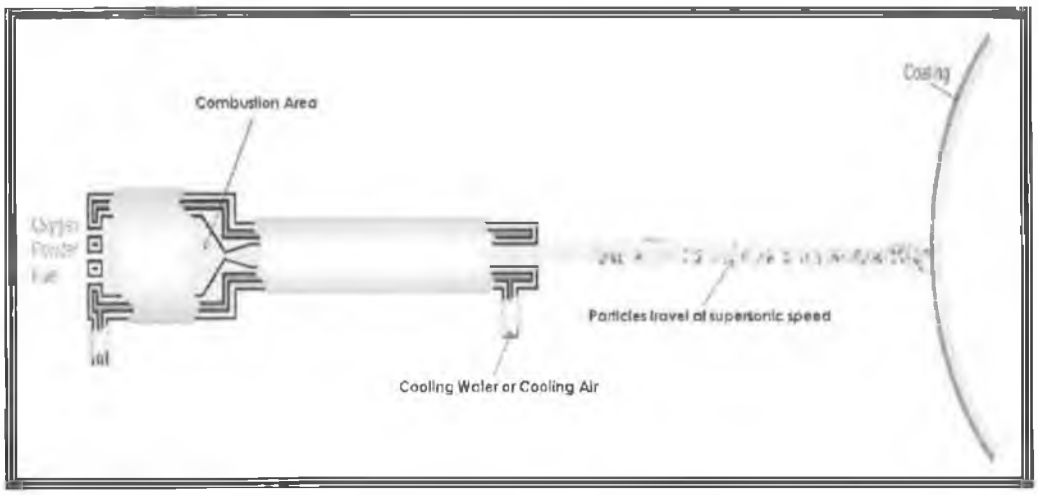

Figure 10 Schematic diagram of the HVOF spray system [52].

2.3.3 Comparison between Thermal Spray Processes

The different thermal spray processes described earlier have different characteristics. Each of these processes can be distinguished based on their coating quality and the requirements of the applications. In other words, it is difficult to permanently prefer any one of these process over another. For example, the only process that could be used for high melting temperatures is plasma spraying. However, this process is still considered complicated and relatively expensive, and has coating properties that differ from those found when using HVOF [52].

The jet parameters; (i) temperature, (ii) velocity, (iii) gas flow, (iv) gas type, (v) power, the particle feed parameters; (i) particle size (ii) temperature, (iii) velocity, (iv) feed rate, and deposit characteristics parameters; (i) density, (ii) bond strength, and (iii) oxides, have a great influence on the coating properties (Table 2).

Research is on-going to optimise the coating end product quality of each of these processes using the above mentioned parameters [49,52]. In this study, the HVOF process was selected to deposit Inconel-625 because it produces low porosity, high bonding strength, with high efficiency and simple process often used in repair industry [51,53].

Table 2 Characteristic of thermal spray processes and coatings [49].

Attribute	Flame spray	High-velocity oxyfuel	Detonation gun	Wire arc	Air plasma	Vacuum plasma
Jet						
Jet temperature, K	3500	5500	5500	>25,000	15,000	12,000
Jet velocities, m/s (ft/s)	50–100 (160–300)	500–1200 (1600–4000)	>1000 (>3300)	50–100 (160–300)	300–1000 (1000–3300)	200–600 (700–2000)
Gas flow, sL/m	300–700	400–1100	N/A	500–3000	100–200	150–250
Gas types	O_2, acetylene	CH_3, C_3H_6, H_2, O_2	O_2, acetylene	Air, N_2, Ar	Ar, He, H_2, N_2	Ar, He, H_2
Power input, kW equiv.	20	150–300	N/A	2–5	40–200	40–120
Particle feed						
Particle temperature (max), °C (°F)	2500 (4500)	3300 (6000)	N/A	>3800 (>6900)	>3800 (>6900)	>3800 (>6900)
Particle velocities, m/s (ft/s)	50–100 (160–300)	200–1000 (700–3300)	N/A	50–100 (160–300)	200–800 (700–2600)	200–600 (700–2000)
Material feed rate, g/min	30–50	15–50	N/A	150–2000	50–150	25–150
Deposit/coating						
Density range (%)	85–90	>95	>95	80–95	90–95	90–99
Bond strength, MPa (ksi)	7–18 (1–3)	68 (10)	82 (12)	10–40 (1.5–6)	<68 (<10)	>68 (>10)
Oxides	High	Moderate to dispersed	Small	Moderate to high	Moderate to coarse	None

2.4 FEEDSTOCK MATERIALS

2.4.1 Types of Thermal Spray Materials

Thermal spray material types are characterised into the following forms: wires, rods, and powders. Wires are made from either metals or alloys and can be used only in the arc spraying or flame spraying processes. The wires are produced using forming technique processes such as wire drawing.

Rods are mainly used in the flame spraying process. The main disadvantage of using rods is the short length of the sintered rod, which gets used up in a very short time; therefore, to continue the process of deposition, a new rod must be added to the torch. This interruption in the process leads to a change in the coating microstructure.

Powders are the most common material used in the field of thermal spraying. This is mainly due to the reliability of their manufacturing route and the variety of their chemical compositions.

It is also important to recognise that composition is not the only important variable. Powder particle shape, size distribution, homogeneity and microstructure all depend on the manufacturing process and these processes influence the spraying process and coating quality [49,50]. The HVOF process uses powder as its coating material, hence this form of material, will be discussed further in the following section.

2.4.2 Methods of Powder Production

Thermal spraying powders can be manufactured according to different methods, the method chosen depending mainly on the material and the process to be used during spraying. Pawlowski [50] describes in detail the different powder types and production methods, including the production of metallic and ceramic powders. The most popular powders that are currently in use are [51]:

- Metals (e.g. Molybdenum) and alloys (self fluxing alloys such Inconel-625)
- Oxide ceramics (e.g. Al_2O_3)
- Cermets (Graphite cladded with Ni or WC agglomerated with 12 wt% Co)
- Carbides (Cr_2C_3)

The method of powder production can be summarised into four groups (Figure 11):

- The atomization method
- Fusing or sintering
- Spray drying (Agglomeration)
- Cladding

The atomization method is mainly applied to the manufacture of metals and alloy powders. The purity of the atomized powder depends on the atmosphere inside the melting chamber, the atomization medium, and the cooling medium in the atomization tower. Powders produced by this process usually have a small internal porosity and, due to their spherical shape, and provide excellent flowability [51].

Fusing or sintering was the first method used to produce oxide, carbide and cermet powders [50]. In this method, the material compound is melted, cast into a mould and crushed into powder form. The powder particles produced by this method are relatively dense with angular and blocky morphologies (Figure 11) [49, 51].

The spray drying or agglomeration technique is the most versatile technique as it permits the agglomeration of any kind of material. The flowability of spherical

powder particles formed using this method can be better than that formed by other methods [50]. This method consists of introducing a slurry containing finely dispersed material to be agglomerated together with an organic binder and water, atomized and dried in a drying chamber and collected using a cyclone for thermal spray use [51].

Cladding powders (composite powder) consists of coating a material with porous or dense layer of another material. This process is applied mainly when materials need to be protected from a flame, to enhance adhesion or to enhance flowability [49, 51]. The powder Inconel-625 under investigation which is mainly made up of Nickel and Chromium was formed using the atomization powder production route.

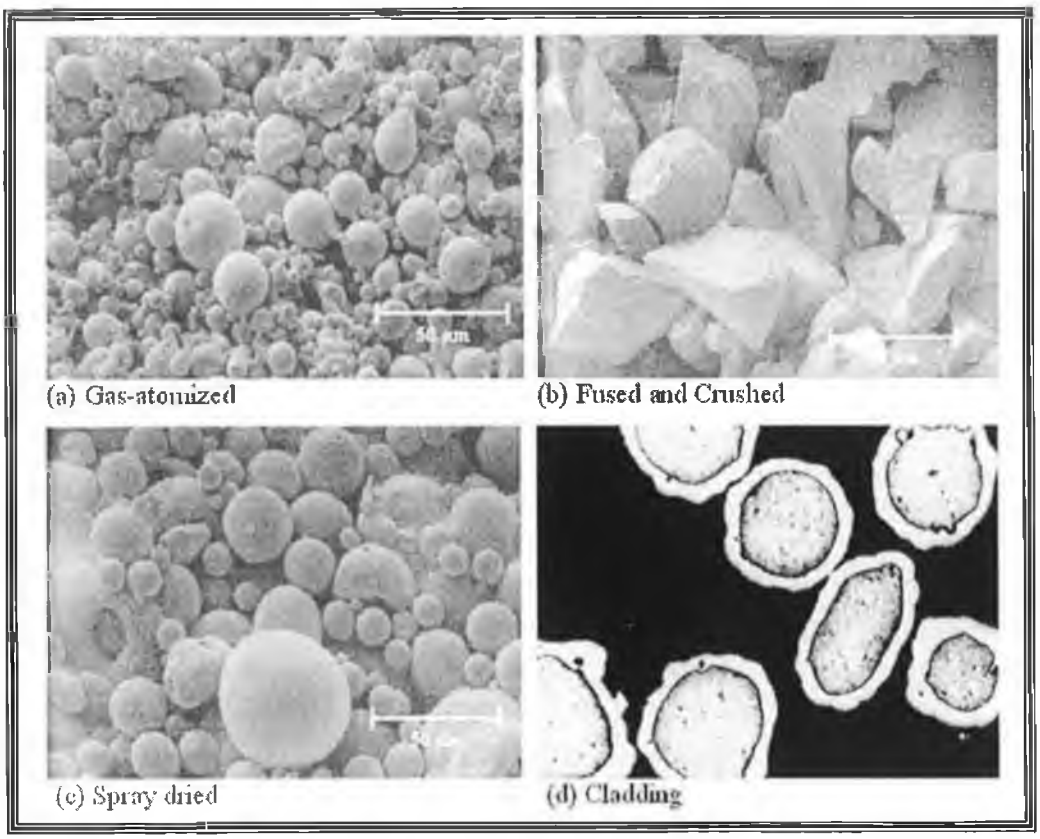

Figure 11 Different produced powder morphologies, as a result of using different powder production methods [49, 51].

2.4.3 Methods of Powder Characterisation

It is mandatory to characterise the powders prior to applying thermal spray coating as the powder size distribution, in combination with shape and particle surface condition, will determine the flow behaviour of the particles within the spray gun and the melting in the torch. Consequently, the end product quality of the coating will be affected. For instance, using small size particles in a high melting temperature system such as the plasma spray process results in powder evaporation which reduces the decomposition efficiency of the coating [51]. Conversely, using large particle size in a moderate flame temperature system such as HVOF results in having non-melted particles in the coating [52].

There are several methods of powder characterisation as well as the techniques used, including [49, 51]:

- Particle size (Mechanical sieve analysis, X-ray absorption)
- Chemical composition (X-ray florescence, XRF spectroscopy)
- Shape of the grain (SEM or Optical microscopy OM)
- Density and flowability (ASTM B 329-76)

2.5 THE HVOF PROCESS

2.5.1 Introduction

During the last two decades, the high-velocity oxy-fuel (HVOF) process has proved a viable technological alternative to the many conventional thermal spray processes such as plasma [52]. In principle, the spray process is similar to the detonation gun process with the exception that HVOF operates using a continuous, steady state process. Fuel (either kerosene, acetylene, propylene and hydrogen) and oxygen are fed into the chamber, combustion produces a hot high pressure flame which is forced down a nozzle, increasing its velocity (Figure 12). The coating material, which is a powder, is fed axially into the high energy gas stream where the expanding gas forces the particles through a nozzle at supersonic velocity. Gas velocities have been measured in the range from 1,500 to 2,000 m/s (4,900 to 6,500 ft/s), on the order of up to five times the speed of sound [54]. The Ideal Stochiometric combustion equation for propane is:

$$C_3H_8 + 5O_2 \longrightarrow 3CO_2 + 4H_20 \qquad \Delta H = -2220 KJ / mol\ C_3H_8 \qquad \textit{Equation 1}$$

The compressed air pinches and accelerates the flame and acts as a coolant for the HVOF gun. HVOF coatings can be very dense, strong and show low residual tensile stress or in some cases compressive stress, which enables thicker coatings of certain materials to be applied than that possible with the other processes [55]. The very high kinetic energy of particles striking the substrate surface does not require the particles to be fully molten to form high quality HVOF coatings. This is certainly an advantage for the carbide type coatings and this is where this process really excels. HVOF coatings are used in applications requiring the highest density and strength not found in most other thermal spray processes. New applications, previously not suitable for thermal spray coatings are becoming viable, such as gas turbines blades, biomedical applications, curvature surfaces (ball valves), to mention a few [56, 57].

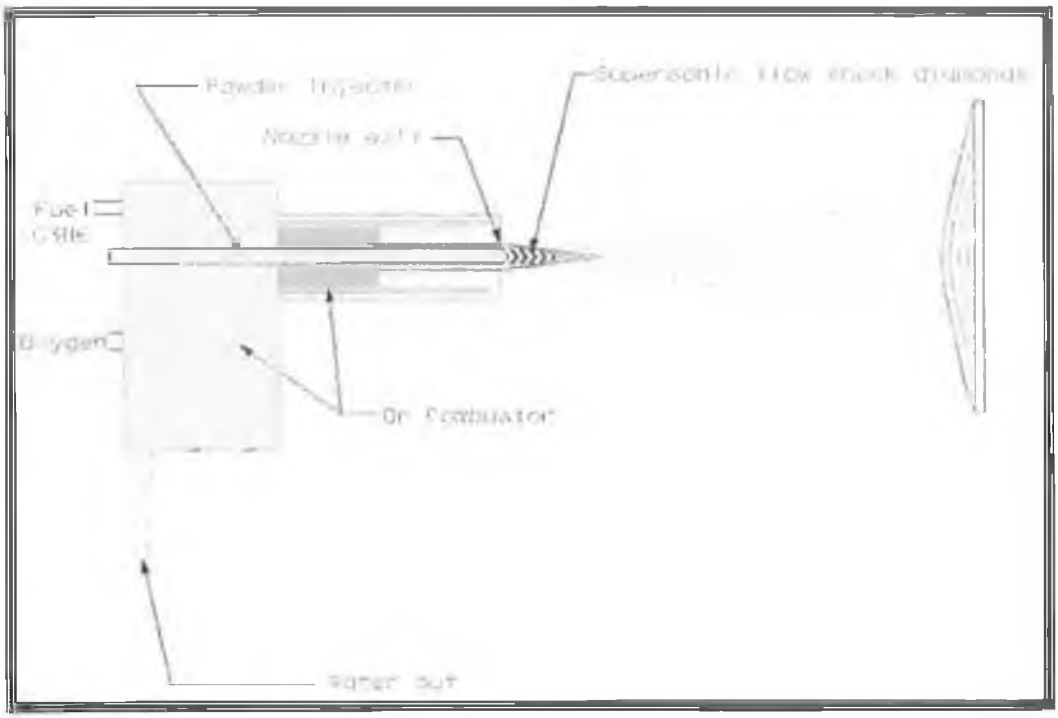

Figure 12 Schematic diagram of the axial feed type HVOF spray gun used in this research.

2.5.2 HVOF Coating Structure and Properties

It is obvious that the mechanical behaviour of industrial materials/coatings depends strongly on their microstructure. Several coating features determine the HVOF deposit properties, including pores, splats (lamellar), unmelted or resolidified particles, grains, oxide inclusions, phases, cracks, and bond interface (Figure 13). Porosity and oxidation are two of the most influencing parameters on HVOF coating characterisation in which all remaining parameters can be deeply related to either one or both of them [58].

(1) Porosity

The HVOF spray deposit usually contains some level of porosity, typically between 0 and 5%. This porosity results from the high number of unmelted or resolidified particles that become trapped in the coating creating poor cohesion that leads to premature coating cracking, delamination, or spalling [59]. Moreover, porosity in HVOF deposits lowers the coating hardness and contributes to poor surface finishes, hence decreasing wear resistance [60, 61]. Table 3 shows porosity results for various Diamond Jet HVOF coatings.

Table 3 Coating porosity in various Diamond Jet HVOF coatings [62].

Coating material	Porosity (%)
Nickel/Chromium Molybdenum Base Superalloy (Inconel-625)	1
Tungsten Carbide-Cobalt	<0.5
Cobalt Base Alloy	1.5
Chromium Carbide/ Nickel Chromium	1
Tool Steel	<1
Al_2O_3–13TiO_2	1.2

(2) Oxides

Oxide inclusions in HVOF deposits are usually detected as dark, elongated phases that appeared as strings in the coating cross section, parallel to the substrate. Oxides are produced when a heated particle interacts with the atmosphere or when the coating surface is heated during deposition [63]. HVOF coating oxides can be minimized using a number of methods: reducing the average temperature of the particle by lowering the heating capacity of the spray jet, reducing the dwell time

of the particle by lowering the spray distance or increasing velocity, or by using the proper powder particle size (30μm ± 5μm) as large particles have a lower surface area to volume ratio [69].

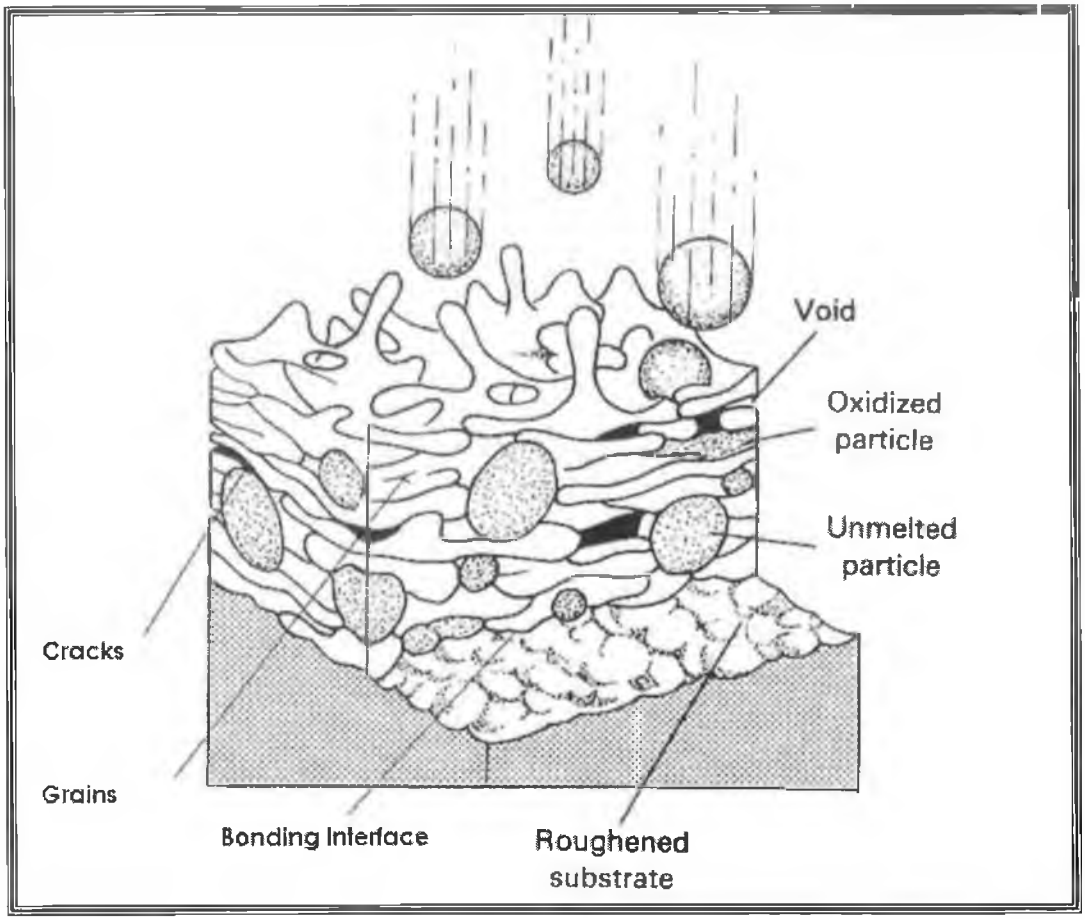

Figure 13 Schematic diagram of the HVOF coating structure showing deposit features [49].

2.5.3 Parameters Affecting the HVOF Coating Quality

There are many parameters that have a direct effect on the HVOF coatings' characterisation. These could be either in the form of surface preparation parameters such as grit type, blasting conditions, grit feed rate and sample surface roughness, or operational parameters like powder feed rate, stand off distance, gun pressure, work piece transfer speed, work piece surface temperature, and equipment from different manufacturers thus producing different coatings structure [65].

Previous research indicates that both spray distance and powder feed rate variations, within the limit of manufacturer specifications, show the highest influence on the coating characterisation [16]. In the plasma spray process alone there are more than one hundred parameters that all have a direct effect on the end product quality of the coating [16, 52, 66]. Figure 14 illustrates the major process parameters that affect HVOF coating quality.

In the HVOF coating process, where the combustion process takes place inside the gun at very high gas flow rates, a supersonic flame speed of up to approximately 2000 m/s can be achieved, leading to very high particle speeds of up to approximately 800 m/s [67]. Although this high kinetic energy leads to a very high degree of particle deformation producing better coating bonding and higher coating density, the number of unmelted or semi-molten particles is increased during spraying. This is mainly due to the fact that higher particle velocities result in shorter dwell time, so there is less time for particle heating. Hence, enhancing one of the process parameters can affect other properties of the deposit [49, 68].

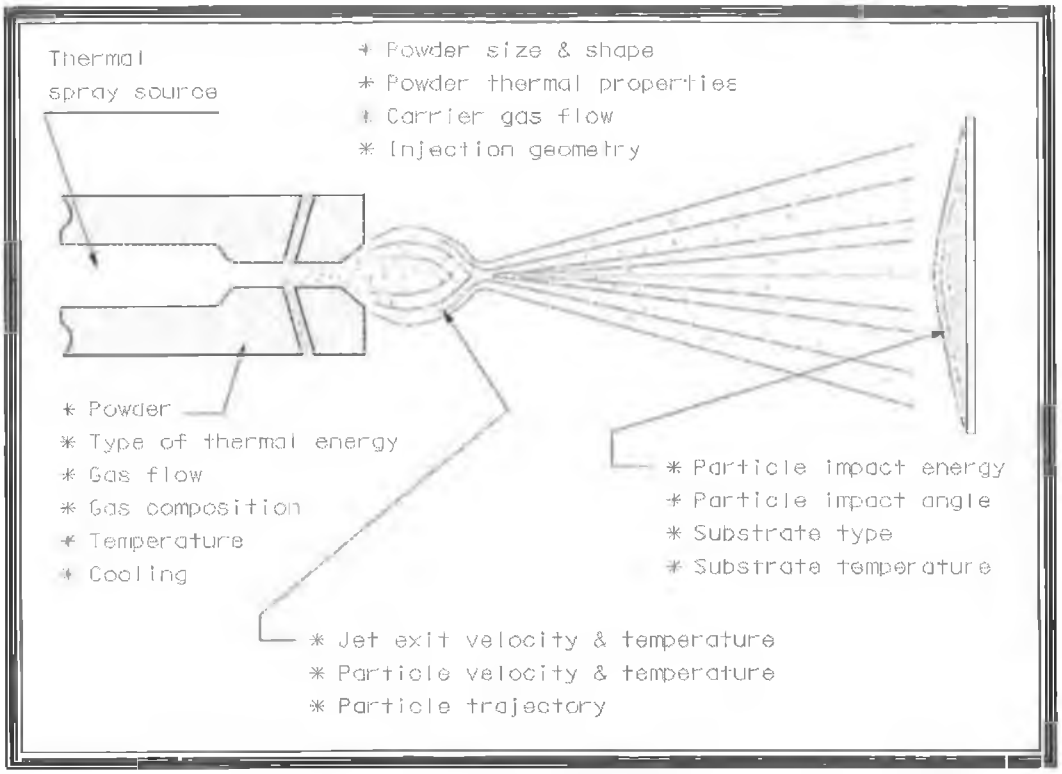

Figure 14 Schematic diagram of the HVOF spray process variables and parameters [49].

2.5.4 Advantages and Disadvantages of the HVOF Coating

(1) Advantages

HVOF coatings, like other thermal spray coating processes, have several overall advantages: a wide range of materials can be deposited as a coating, low processing cost, wide range of coating thickness, wide range of applications, and minimal thermal degradation to substrate. However, the HVOF process offers a number of advantages over, and alternative to, competing processes including higher bond strength, lower porosity, lower flame temperature and lower capital

cost. The HVOF thermal spray process is a uniquely distinguished process due to its high particle velocity produced via the supersonic velocity of the jet gun.

Consequently, several advantages are maintained due to this high particle velocity, including [49, 62]:

1. Much shorter exposure (to temperature) time in flight due to high particle velocities
2. Short particle exposure time in ambient air once the jet and particles leave the gun, which results in lower surface oxidation of particles
3. Uniform and efficient particle heating due to the high turbulence experienced by the particles
4. Lower ultimate particle temperatures compared to other processes

Table 4 summarises the reasons the HVOF process produces such high quality coatings.

Table 4, Benefits of using HVOF coatings [62].

Coating benefit	**Main reasons for this benefit**
Higher density (Lower porosity)	Higher impact energy
Improved corrosion barrier	Less porosity
Higher hardness ratings	Better bonding, less degradation
Improved wear resistance	Harder, tougher coating
Higher bond and cohesive strength	Improved particle bonding
Lower oxide content	Less in flight exposure time to air
Fewer unmelted particle content	Uniform particle heating
Greater chemistry and phase retention	Reduced time at higher temperature
Thicker coatings	Less residual stress
Smoother as sprayed surface	Higher impact energies

(2) Disadvantages

HVOF coatings also have some disadvantages, and it is important to understand these so that design or repair engineers can avoid placing HVOF deposits in situations where the required performance is not achievable [62, 69]. These disadvantages include:

1. Flame temperature is relatively low, in the order of 2,900°C (5,250°F), making it difficult to spray ceramics and refractory metals. Since dwell time (the amount of time the powder is in the flame) is short, heat transfer to large powder particles may not be sufficient. It requires finer powder particle size and tighter tolerance on particle size distribution than other processes.

2. The amount of heat content in the HVOF system is very high, so over-heating of the substrate is quite likely. Therefore, extra cooling of the substrate is necessary, and cooling with liquid CO_2 is now a standard with the new HVOF process [62, 69].

3. Masking (Covering off of certain parts of a component to deposit only on specified areas) of the part is still a great problem as only mechanical masking is effective. It is very difficult and time consuming to design an effective mask for a complex component with areas which do not require deposition.

2.5.5 Applications of the HVOF Coating

HVOF coatings have numerous applications that can be used in several industries including oil and gas, aerospace, automotive, chemical, electronic, energy,

shipbuilding, medicine, printing, paper, and decorative. A brief list of these applications include coatings used for [49, 51, 70]:

1. Dimensional restoration and repair
2. Corrosion resistance
3. Wear prevention
4. Oxidation resistance
5. Thermal insulation and control
6. Abrasive activity
7. Abradable seals
8. Biomedical compatibility
9. Lubricity and low friction surface.

It is important to note that Inconel-625 powder is used extensively in the (oil/gas) repair industry due to its excellent corrosion resistance. This material has both Chromium and Nickel that enhance the property of corrosion resistance and can be easily made using gas atomised process as indicated previously. Also, it has outstanding characteristics in terms of lower porosity and reduced oxide content [71]. However, as the application of this material is influenced by the substrate type and behaviour, it needs to be thoroughly examined and evaluated in aggressive environments and over different metallic substrates.

The specific application considered in this work is the repair of sea water pump shafts for dimensional restoration, wear and corrosion protection using HVOF Inconel-625 thermally sprayed coating.

2.6 REVIEW OF PREVIOUS STUDIES WITH FOCUS ON HVOF THERMALLY SPRAYED INCONEL-625 COATINGS TESTING

The following section gives a brief review of the previous testing investigations carried out in the field of HVOF thermally sprayed Inconel-625 coatings including bending (flexural), fatigue, erosion-corrosion, tensile as well as residual stresses determination.

2.6.1 Bending Test

The work that has been carried out on the three-point bending test of HVOF thermally sprayed Ni-based coatings is very limited [72-74]. Yilbas et al. [72] investigated the effect of laser treatment on HVOF sprayed Inconel-625 coatings when subjected to a three-point bending test. The results indicated that the elastic limit of the coating reduced after the laser treatment. Also, the origin of crack sites was in the coating/substrate interface. During the four-point bending test, the stress profile of coating showed similar behaviour for the same powder sprayed using two different coating systems, namely HVOF and Plasma [73]. It was also observed that the four-point bending stress profile for the coated sample was similar to the tensile test profile. The four-point bending test was utilised by Hjornhede et al. [74] to compare the adhesion strength of HVOF, arc spray and laser cladding applied over (Fe1Cr0.5Mo) base material. Coating delamination occurred due to the initial formation of transverse cracks in the coating post bending.

2.6.2 Fatigue Test

One important application of HVOF coatings is their use in dynamic components in oil and gas industrial equipment [75]. These coatings are widely used to restore worn or undersized high strength steel parts and components that were once

previously repaired using the conventional arc welding technique, hence the microstructure of the substrate has changed [76]. In service, these components are generally subjected to severe cyclic loading in an aggressive environment [77]. Consequently, investigations into corrosion and fatigue properties of HVOF coating over plain or welded surfaces are now of the utmost importance [78]. Considerable research studies have been carried out to investigate various affecting parameters on the fatigue properties of HVOF coated surfaces [79]. However, the study of HVOF coating over welded surfaces has to date been very limited [80-97].

The evaluation of the fatigue strength of a material is strongly affected by substrate type and sprayed coating [80]. However, the fatigue strength of a coated specimen was not as greatly affected as that of a non-coated specimen when both were evaluated under the same testing conditions in highly corrosive environments [81, 82]. Previous work indicates that Nickel based alloy coatings such as NiCrMoAlFe and Colomonoy 88 shown good resistance to fatigue when tested in various corrosive mediums [16]; however, varying the spraying system parameters, adjusted these resulting fatigue properties [83, 84].

The HVOF coating process produces significantly less pit formations when compared to other techniques such as Atmospheric Plasma Spraying (APS) and High Frequency Pulse Detonation (HFPD), hence the process produces coatings with high fatigue strengths [85, 86]. Proper control of the coating thickness significantly enhances the coating fatigue strength properties and it is possible to combat interfacial delamination by selecting an appropriate coating thickness [87]. This may be related to the variation of residual stresses with the coating thickness [88]. The fatigue behaviour of thinner coatings (200 μm) has been found to be better than thicker ones (450 μm), as the possibility of crack initiation within thicker coatings is higher, as well as the fact that compressive residual stresses are higher in thicker coatings [89, 62].

Although surface preparation enhances the coating-substrate bond, the fatigue strength of substrate may decrease due to blasting [90]. During the grit blasting process, particles that are retained in the substrate act as stress concentrators and enhance the nucleation of fatigue cracks and give a rise to a decrease in the fatigue strength of the blasted material [91-94]. Various studies have indicated that there is a relationship between compressive residual stress on both the coating bonding and its fatigue strength [95-96]. In general, fatigue failure can mostly be attributed to micro and macro-cracking of either the coating material or the coating substrate interface, which is also a result of the attenuation of compressive residual stresses that arise during the quenching process during deposition [97].

2.6.3 Erosion-Corrosion Test

One of the most prominent concerns in the oil and gas production industry is the behaviour of materials in an aggressive corrosive environment with the presence of suspended sand particles which contribute to corrosion, erosion and overall wear of the surface. Surface metal loss of internal components in rotating and stationary equipment can be attributed to pure electrochemical corrosion, pure mechanical erosion and the synergistic interaction of the two [98]. This effect plays a major role in equipment reliability and maintenance costs, especially if the equipment operates in off-shore industries where the internal components are exposed to corrosive environments. The erosion-corrosion, wear and thermal resistance of metallic alloys used in a wide range of such equipment have been shown to be improved in an effective and economical way by means of High Velocity Oxy-Fuel (HVOF) coatings [99, 100].

The rapid development of the HVOF coating process has increased the demand for various types of coating materials including Inconel-625. This material has outstanding properties which make it superior when applied as a HVOF coating in order to prevent corrosion [101-103]. However, the coating material can significantly deteriorate when subjected to the impact of dry or solid erodent

particles where the erodent particle size and the degree of fluid impingement are the principal affecting parameters [104, 105]. Other parameters, such as the influence of time, solid loading, impingement angle, temperature and particle size and velocity, as well as the erosion-corrosion mechanism, must also be taken into consideration [106, 107].

When comparing the influence of dry and slurry erosion on HVOF coatings, it was shown that erosion rates in dry particles impact were about three orders of magnitude higher than those in slurry systems [108]. This difference probably reflects the real erodent target impact velocities which are mitigated in the slurry test by the water medium [109]. Various studies on the erosion-corrosion of HVOF sprayed Ni-based coatings indicated that material loss rates, considered to be low during solid-free impingement, increased significantly when solid particles were added [110]. However, most of these tests were carried out on single substrate type and only a limited number of tests considered the combination of HVOF erosion-corrosion of coatings applied over different substrates [111]. Moreover, the testing of coatings applied over welded surfaces has not yet been fully understood. In order to select appropriate coating materials for fluid machinery, both coating erosion-corrosion behaviour and the substrate material response needs to be clarified.

2.6.4 Tensile Bonding Test

Bond strength is considered to be one of the most influential properties of HVOF coatings. This is because it represents a measure of the HVOF coating's ability to adhere to the substrate. Practical experience as well as theoretical analysis performed on different HVOF systems and materials have shown that there are several factors which influence coating-substrate bonding. These factors include heat treatment and surface preparation prior to deposition, the properties of the powders used for spraying, the contact temperature between the particles of the coating and substrate, and the physical properties of the specimen material and

coatings. Reports indicate that the fuel/oxygen ratio and spray distance have the most significant effect on coating-substrate bonding [112, 113]. When optimising these parameters for the deposition of NiCrBSi thermally sprayed powder using the HVOF process, a bond strength of 41-52 MPa was achieved [114].

Further investigations indicated that the tensile bonding strength of Ni-Cr coatings decreases when the coatings were subjected to very high temperatures, such as using coatings in boiler components. For instance, when 80Ni-20Cr was tested at 750°C using the adhesion test as per ASTM C 633, the tensile bond strength decreased from 68 MPa to 56 MPa [115]. Moreover, the bonding strength of NiCrBSi increased as the substrate surface roughness increased, where maximum bonding was achieved when a surface roughness of Ra 5.8μm was used [116]. It was also shown that adding WC-Co to NiCrBSi during spraying changes the adhesion mechanism from mechanical interlocking only to chemical bonding and mechanical interlocking [117, 118]. Li et. al. [119] found that when a bond coat of about 50μm thickness was introduced between the coating (NiCrBSi) and the substrate (mild steel), the adhesive strength of the coating increased from 40 MPa to 56 MPa. Moreover, when a WC-Co interlayer bond coat was applied to NiCrBSi-40wt%(WC-Co) composite coating, the bond strength then increased to 65 MPa.

The tensile bonding strength of HVOF sprayed Ni-based coatings can be significantly affected by the state of the deposited particles, where significant melting of the sprayed particle did not contribute to an increase of bonding strength [120]. The deposition of partially melted large particles presented a dense microstructure and yielded strengths of more than 76 MPa [121]. However, Wang et al. [122] states that spray particle temperature, velocity and momentum do not correlate directly with bond strength. As coating corrosion resistance affects bonding, HVOF sprayed Ni-based coatings showed better corrosion resistance than stainless steel coatings when both were tested under highly corrosive environments [123].

It is important to note that the tensile test for coating to substrate adhesion is often used as a determination of the point of failure of coatings. However, for most coating materials, including Inconel-625 powders, several factors can affect the methodology of the tensile test and the resultant behaviour of the coating. Firstly, in practical applications, the coating does not experience a pure tensile stress. There are in fact several stresses, including shear, bending, tensile and compressive, all acting on the deposit. Secondly, during the ASTM tensile test, the coating/adhesive interface or interior coating material often fails, instead of the coating/substrate interface [124].

2.6.5 Residual Stress

There are mainly two mechanisms of residual stress development in thermally sprayed coatings, quenching stress and cooling stress.

(1) Quenching Stress

According to Pawlowski [50], as many as 5 to 15 lamellae exist in a single pass of spray. As the lamellae solidify they contract, but are constrained by each other, and by the substrate, thus generating high tensile stresses in the individual lamellae as shown in Figure 15. Tensile quenching stress is unavoidable and may be estimated by the following [62]:

$$\sigma_{ij} = \alpha_c (T_m - T_s) E_c \qquad \textit{Equation 2}$$

Where σ_q is the quenching stress (Pa), E_c is the elastic modulus of the coating (Pa), α_c is the coefficient of thermal expansion of the coating (/°C), T_m is the melting temperature of individual lamella (°C), and T_s is the temperature of the substrate (°C).

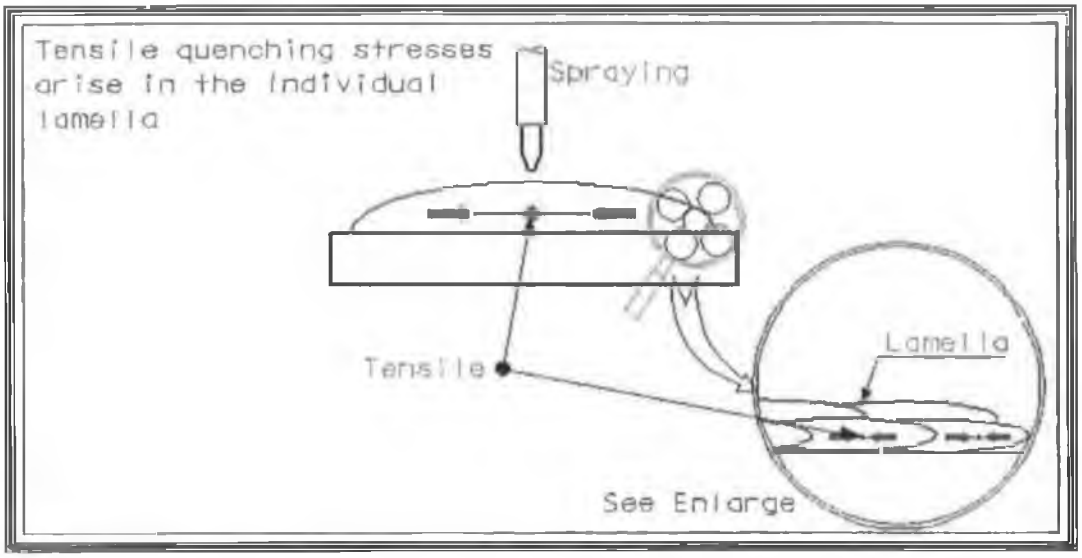

Figure 15 Schematic of quenching stresses in the individual lamellae, [62].

(2) Cooling Stress

When deposition is eased or interrupted, cooling stresses generate, mainly due to the thermal expansion co-efficient mismatch between the substrate and the coating material. If the coating contracts to a greater extent than the substrate ($\alpha_c > \alpha_s$), a tensile stress is generated in the coating [62]. This may lead to adhesion loss and cracking of the coating. If the coefficients are equal, then no cooling stress will develop. If the coating contracts by a smaller amount than the substrate ($\alpha_c < \alpha_s$), the resulting cooling stress will be compressive as shown in Figure 16 [62]. The cooling stress can be estimated using the following equation [62, 64, 124]:

$$\sigma_c = \left[\frac{E_c (T_f - T_R)(\alpha_c - \alpha_s)}{1 + 2\frac{E_c T_c}{E_s T_s}} \right] \qquad \textit{Equation 3}$$

Where σ_c is the cooling stress (Pa), E_c is the Young's modulus of the coating (Pa), E_s is the Young's modulus of the substrate (Pa), α_c is the coefficient of thermal expansion of the coating (/°C), α_s is the coefficient of thermal expansion of the substrate (/°C), T_c is the temperature of the coating (°C), T_s is the temperature of the substrate (°C), T_f is the deposition temperature (°C), and T_R is the room temperature (°C). However, this equation does not take into account; conduction and the temperature gradient across the sample.

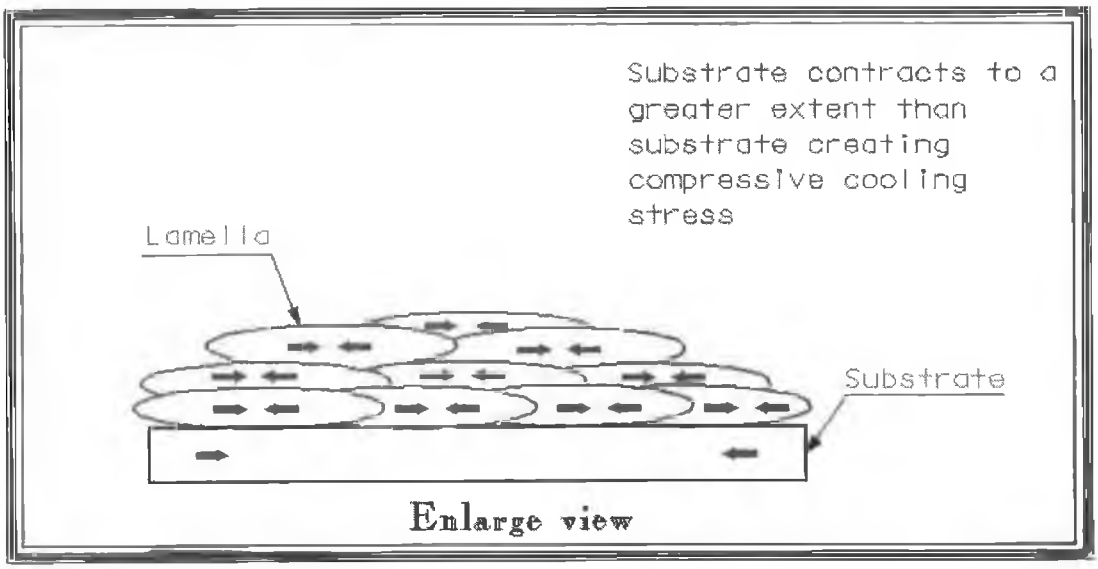

Figure 16 Schematic of cooling stresses, [62].

2.7 SPRAY PROCESS MODELLING

Considerable research studies have been carried out on the development of models capable of predicting what happens at various stages during and after the thermal spraying process. Previous research carried out in the MPRC (Materials Processing Research Centre) included simulation of heat transfer though a thermally sprayed sample, analysis of residual stresses due to deflection loading using the ANSYS Finite Element Analysis (FEA) Package [62]. Other work has considered the simulation of multi powder/gas flow through a multi powder HVOF (High Velocity Oxy-Fuel) feed device using the FLOTRAN CFD (Computational Fluid Dynamics) [69].

Simulation results obtained from the FEA demonstrate the capability for residual stresses prediction in thermally sprayed layer composite and stresses that arises during the production processes of coated work pieces such as engine liners [125]. Ghafouri et al. [126] use FEA for the prediction of residual stresses at the coating/substrate interface and upon variation in coating thickness. Results showed that high stresses were present at the coating/substrate interface and stresses increased with an increase in coating thickness and temperature.

FEA can be used effectively to explain the behaviour of coating during the deposition process based on the variation of some influencing factors including coating thickness, coating modulus. Moreover, residual stresses have been shown to be influenced by the deposit fracture toughness [127].

It is important to note that all previous works involved the simulation of HVOF coating applied on one substrate type. However, the present work includes the simulation and modelling of HVOF coating applied on different substrate material types. This work also includes the analysis of residual stresses during the deposition process for thermally sprayed sample applied over different substrate materials.

3

EXPERIMENTAL EQUIPMENT AND PROCEDURES

3.1 INTRODUCTION

The present study investigates the bending, fatigue, erosion-corrosion, and tensile characteristics of HVOF thermally sprayed Inconel-625 coating material which in some cases were subjected to aqueous static corrosion. Investigations of each test were carried out when the coating material was applied over three different metallic surfaces: (a) plain stainless steel (SS), (b) spot-welded stainless steel (SW-SS), and (c) a composite surface of stainless steel and carbon steel welded together (C-SS-CS).

In this chapter, the HVOF thermal spray facility used to deposit the Inconel-625 coating is described followed by a description of the powder morphology, size and characteristics used in this research. Information is provided on the fabrication of the workpiece fabrication, surface preparation, and welding procedure undertaken. This is followed by a full description of the coating process and characterisation techniques used to analyse the coated specimen. The experimental procedures of each mechanical test is described according to their associated standard. The chapter concludes with a description of the residual stresses calculation procedure and the finite element method used in this work.

3.2 HVOF THERMAL SPRAYING SYSTEM

A Sulzer Metco Manual Hybrid Diamond Jet (using propylene fuel gas) with gas supply unit, DJ9H - Hand held gun body, 9MP-DJ powder feed rate control, and DJFW flow meter were used to produce the Inconel-625 coating (Figure 17). The air, fuel and oxygen were maintained at pressures 7.2, 6.2 and 10.3 Bar, respectively. The work specimen was maintained at 475°C (by the flame of the gun) and rotated at 250 rev/min using a Dean Smith B-5 lathe machine. The combustion process took place within the gun. This has a prominent influence on the coating integrity, hence more details about the DJ9H gun are discussed in the next section.

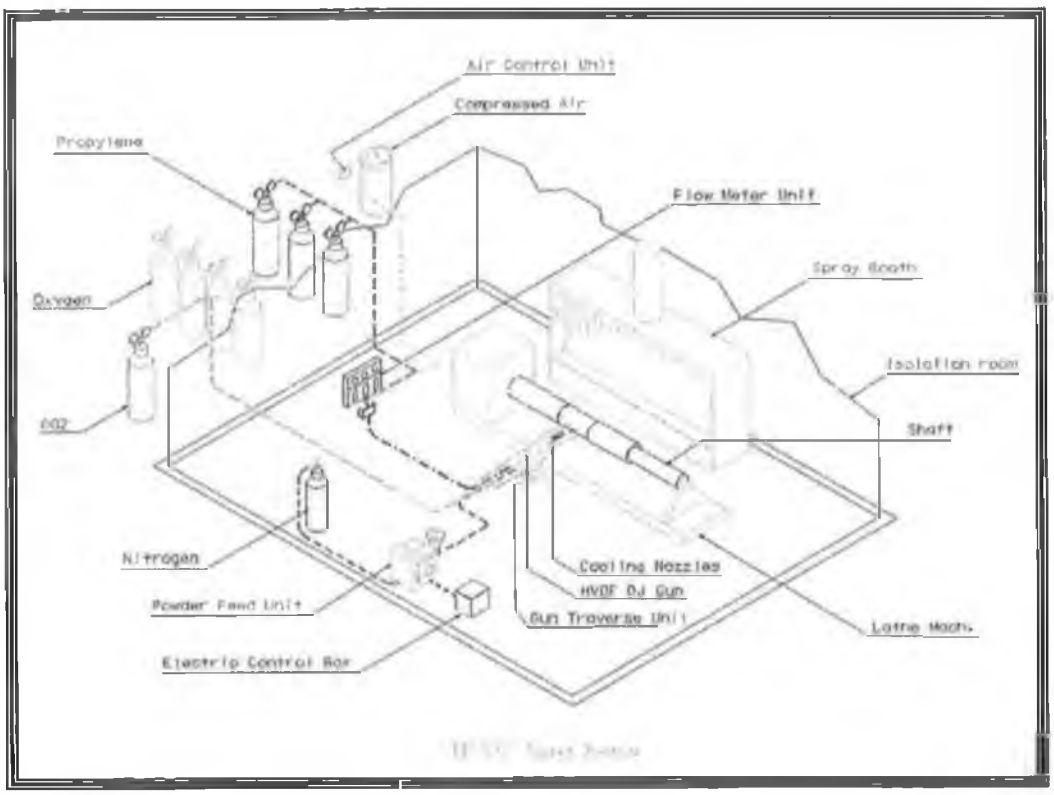

Figure 17 High velocity oxygen fuel system.

3.2.1 DJ9H Gun

The Sulzer Metco HVOF spraying process uses oxygen and fuel gas to produce a high velocity gas stream in the gun nozzle. This gas stream, when ignited exits the gun, as a luminous white, supersonic flame containing diamond-shape shock waves hence the name "Diamond Jet", (Figure 18). The combination of high fuel gas and oxygen flow rates and high pressure leads to the generation of this supersonic flame. The gun can accommodate different fuel gases including acetylene (C_2H_2), ethylene (C_2H_4), hydrogen (H_2), propylene (C_3H_6), and propane (C_3H_8). Each gas provides different combustion temperatures. The latter was used in this research as this is the fuel used in repair applications and has the ideal combustion for the powder material used Inconel-625 [49]. The powder coating material is fed into the high energy gas stream where the expansion gas, forces the particles through a series of nozzles at supersonic velocities. The high kinetic energy of the powder produces well bonded coatings with high bond strength and low porosity [52]. It should be noted that HVOF systems from different manufactures produce quite different coating properties. Harvey et al. [128] described different HVOF systems and the important differences between them. Significant details making them quite different from each other are; powders feed position in the spraying gun, gas flow rates and choice of fuel gas. In some systems the powder is fed into the combustion zone, in other systems it is fed into the exhaust barrel. Feeding powder into the combustion chamber as used in this research, maximises the heat transfer between the flame and the powder particles. This increase in the heat transfer, in parallel with spray distance and powder feed rate, plays a major roll in controlling coating oxidation. Hybrid cooled spraying gun specifications are also available, where instead of air (as used in this research), cold water can be used to keep the gun cool around the outside of the nozzles to prevent deformation of the internal section of the gun (Figure 18).

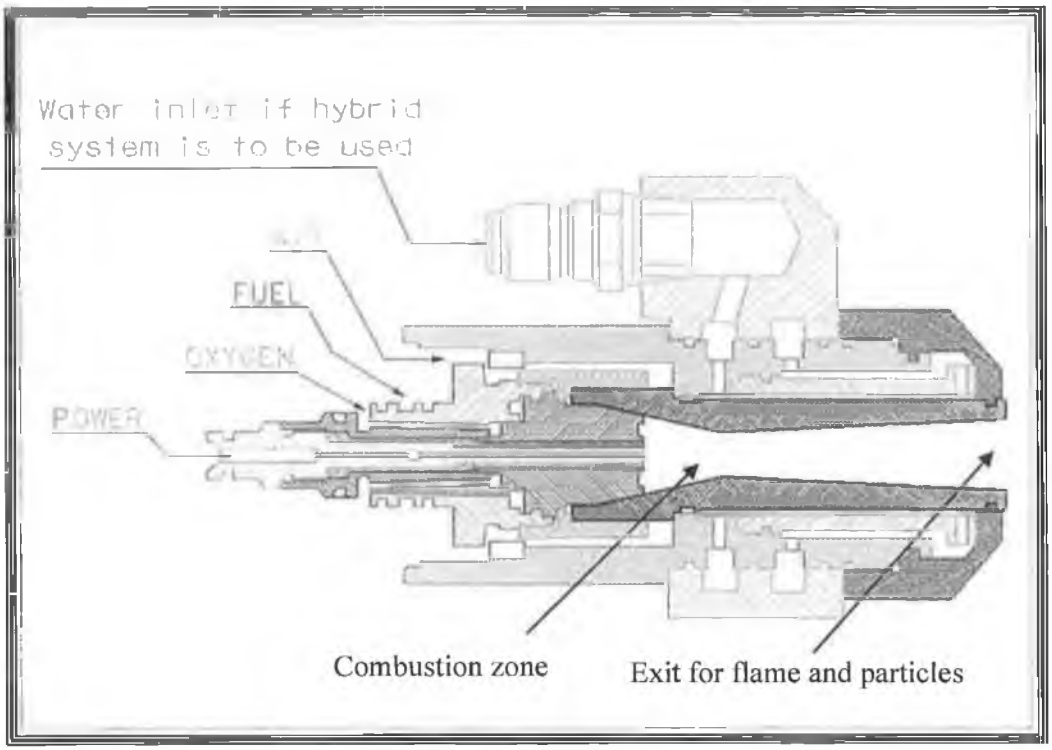

Figure 18 Schematic diagram of DJ9H HVOF spraying gun, [49].

3.3 POWDER MATERIAL

The powder under investigation was Inconel-625 powder (or known as Sulzer Metco Diamalloy 1005). Its commercial composition is presented in Table 7. Figure 19 show the morphology of the atomized powder. These particles had spherical shape and a size range of 40 ± 11 μm. The Inconel-625 powder is typically used as a coating in corrosive and erosive applications like seawater environments [16, 129].

Table 5 Chemical Composition of Diamalloy 1005 Powder [16].

Powder Material	**Chemical Composition %**				
	Ni	Cr	Mo	Fe	Co
Inconel-625	66.5	21.5	8.5	3	0.5

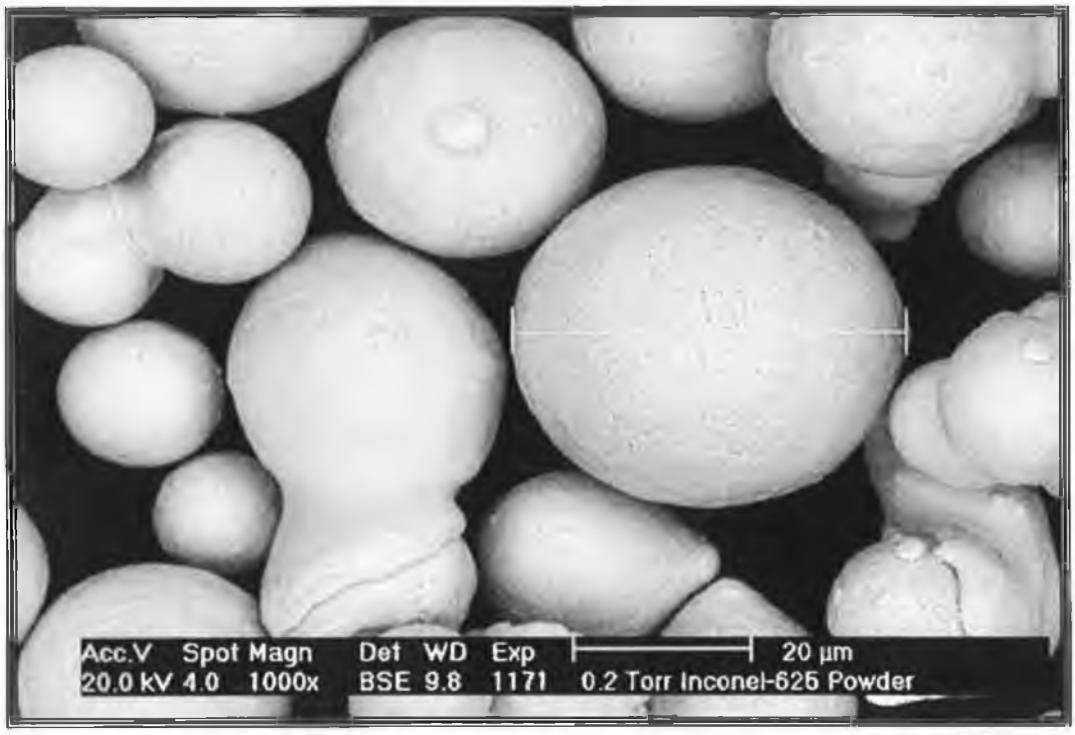

Figure 19 Scanning Electron Microscope view of the manufactured Inconel-625 powder.

3.4 EXPERIMENTAL MATRIX

To evaluate the effect of each substrate type and service medium, nine sets of test specimen were proposed. These sets of specimens selected represented a combination of three substrate types: (i) Plain stainless steel (SS), (ii) Spot-welded stainless steel (SW-SS), (iii) Composite surface of Stainless Steel and Carbon Steel welded together (C-SS-CS); in three environmental service mediums: (i) as coated, (ii) as coated and subjected to aqueous static corrosion for two weeks, (iii) as coated and subjected to aqueous static corrosion for four weeks. Twenty eight specified specimens of each set type were manufactured, where seven test samples were dedicated for each of the four main mechanical tests (Bending, Fatigue, Erosion-Corrosion, and Tensile), with the proviso that some of the specimens were kept as back up in the case of the need to repeat tests. Some of the testing standards required less than seven samples to analyse and obtain reliable data. For example, three samples of each case for the erosion-corrosion test and four samples for the tensile test were adequate for reliable analysis. Coating characterisation was then performed post mechanical testing on each test sample, (total of 252 samples were fabricated of which 189 were analysed) (Table 6).

Table 6, Shows the test matrix used in this research.

Powder	Substrate	Service Medium	Number of Samples			
			Bending	Fatigue	E-C*	Tensile
Inconel-625 (Diamalloy 1005)	Plain stainless steel (SS)	As coated	4	7	6	4
		As coated and subjected to aqueous static corrosion for two weeks	4	7	6	4
		As coated and subjected to aqueous static corrosion for four weeks	4	7	6	4
	Spot-welded stainless steel (SW-SS)	As-coated	4	7	6	4
		As coated and subjected to aqueous static corrosion for two weeks	4	7	6	4
		As coated and subjected to aqueous static corrosion for four weeks	4	7	6	4
	Composite surface of Stainless Steel and Carbon Steel welded together (C-SS-CS)	As coated	4	7	6	4
		As coated and subjected to aqueous static corrosion for two weeks	4	7	6	4
		As coated and subjected to aqueous static corrosion for four weeks	4	7	6	4

* E-C = Erosion-corrosion test

3.5 WORKPIECE

3.5.1 Substrate Samples

AISI 4140 carbon steel and AISI 316 stainless steel (150x40x4 mm^3) substrates were used. These can be considered the most common materials used in the oil and gas industries and are normally subjected to highly corrosive and erosive environments. Three different sample types were used: (a) plain stainless steel (SS), (b) spot welded stainless steel (SW-SS), and (c) composite surface of stainless steel and carbon steel welded together (C-SS-CS), (Figure 20).

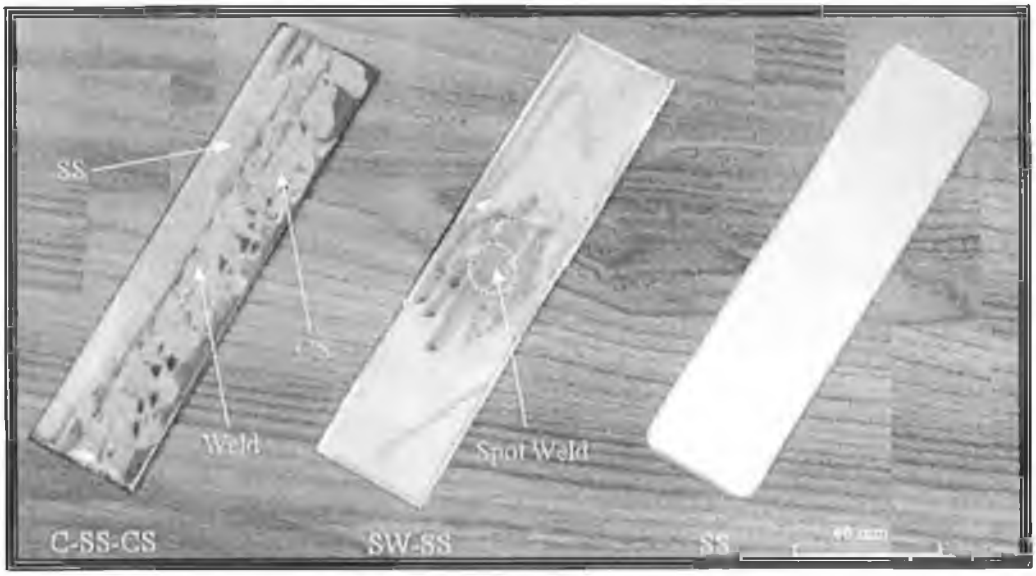

Figure 20 Photograph of the substrate types used in the test.

3.5.2 Welding Procedure

Samples fabricated were degreased in benzene and washed with de-ionized water prior to welding process. Samples were spot-welded using Gas Tungsten Arc Welding (GTAW) manual process. The GTAW process consisted of a power source, manual gas tungsten arc torch and filling wire as shown in Figure 21. The stainless steel 309L electrode used was 2.4 mm in diameter and can be applied on any austenitic stainless steel. During the welding process the arc was placed at a distance of 2 to 3 mm from the work piece. The weld spot was 3 mm in depth and 5 mm in width. Pure argon was used as shielding gas at flow rate of 7l/min. The specifications of the rod welding process used in this research are shown in Table 7.

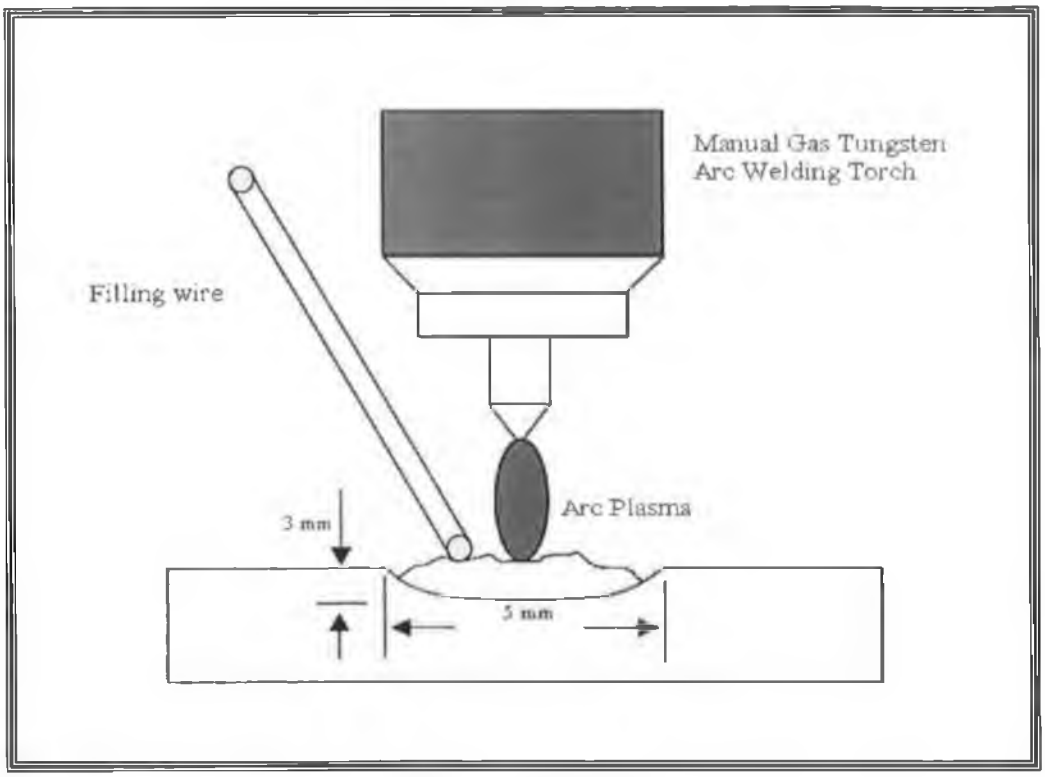

Figure 21 Schematic diagram of the GTAW welding process.

Table 7, Specification of the rod welding used in the experiment tests.

BASE METAL		FILLER METAL			HEAT TREATMENT		
Substrate Material Specification	Thickness Range	AWS No (Class)	Size	Max Deposit Thickness	Pre-Heat Temp.	Inter-pass Temp.	PWHT
Carbon Steel to Austenitic Stainless Steel	1.6-12 mm	SS309L	2.4 mm	12 mm	100°C	177°C	None

3.5.3 Surface Preparation

The samples were subsequently cleaned, preheated to 450°C in a furnace for three hours to takeout any contamination in the substrate and then grit blasted with Al_2O_3 particles 20 mesh (83 μm), manufactured by K. C. Abrasive Company with the following chemical composition Al_2O_3 (96-97%), TiO_2(2.75%), SiO_2(0.61%), Fe_2O_3 (0.54%), [16]. Blasting was conducted at a pressure of 550 kPa, (80 Psi) and at a distance of 38 cm, (15 inches) normal to the surface of the specimen, (Figure 22). The surface roughness of the substrate ranged from 5 to 6 (Ra, μm).

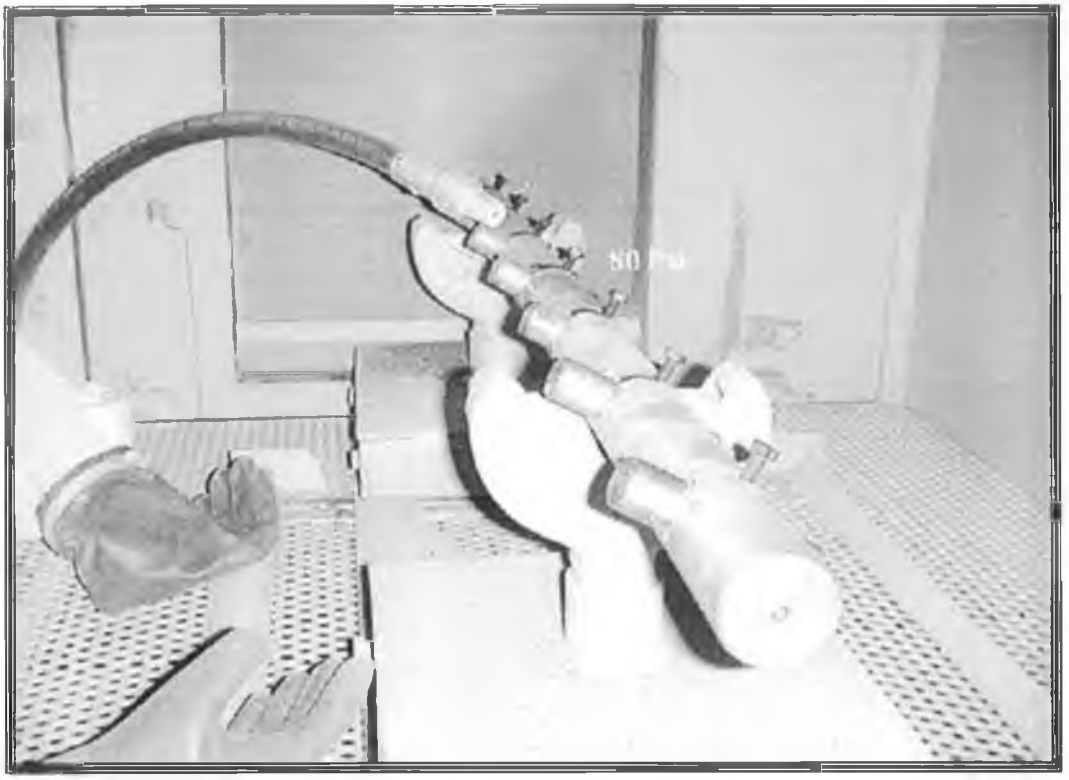

Figure 22 Photograph of grit blasting chamber.

3.5.4 Spraying

The spraying parameters used to produce the HVOF coatings used in this work are given in Table 8. Firstly, special samples holder were fabricated to allow the spraying of 24 samples all at once, (Figure 23). Later, it appeared that this holder was unable to maintain a spraying angle of 90° on each sample as the assembly rotated which is recommended to avoid splats overlapping that result in increased coating porosity and thereby decreasing coating bonding (Figure 24), [49]. Hence, another holder was fabricated to maintain 90° spraying angle for each samples (Figure 25 (a)) which also resembles the real life application of repairing shafts (Figure 25 (b)). The coating thickness was fixed at 400 ± 10 μm, whatever the working conditions, (Figure 26).

Table 8 Process parameters of HVOF thermal spray.

Spray Parameters	Oxygen Pressure (kPa)	Fuel pressure (kPa)	Air pressure (kPa)	Powder feed rate (m^3/h)	Spray rate (kg/h)	Spray distance (m)
Value	1034	620	724	0.81	6.35	0.28

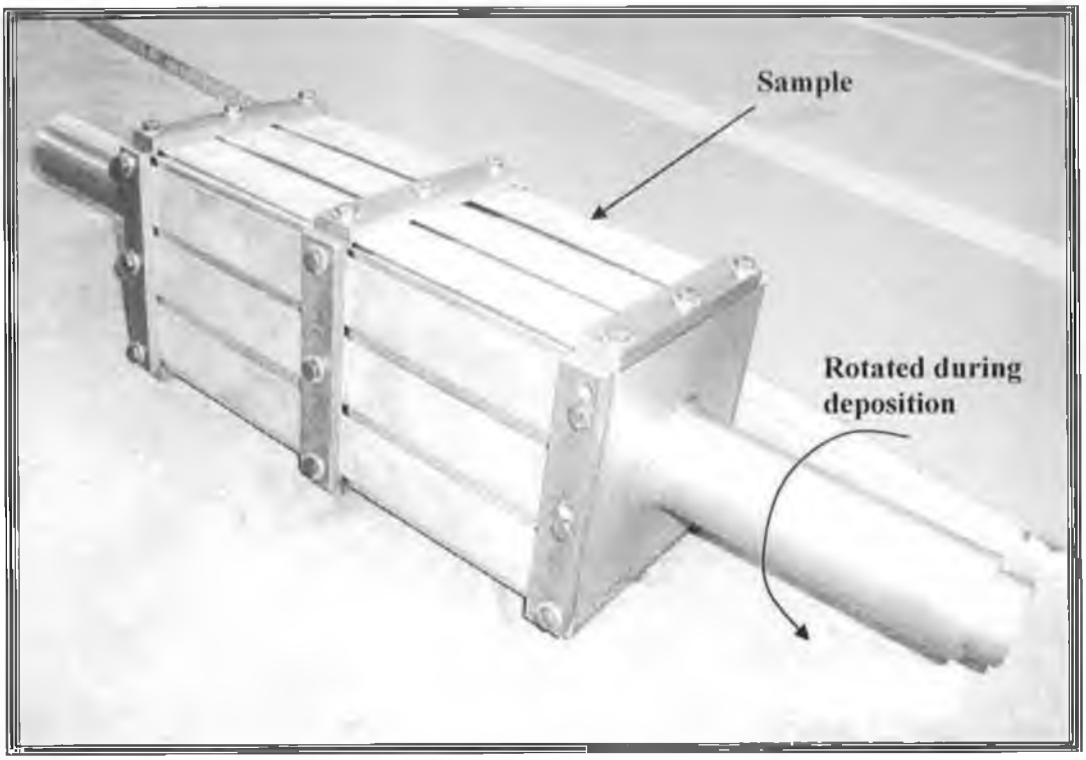

Figure 23 Photograph of the first test samples holder.

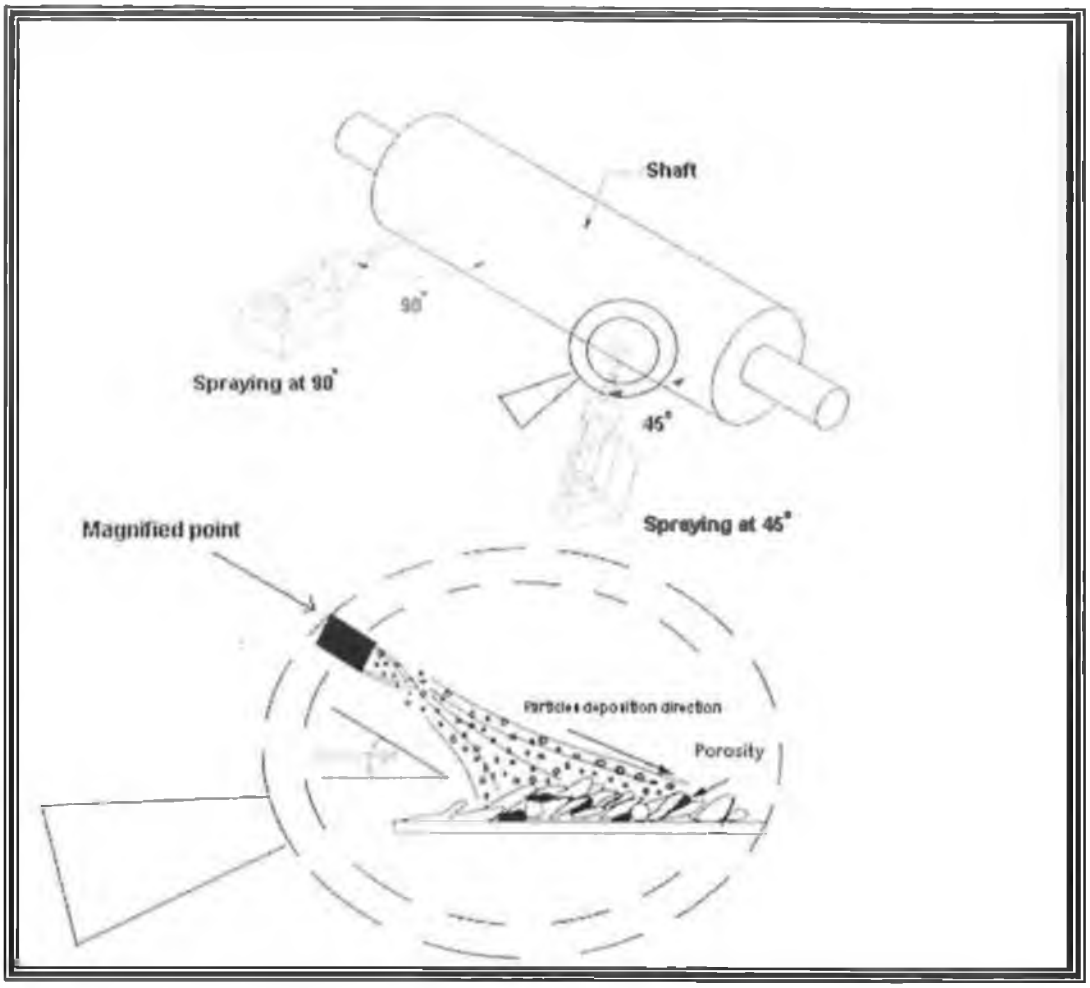

Figure 24 Schematic diagram showing the effect of spraying angle.

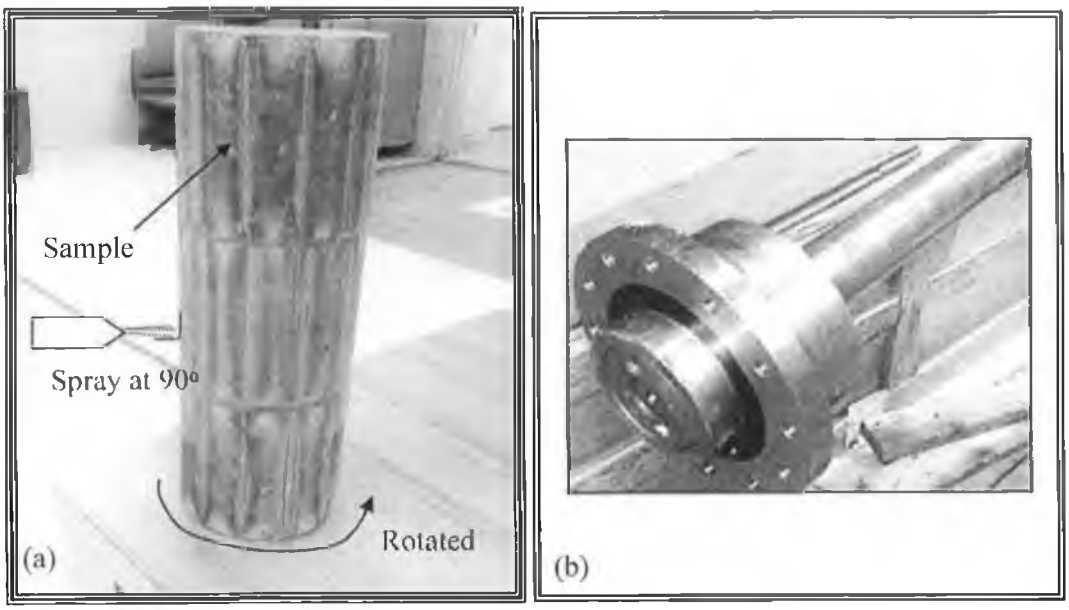

Figure 25 Photograph of the modified test samples holder, for spraying angles of 90 (a) and shaft requiring repair (b).

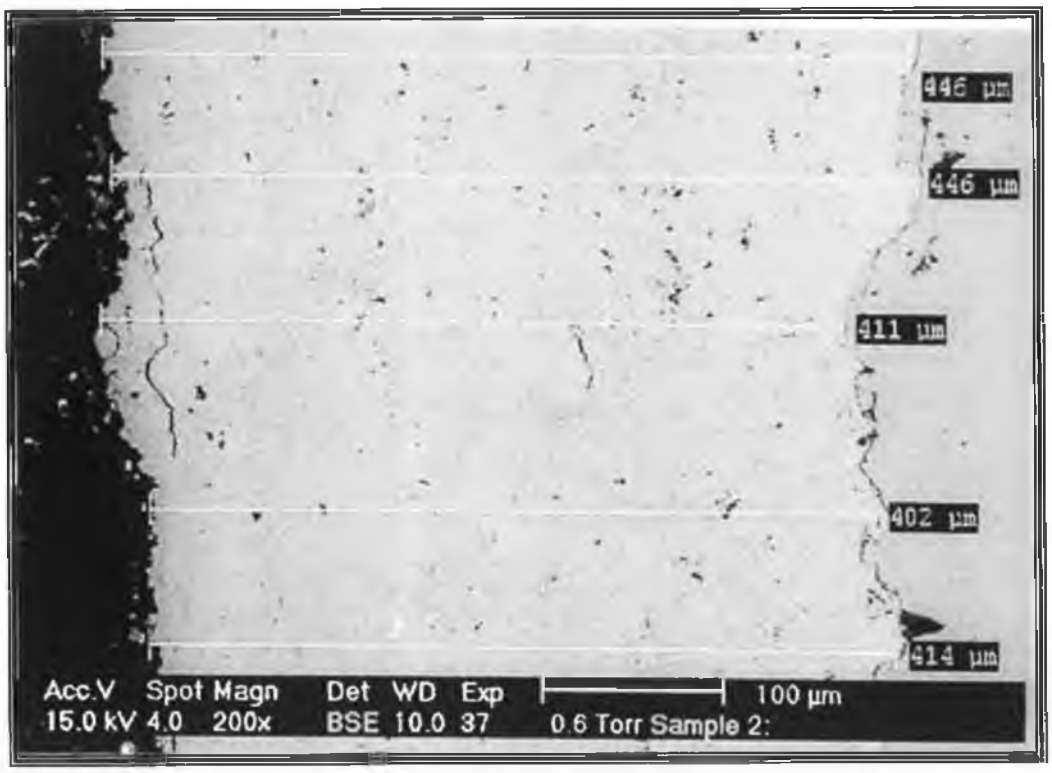

Figure 26 SEM image showing the coating thickness.

3.6 COATING CHARACTERISATION TECHNIQUES

Coating characterization is a critical step in the assessment of thermal spray coating quality. It is important to note that the preparation of the test specimens prior to characterisation has a prominent influence of the coating microscopy. Different grinding or polishing techniques can result in a completely different coating microstructures [130]. The following sections will explain the metallographic preparation process used, and the microscopic analysis techniques such as; Optical, SEM and EDS used to characterise the deposit.

3.6.1 Metallographic Preparation

Metallography is the technique taking image for topographical or microstructural features on prepared surfaces of materials [131]. The properties and performance of coating materials may be controlled by studying the microstructures using metallography. Metallographic specimen preparation is an important tool for the characterisation of thermally sprayed coatings in terms of revealing the coating/substrate interface, coating layer morphology, and location. The metallographical process can be divided into four different stage; sectioning, mounting, grinding and polishing.

(1) Sectioning

Sectioning is a necessary step before the mounting to reduce the size of test samples or to explore its hidden cross-section. The test samples were sectioned using an ISOMET low speed diamond cutting saw manufactured by BEUHLER. An Oil-base lubricant was used as the cooling medium. A low speed cutting saw was used to minimise stresses and distortion of the sectioned surface, which can often be introduced by cutting processes.

(2) Mounting

There are two basic techniques of mounting; cold and hot. Cold mounting requires very simple equipment consisting of a cylindrical ring which serves as a mould and a flat piece of glass which serves as the base of the mould. The sample is placed on the glass within the cylinder and the mixture poured in and allowed to set Cold mounting takes about 40 minutes to complete. However, hot mounting uses both heat and pressure to thermoset resin. This method, in some cases, is not preferred particularly if the sample has a loose layer on its surface. However, in the thermal spray deposits case the coating has adequate adherence to its substrate, hence it is not effected by the hot mounting. In hot-mounting the sample is surrounded by an organic polymeric powder (thermoset resin) which melts under the influence of heat (up to 200°C). Pressure is also applied by a piston, ensuring a high quality mould free of porosity and with intimate contact between the sample and the polymer. Therefore, in the current research, the hot mounting process SIMPLIMET 2000 made by BUEHLER was used to mount different types of coatings and powder samples.

(3) Grinding

The prepared mount (sample contained in a thermoset mould) was then subjected to a series of grinding steps, with the aim of producing a surface which would reveal its microstructure characteristics. The BUEHLER MOTOPOL unit was used to grind samples, automatically. Automation of grinding and polishing stage was essential as it eliminates operational error such as applied load and rotation per minute [64]. The grinding was divided into two stages; plane grinding and fine grinding.

(a) Planar Grinding

The purpose of using plane grinding was to remove the damage due to the sectioning stages and to produce a flat plane for subsequent grinding. A P60 grit (very coarse) Silicon Carbide paper was initially used to remove all damage without creating new defects in the coating. This paper lasted a duration of around 60sec, after which the abrading particles were washed away. Planar grinding was performed in a contact pressure of 100 to 150 kPa and using water as a lubricant for 60sec.

(b) Intermediate Grinding

The intermediate grinding step was concerned with the removing the damage caused by the planar grinding. Silicon carbide paper was used to fine grind the samples, but this procedure went from a coarse P200 grit up to fine paper P1200 grit. Each abrasive size can be used for five minutes in turn, starting from P200 grit and finishing with P1200 grit. In the current work, only the P240 and P600 grit papers were used to fine grind the different coating samples. As this found to adequately reveal the characteristics received from this research. Each paper was used for duration of 4 minutes. Intermediate grinding was performed at a contact pressure of 100 to 150 kPa and using water as a lubricant.

(4) Polishing

The objective of the polishing stage was to remove the abrasion-damage layer that may appear as scratches or as slip/twin/shear damage beneath the surface caused by the intermediate grinding stage. Optical microscopy requires that a specimen must be both flat and highly reflective [132]. There were two steps involved in the polishing procedure; diamond polishing and fine oxide particle polishing. Diamond abrasives are very effective during the polishing stage and considered as an adequate tool to prepare a coating for general microscopic examination. The most common diamond particle sizes are 6, 3 and 1 micron. Normally each abrasive size can be used for 5 minutes in turn, starting from 6 micron finishing by 1 micron [64]. In the current research, Aluminium oxide polish with 0.05 micron of particle

size was used for a duration of 3 minutes to prepare the coated specimens. Polishing was performed at a contact pressure of 100 to 150 kPa and using water as a lubricant.

3.6.2 Microscopic Analysis Techniques

(1) Scanning Electron Microscope (SEM)

Scanning electron microscopy (SEM) is a method for high-resolution imaging of surfaces. The SEM uses electrons to form image, much as a light microscope uses visible light to reflect an image. The advantages of SEM over optical microscopy include greater magnification (up to 300,000X) and much greater depth of field producing high image resolution [133]. An incident electron beam is raster-scanned across the sample's surface, and the resulting electrons emitted from the sample are collected to form an image of the surface trough a cathode tube. The image is typically obtained using secondary electrons to get the best resolution of fine surface topographical features. Alternatively, imaging with backscattered electrons gives contrasts based on atomic number to resolve microscopic composition variations, as well as, topographical information [133]. Qualitative and quantitative chemical analysis information can also be obtained using an energy dispersive x-ray spectrometer, a devise attached to the SEM, will be explained in the next section. The scanning electron microscope used in the current study, was a Philips XL-30 SEM equipped with Energy Dispersive Spectrometer (EDS), Model DX-4 by EDAX, (Figure 27). Polished/as sprayed samples were placed in the SEM vacuum chamber, and analysed to reveal coating characteristics such as; voids, non-melted particles, coating thickness, and oxides inclusions.

Figure 27 Photograph of the ESEM (Philips XL-30).

(2) Energy Dispersive X-Ray Spectroscopy (EDS)

Energy dispersive x-ray spectroscopy (EDS) is defined as an analytical method used in the determination of elemental chemical composition, and normally performed in conjunction with a scanning electron microscope (SEM) [134]. The technique utilises x-rays that are emitted from the sample during the bombardment by the electron beam to characterise the elemental composition of the analysed material. Features as small as about 1μm can be analysed [134]. When the test sample is bombarded by the electron beam, electrons are ejected from the atoms along the sample's surface. A resulting electron vacancy is filled by an electron from a higher shell, and an x-ray is emitted from the sample to balance the energy difference between the two electrons. The EDS x-ray detector measures the number of emitted x-rays versus their energy. The energy of the x-ray is characteristic of the element from which the x-ray was emitted.

A spectrum of the energy versus relative counts of the detected x-rays can be obtained and evaluated for qualitative and quantitative determinations of the elements present in the sampled volume [135]. It is important to note that EDS analysis of light elements such as oxygen is at best semi-quantitative and the relative accuracy depend on the amount present in the sample. For examples, the errors in the analysis for concentrations below 5 % can be as high as ± 50% [136,137].

In the current research a scanning electron microscope with an EDS X-ray instrument, provided by EDAX company was used to investigate elemental analysis of the HVOF thermally sprayed Inconel-625 coatings. The analysis was used to measure the amount of element contained in the steel samples such as; Oxygen, Aluminium, Silicon, Nickel, Chromium, and Molybdenum.

3.7 MECHANICAL TESTS PREPARATION

The mechanical tests carried out in this research include: bending, fatigue, jet impingement (erosion-corrosion), and tensile tests. These tests were prepared according to the international standards; ASTM D 790, ASTM E-739, ASTM G 73, and ASTM E8 for bending, fatigue, jet impingement, and tensile tests respectively. 70% of the tested samples were subjected to static corrosion test prior to subjecting these samples to each of the mentioned mechanical tests. The following sections will explain the preparation of each test in detail.

3.7.1 Static Corrosion Test

The static corrosion test were carried out in an aqueous environment simulating the sea water in the gulf region. The electrolytic solution used in the immersion tank was 0.1N H_2SO_4 + 0.05 NaCl. The specimens prior to testing were degreased in benzene and washed with de-ionized water. The immersion tank facilitated the circulation of the electrolytic solution and it had capacity of accommodating ten flat samples at a time. Consequently, specimens were hung into the immersion tank and checked with the conditions on a regular base. The specimens were left in the immersion tank for two and four weeks duration.

3.7.2 Bending (Flexural) Test

A bending test method was used to determine the flexural properties of the HVOF coated specimens and how these properties varied with specimen substrate type and atmospheric conditions. The bending test was carried out using the 3-point bending test according to the ASTM D 790 international standard [138]. Test samples of rectangular cross-section was placed on two supports and loaded by means of a loading nose midway between the supports, (Figure 28). The specimens were allowed to deflect up to maximum displacement of 20 mm for all

types of coated samples. The test was carried out using an INSTRON 300 instrument equipped with a deflection measuring device where the error in the load measuring system was ± 1 % of the maximum applied load. The loading nose had a cylindrical surface with a radii of 5mm (0.197 in), to avoid excessive indentation, or failure due to stress concentration directly under the loading nose. The test was carried out at room temperature 23 ± 2°C and 50 +/- 5% relative humidity. To ensure reliability a total of five samples for each test condition were tested. Figure 29 shows the shape and conditions of the sample after a typical 3-point bending test.

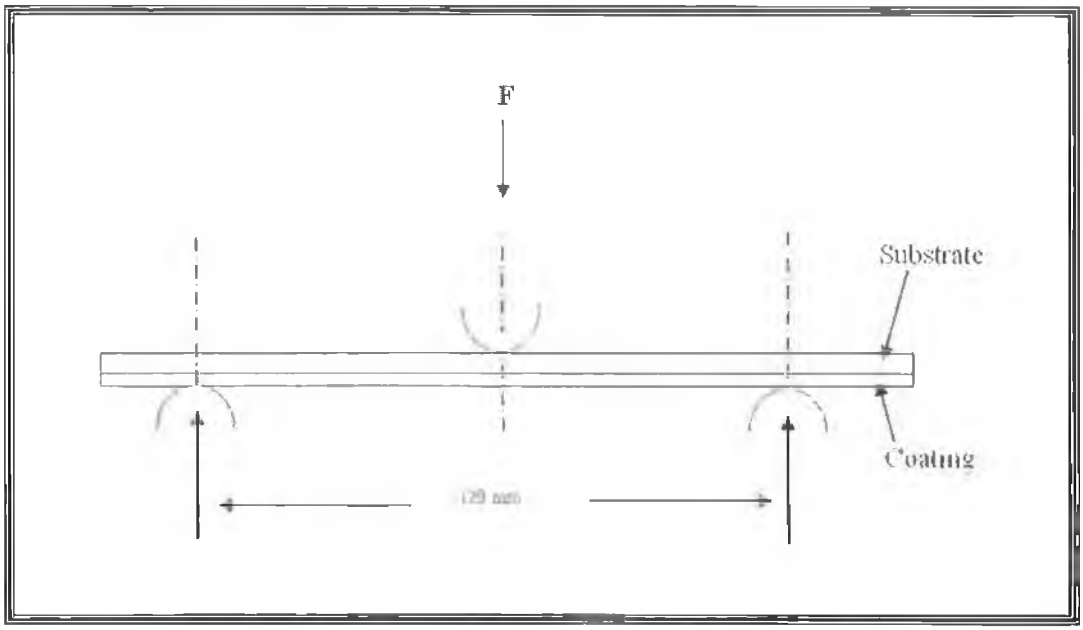

Figure 28 Schematic diagram of the 3-point bending test.

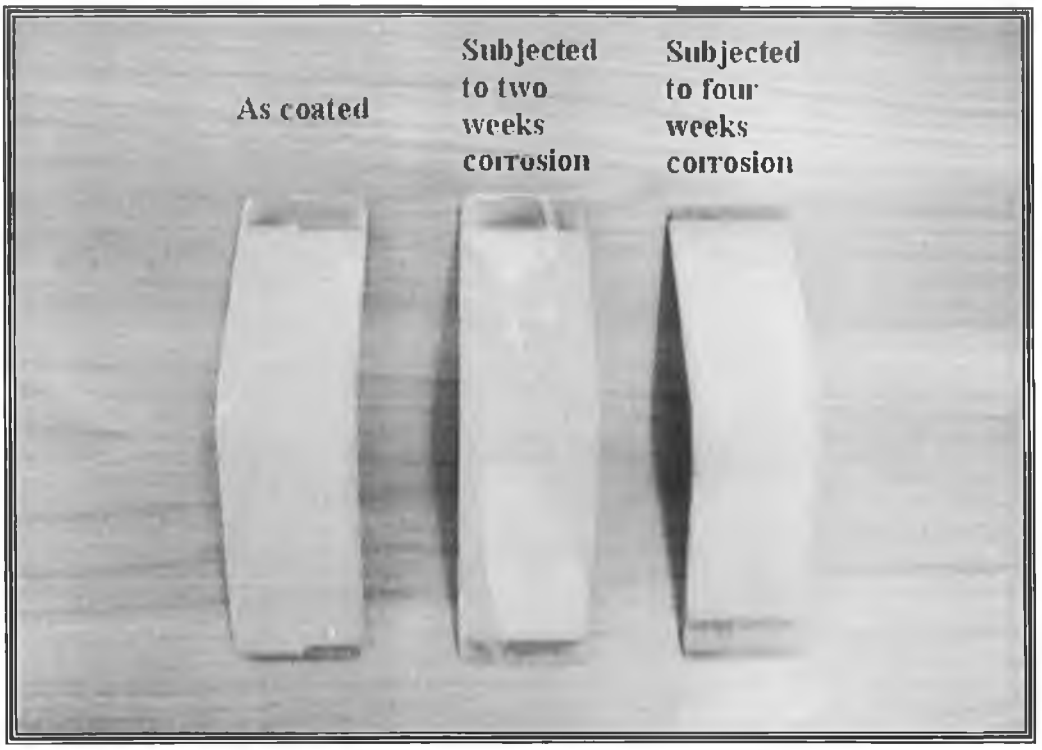

Figure 29 Photograph of the three types of samples used in the bending test.

3.7.3 Fatigue Test Preparation

An INSTRON 8501 material testing system was used to obtain the fatigue data as it had a capacity of ± 100 kN, (Figure 30). The displacement and percentage strain was set to ± 75 mm, ± 25% respectively. The fatigue tests were conducted using the Wave Maker FLAPS Software initially ramped to a mean load level and then a sinusoidal loading with a frequency of 20 Hz at a stress ratio of R ($R=\sigma min/\sigma max$)= 0.1 of the specified value of σm. The maximum cyclic stress ranged was set to approximately 70% to 90% of the tensile strength of the substrate material. All tests were carried out in air at room temperature 23 ± 2 °C and conducted according to the Statistical Analysis of linearized Stress-Life (S-N) Fatigue Data found in ASTM E-739-91 [139]. A total of 42 samples were employed for evaluating the corrosion-fatigue properties of the coated specimens, (21 plain stainless steel substrate and 21 spot welded stainless steel substrate,

which was within the range of specimens required in S-N testing for reliability data according to the ASTM E-739 standard (12-24) [139]. Three samples were tested at each stress level which ranged from (150 to 450 MPa), where each sample represent the test condition (as coated, as coated and subjected to corrosion for two weeks period and as coated and subjected to corrosion for four weeks period). The test samples geometry employed is shown in Figure 31.

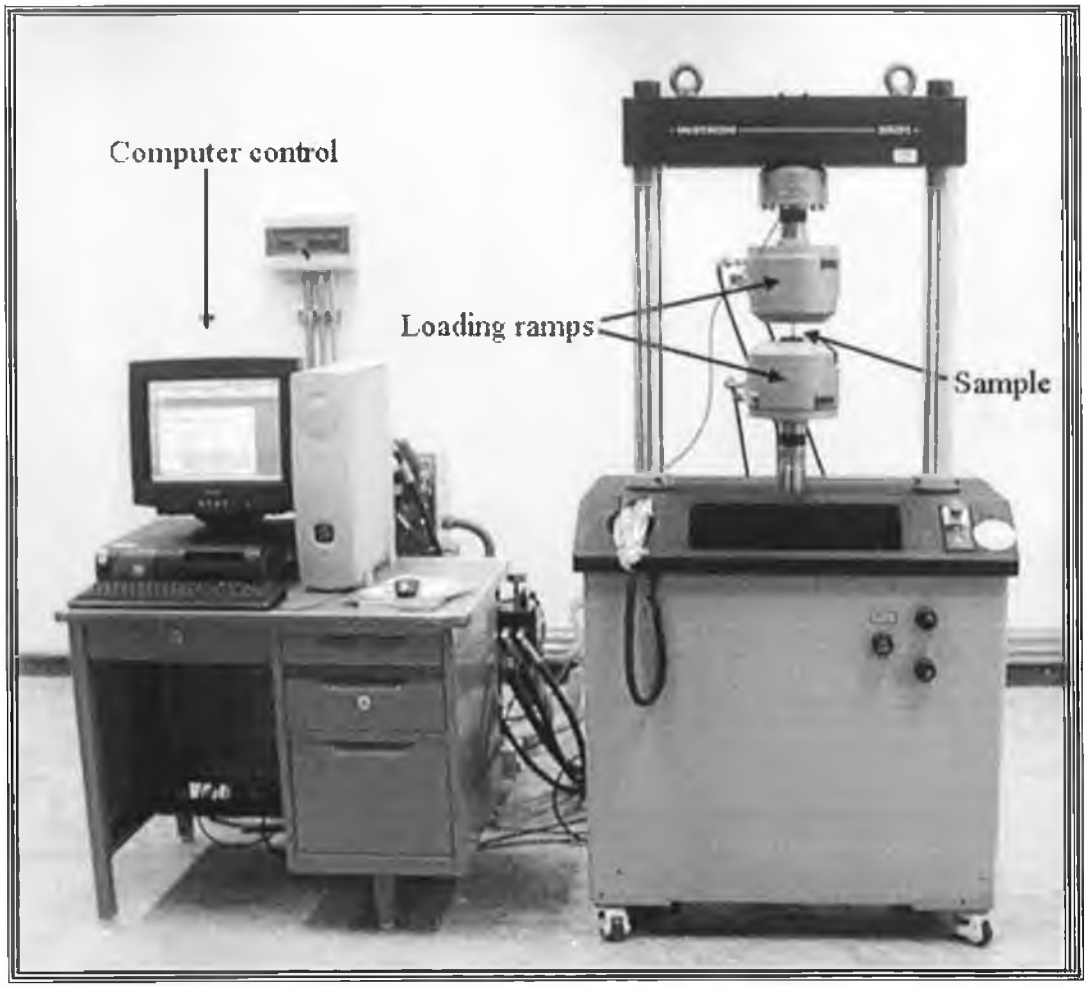

Figure 30 Photograph of the INSTRON 8501 fatigue/tensile testing machine.

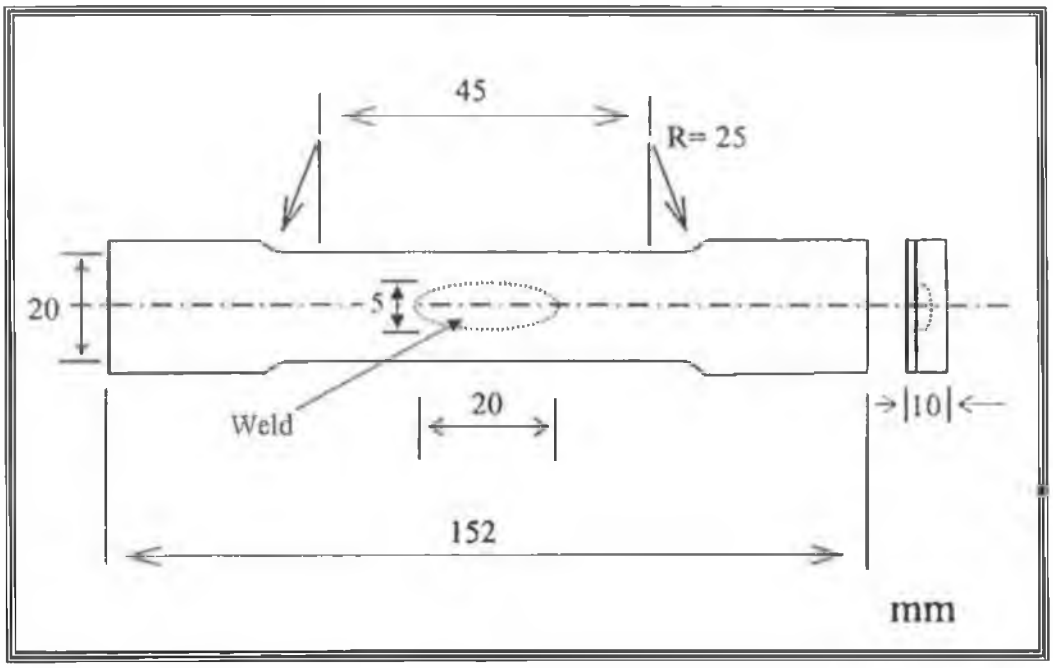

Figure 31 Geometry of the spot welded fatigue/tensile samples used in each test.

3.7.4 Jet Impingement (Erosion-Corrosion)

The erosion corrosion experiment was carried out using a jet impingement rig (Figure 32). This consisted of a flow loop through which natural seawater (pH 8.3) or sand slurry was circulated. The system was designed to test three samples at the same time. The jet angle was set at 90^{o} to the sample surface and the fluid impinged at a velocity of 40 m/s, at a water slurry temperature of 50^{o}C and a pressure of 14 Bar and 17 Bar after heating to simulate the erosion-corrosion effect on the coating at extreme summer temperatures. The specimens were rinsed in water, dried and weighed with a precision balance which had an accuracy of ± 0.1

mg. Special Teflon holders were fabricated to ensure the prevention of any eventual leakage. The methodology of the test was to consider two conditions: (i) different substrate types tested every 20 hours, up to 100 hours, (ii) different substrate types tested in 500 hour runs. Figure 33 shows the three forms of sample used in the jet-impingement test.

The test was performed according to ASTM G73 "Practice for Liquid Impingement Erosion Testing" [140]. To improve the chance of reliability, a total of six samples for each test condition were tested.

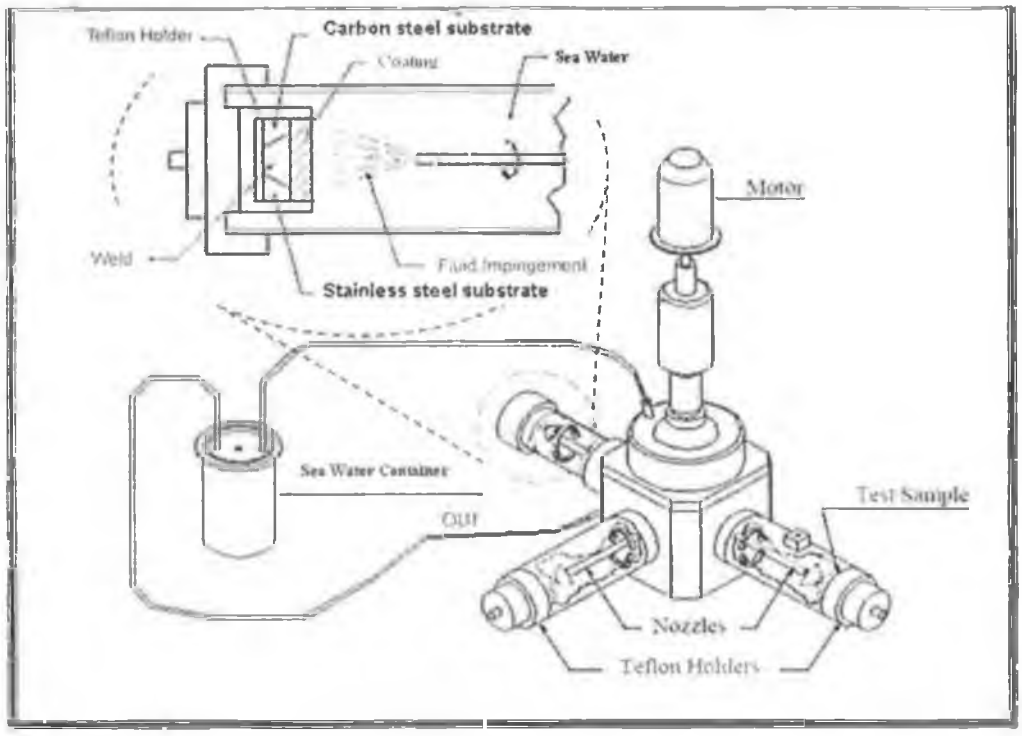

Figure 32 Schematic representation of the erosion-corrosion testing rig.

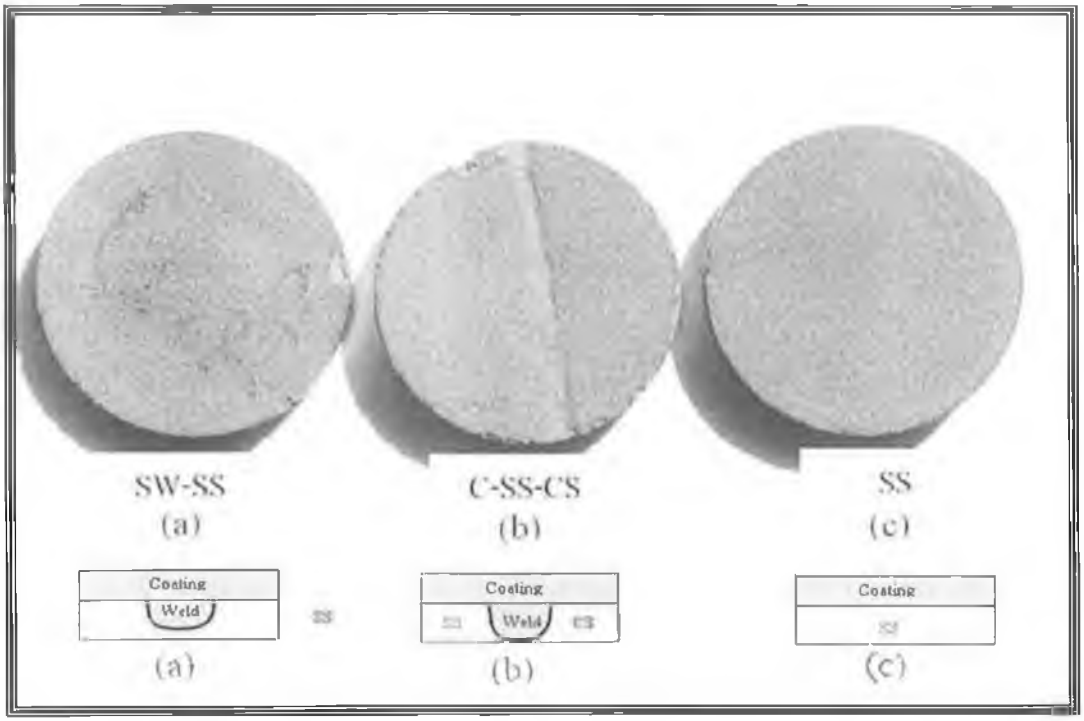

Figure 33 Photograph of the three forms of samples types used in the jet-impingement test.

3.7.5 Tensile Testing

The aim of conducting the tensile test was to evaluate the tensile strength of the different substrate materials coated with HVOF thermally sprayed Inconel-625 powder and subjected to different corrosive environments. The tests were conducted using the INSTRON 8501 hydraulic testing machine. Statics tests were conducted to acquire stress strain plots for all test specimens, considering the variations produced by the processes shown in Table 6. The tests were performed under load controlled at a displacement rate of 0.08 mm/sec, largely as per ASTM E8, "Standard Method of Tension Testing of Metallic Materials" [141]. The test specimen employed for determining the stress strain behaviour of the coated materials were of rectangular geometry and not dog-bone shape. The reason for that was because the spot welded samples were assured to fail in the mid-section region of the sample due to the deterioration in the material properties because of

the heat affected zone resulting from the weld. Another reason was to ensure the coating would fail before the substrate, making it unnecessary to reduce the cross-section area by dog-boning to force the failure to occur in the specimen mid-section. To effectively evaluate the coating performance, both stainless steel and carbon steel uncoated materials were also tested. The grips were placed 25 mm from each end of the sample in size of (150x40x4 mm^3) and the test was carried out at room temperature.

3.8 MEASUREMENT OF RESIDUAL STRESS

Residual stresses in HVOF coatings has been recognised as one of their most important characteristics. Coating deformations such as spalling or cracking can result from residual stress variations between the coating and substrate [142]. Moreover, several coating performance indicators including bonding strength, thermal resistance, erosion-corrosion, fatigue, and bending characteristics are strongly influenced by the nature of thermal stresses [143]. There are several methods used to measure residual stresses including hole drilling method, X-ray diffraction method, and deflection method (Almen) [143-147]. X-ray diffraction and the Hole drilling methods were found to be the most used methods in recent time [148]. Similarly, Clyne derived a simpler analytical method to determine the residual stresses variations across the coating and substrate [149]. In this study, the prediction of residual stresses of coatings applied over different metallic substrates were determined using two methods; (i) Clyne's analytical method, and (ii) Modelling using ANSYS Finite Element Analysis.

3.8.1 Clyne's Analytical Method

Residual stress determination using Clyne's analytical method is a quick and reliable method compared with other methods such as the X-ray diffraction and hole drilling method [150]. In this method, a simple coating system (just two layers), can be considered. It is useful to consider the situation of a two layered system in terms of misfit strains, that is, relative differences between the stress free dimensions of the two layers [151]. Tsui and Clyne [152] used an analytical method, which considered a pair of plates bonded together with a misfit strain $\Delta\varepsilon$ in the x-direction as shown in Figure 34. The stress distribution through the coating thickness, stress at the coating-substrate interface, as well as at the bottom of the substrate can be analytically predicted using Clyne's method [153]. The stress distribution was derived by Clyne [153], using the following equations:

[Stress at the top of the deposit]

$$\sigma_d\Big|_{y=h} = -\Delta\varepsilon\left(\frac{E_d' H E_s'}{h E_d' + H E_s'}\right) - E_d' \kappa (h-\delta) \qquad \text{Equation 4}$$

[Stress at the Bottom of the deposit]

$$\sigma_s\Big|_{y=0} = -\Delta\varepsilon\left(\frac{E_d' H E_s'}{h E_d' + H E_s'}\right) - E_d \kappa \delta \qquad \text{Equation 5}$$

[Stress at the Top of the Substrate]

$$\sigma_s\Big|_{y=H} = \Delta\varepsilon\left(\frac{E_d' h E_s'}{h E_d' + H E_s'}\right) - E_s' \kappa (H+\delta) \qquad \text{Equation 6}$$

[Stress at the Bottom of the Substrate]

$$\sigma_s\Big|_{y=0} = \Delta\varepsilon\left(\frac{E_d' h E_s'}{h E_d' + H E_s'}\right) - E_s' \kappa \delta \qquad \text{Equation 7}$$

Where $\Delta\varepsilon$, E_c' and E_s', κ (Curvature) are given as,

$$\Delta\varepsilon = (\alpha_s - \alpha_c)\Delta T \qquad \text{Equation 8}$$

$$E_c' = \frac{E_c}{(1-\nu_c)} \qquad \text{Equation 9}$$

$$E_s' = \frac{E_s}{(1-\nu_s)} \qquad \text{Equation 10}$$

$$\kappa = \frac{6 E_d E_s (h+H) h H \Delta\varepsilon}{E_d^2 h^4 + 4 E_d E_s h^3 H + 6 E_d E_s h^2 H^2 + 4 E_d E_s h H^3 + E_s^2 H^4} \qquad \textit{Equation 11}$$

Where

α_c = co-efficient of thermal expansions of the coating $(K)^{-1}$

α_s = co-efficient of thermal expansions of the substrate $(K)^{-1}$

ν_c = poison's ratio of the coating

ν_s = poison's ratio of the substrate

ΔT = temperature difference between the substrate and coating (K)

δ = overall deflection of the beam (m)

κ = the curvature of the beam (given as 1/R, R is bending radius of the sample, m^{-1})

Stokes [62] found this method to be very effective in measuring residual stress in WC-Co deposits; hence the method was used in the present study. In this method a sample of substrate size (40mm wide x 150 mm long x 4 mm thick) and coating thickness of 0.4mm was considered. The coating material was applied over three different metallic surfaces: (a) plain stainless steel (SS), (b) spot-welded stainless steel (SW-SS), and (c) a composite surface of stainless steel and carbon steel welded together (C-SS-CS). Following deposition, the distributed stresses on the coating and the different metallic substrates were deduced by measuring the resulting deflection of the samples and using Equations 4 to 7.

Equation 2 was used to calculate the quenching stress in the deposit [62], and the stress generated in the coating due to thermal expansion mismatch between the coating and substrate can be estimated using Equation 3. Residual stress due to deposition can be estimated by adding both quenching and cooling stresses. It is important to note that these equations were used to estimate the overall residual stresses in the coating during the deposition and cooling processes and it was not possible to use these to determine the residual stress at specific points like equations (4-7). This is because determining the residual stress at specific points is dependent of the coating and substrate thickness.

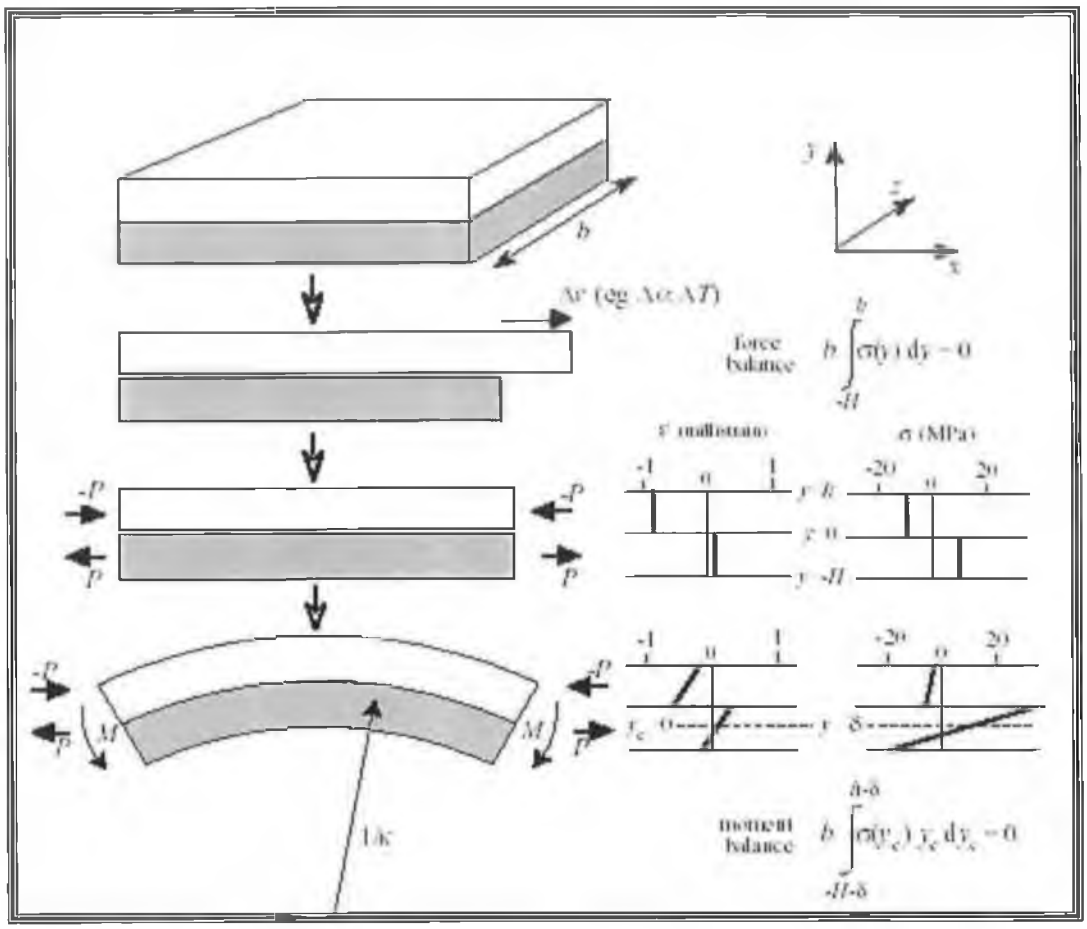

Figure 34 Schematic description of the generation of curvature in a bi-material plate as a result of misfit strain, adapted from [151].

Table 9 Material properties of the coating and the different metallic substrates used in the modeling. [16, 49].

Material (Bulk)	E (N/mm^2)	α (K^{-1})	*k (W/m.K)	υ	Bulk Yield (MPa)
C.S (AISI) 4140	205×10^3	13.7×10^{-6}	42.7×10^{-3}	0.3	675
SS 316	193×10^3	15.9×10^{-6}	16.3×10^{-3}	0.3	290
SS 309	200×10^3	15×10^{-6}	15.9×10^{-3}	0.3	280
Inconel-625	207×10^3	12.8×10^{-6}	9.8×10^{-3}	0.31	483

*k here represent conductivity required in the ANSYS model.

3.8.2 Modeling Using ANSYS Finite Element Analysis

Two of the samples involved welding, this resulted in inhomogeneity of the substrate, Clyne's method can not be used in this situation as it only deals with plain substrates. Hence, prediction the residual stress of the coating over different metallic substrates require another method of modelling. Equation 2 and 3 were used to calculate the variation of residual stresses due to substrate type change. These results were then compared to the model results.

During the deposition of Inconel-625 coating over metallic substrate, stresses due to the quenching of the lamella and cooling of the coating generated a moment at the end of the sample, causing a deflection, (Figure 35). As the simulation of both quenching and cooling in one system is quite difficult, the method of simulation used in this research relies on the deflection of the sample post-spraying, as proposed by Stokes [62].

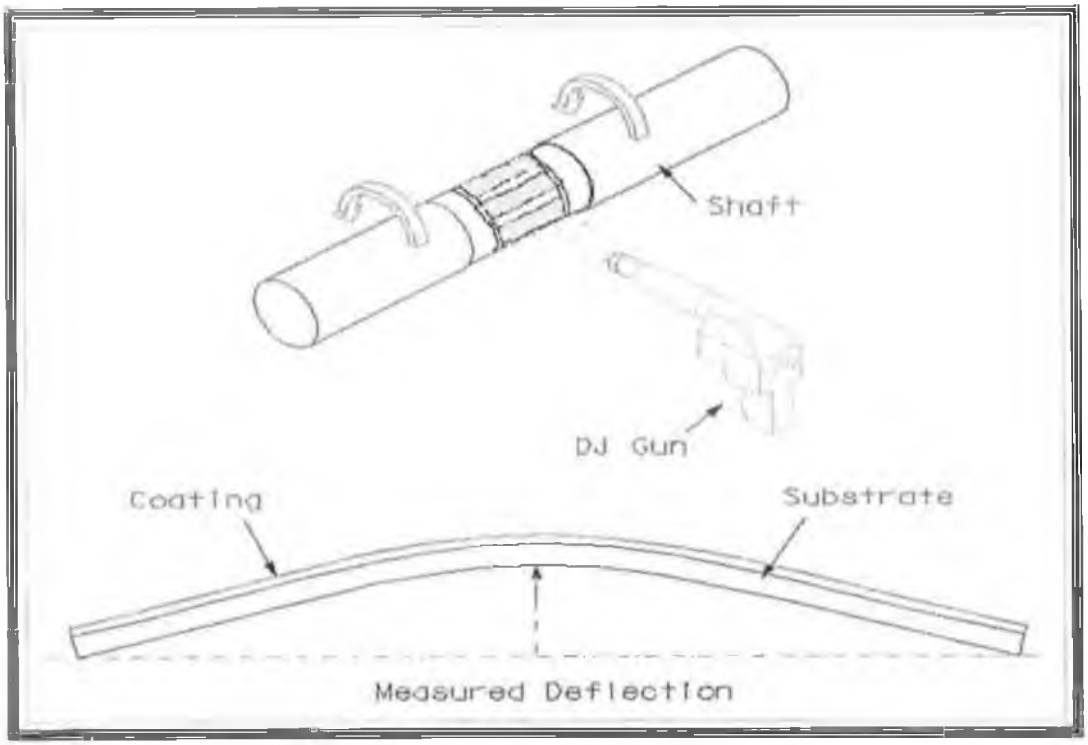

Figure 35 Clyne's method used to determine distributed stress in thermal spray coatings, adapted from [62].

Two approximate methods were approached to demonstrate the numerical formulation of this system. The first method was to apply a known displacement (deflection) to the sample while both ends were locked, (Figure 36). This would generate a known deflection that was found from the curvature in equation 11. This deflection would cause an internal stresses in the deposit and the substrate (moment model).

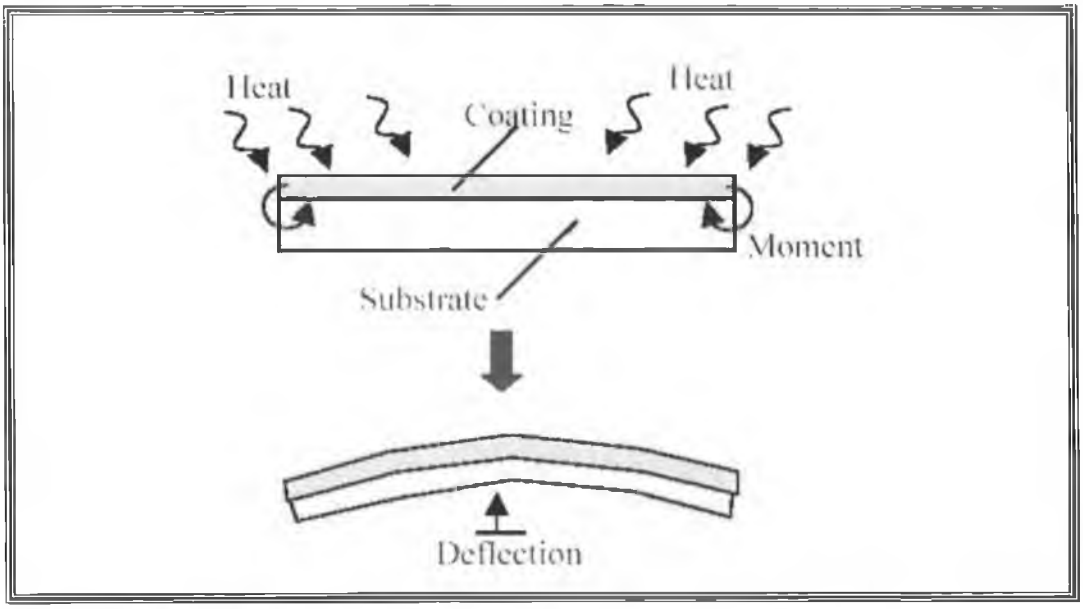

Figure 36 Sample deflection caused by moment, adapted from [62].

The second method (Thermal model) was to apply a series of temperature loads (as produced by the convective thermal gradient across the sample) to the coated sample until the desired deflection was achieved (that found using equation 11). To correctly model the residual stresses in deposit, Stokes [62] found that if one used the stress at the top of the coating and the bottom of the substrate from the moment model and the stress at the bottom of the coating and the top of the substrate (interface) from the thermal model this would provide results similar to that found experimentally, Figure 37 [62]. This would then give a predictive model of residual stresses distributed across the deposit.

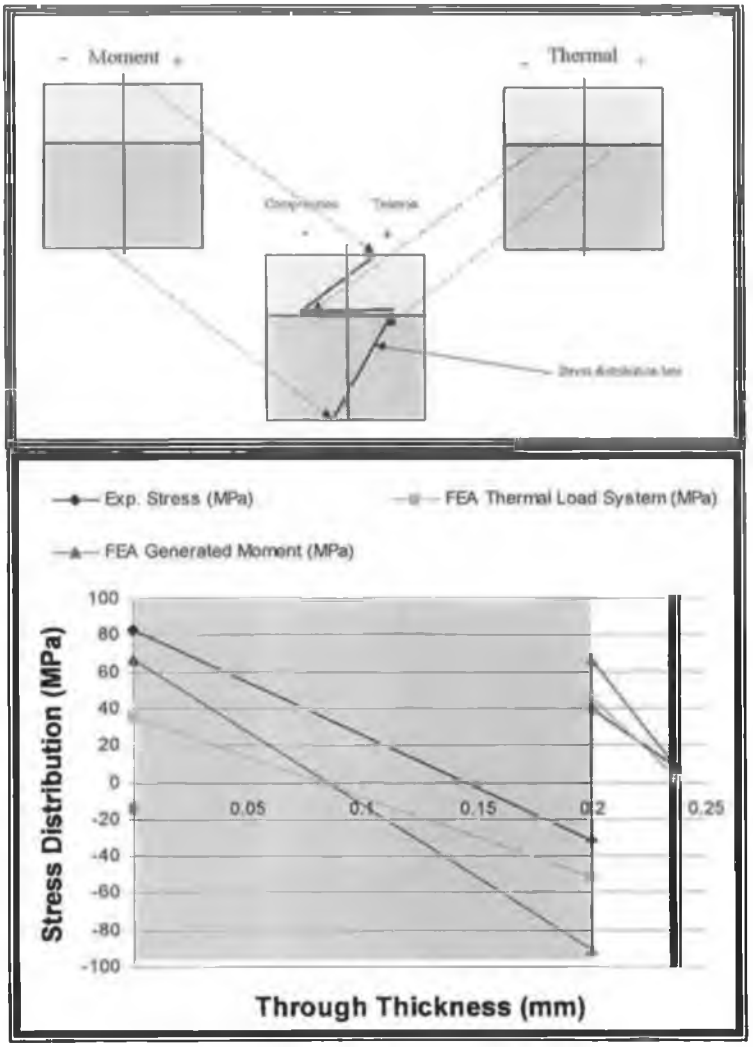

Figure 37 Stress distribution in the coating during deposition process.

This work considered the development of residual stresses during the spraying process. The presence of a weld in the base material generated a residual stresses as shown in Figure 38. However, the effect of this residual stresses was reduced during the surface preparation (shot peening) of the sample prior to spraying. Heat treatment in the oven for three hours at 450°C before and after spraying also reduced the effect of residual stresses generation in welded substrates [154]. Therefore, any stresses arising in the samples were purely due to thermal spraying.

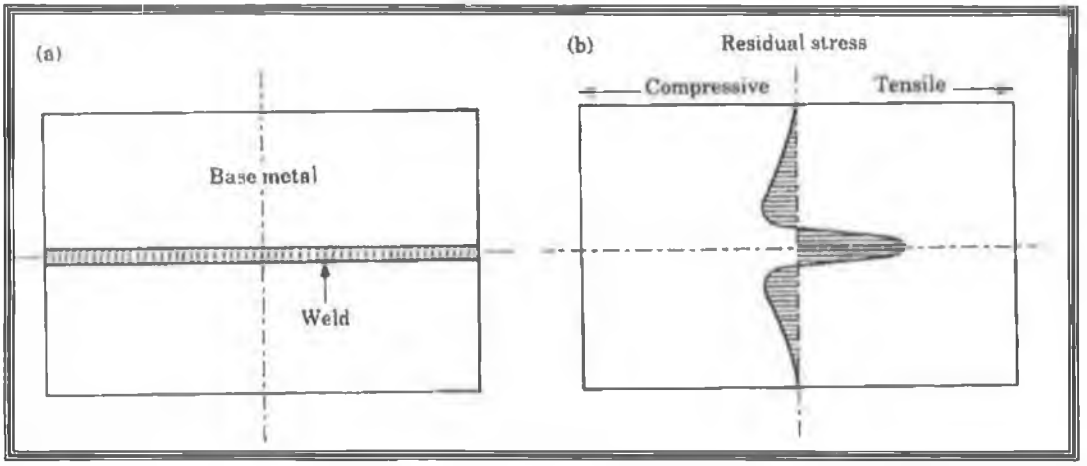

Figure 38 Schematic of residual stresses developed in welding joint [154].

4

RESULTS AND DISCUSSION

4.1 INTRODUCTION

The present study experimentally analysed the mechanical properties of the Inconel-625 coated material, through coating characterisation and mechanical testing. The material's resistance to several mechanical tests - including bending, fatigue, erosion-corrosion, and tensile testing, where the coating material are applied over plain, welded and composite substrate materials was investigated to determine the effect of possible failures of this material when subjected to sever corrosive and erosive environments combined with different mechnical loadings during operation. Furthermore, residual stresses evaluation using modelling and analytical methods were used to predict the influence of residual stress when this coating was applied over different metallic substrates.

4.2 COATING AND SUBSTRATE CHARACTERISATION

Detailed characterisation for the Inconel-625 coating material applied over different metallic substrates was performed prior to mechanical testing to compare the characteristics of the present coating with manufacturer specifications and ensure that the coating under testing was produced at its best quality.

Figure 39 shows a typical cross section of a coated sample where the Inconel-625 deposit (A) is approximately 400μm in thickness deposited onto the substrate (B). The coating porosity (measured microscopically) ranged from 1% to 3% with the noticeable presence of oxide formation around the resolidified splats. The lamella structure can be observed in the coating and some randomly distributed cavitations at the interface between the coating and the substrate are also evident. Figure 40 shows a magnified view of the area depicted as (A) in Figure 39, illustrating that such a deposit contains large semi-molten powders (C), which presumably were formed due to one or all of the following: (i) the non-uniformity of the powder manufactured - in some cases several particles are attached together (as shown in Figure 19), and (ii) the high cooling rate of splats during inflight time. Moreover, the melting of such joint particles is more difficult than that of small spherical particles when one considers the energy and particle thermal exposure time (dwell time) during the HVOF process.

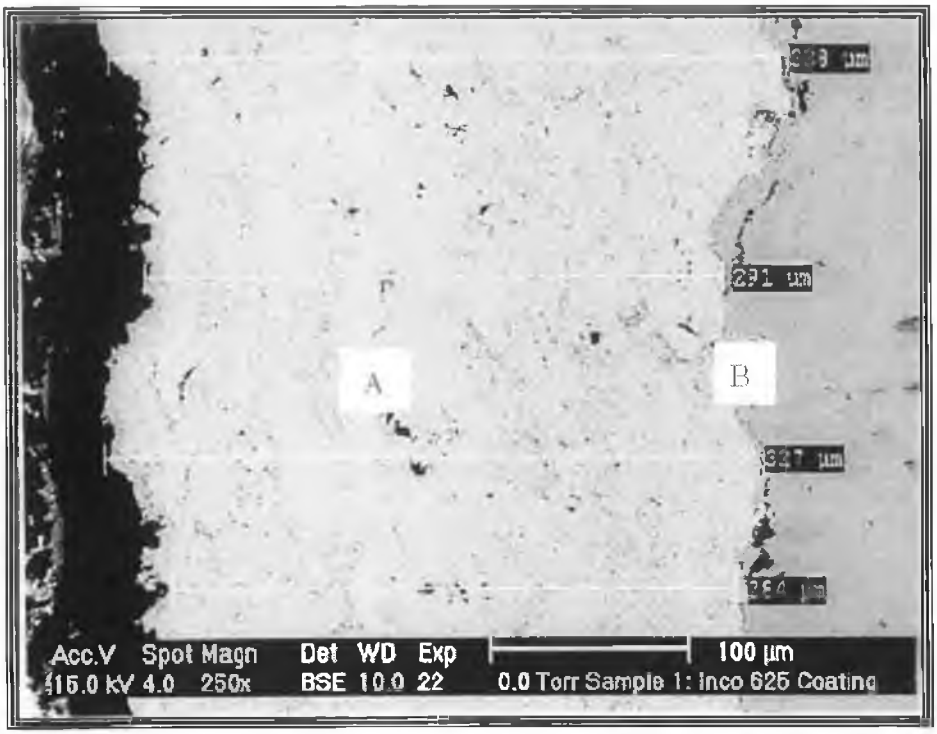

Figure 39 Typical cross section of the coated sample

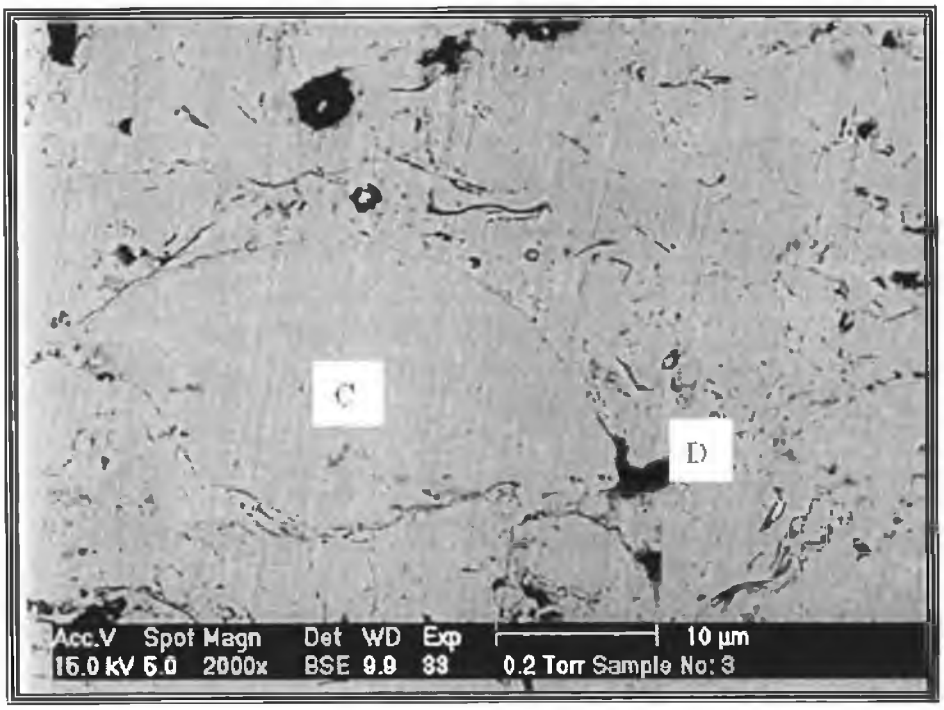

Figure 40 Magnified view of the area depicted as A in Fig. 39.

The EDS analysis was conducted on three selected points across the deposit to determine its approximate local chemical composition (wt%) and the variation of oxygen presence in the coating along with thickness. Figure 41 (a) shows the EDS spectrum of the particle identified as (C) in Figure 40 and indicates the presence of large peaks of Ni, Cr, and Mo, which are the three main elements of the Inconel-625 powder. However, Figure 41 (b) shows the EDS spectrum of the particle identified as (D) in Figure 40. The EDS analysis showed that the oxide formed in the coating contained mainly the Cr_2O_3 phase. This is mainly due to the high temperature of the splats and presence of air molecules captured in voids between the non-melted or semi-molten particles and the next bonded splats. It was also observed from the EDS analysis that other types of oxides were present at the interface between the coating and the substrate, namely and SiO_2 (from the Al_2O_3, TiO_2, SiO_2, Fe_2O_3 grit blast) as shown by Figure 41 (c). This is because some grit blasting material remained after the surface preparation process. Coating porosity, microhardness and bond strength, and variation of thickness were as follows: porosity ranged from 2-3%, microhardness ranged from 350 to 450 (Vicker), and tensile bonding measured using ASTM C 633 ranged from 700 to 850 Bar, comparable with earlier observations [16].

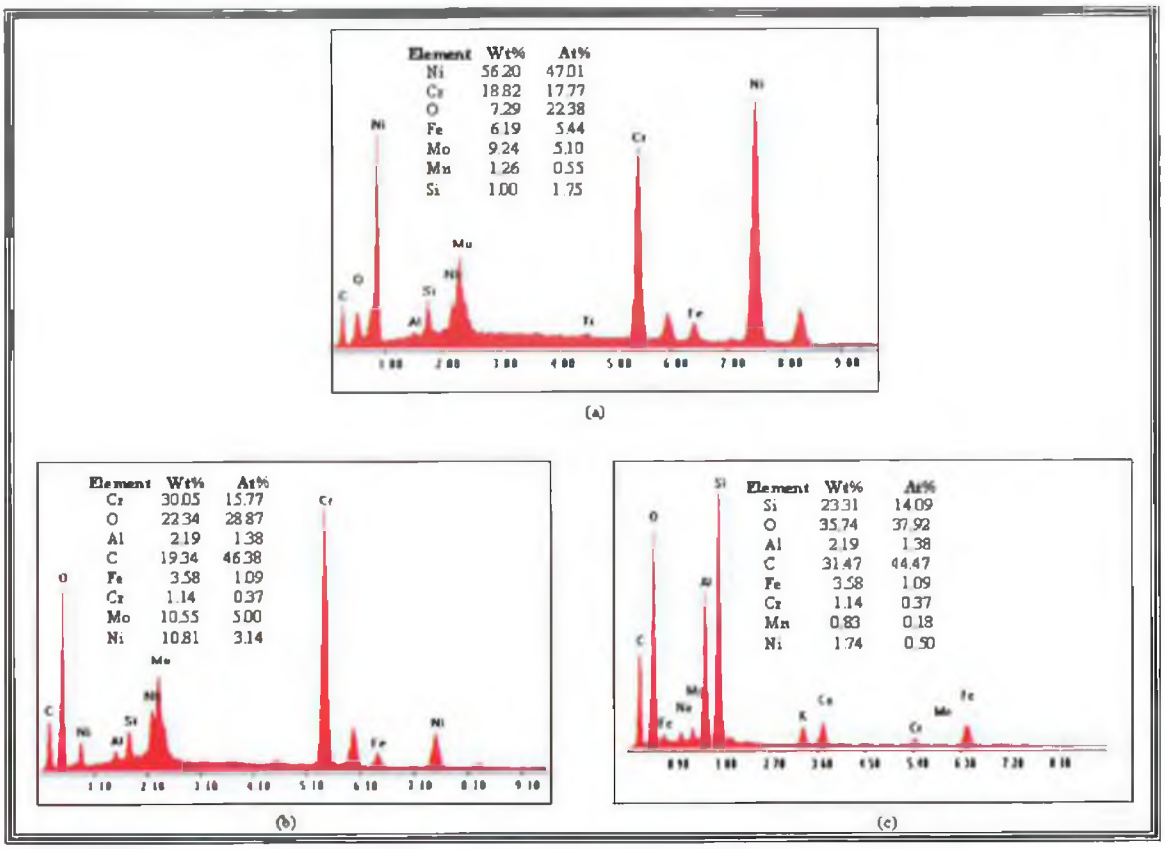

Figure 41 (a) EDS spectrum of the particle identified as C in Figure 40, indicating high Ni, Cr, and Mo peaks. (b) EDS spectrum of the dark inclusions as D in Figure 40, indicating presence of Cr_2O_3. (c) EDS spectrum of interface between coating and substrate as b in Figure 39, indicating presence of SiO_2.

Figure 42 shows the X-ray linescan of the coatings cross section at 2000X magnification. The linescan represents 128 consecutive analysis points on an arbitrary line **A**_____**B** across the coating. At each of the 128 analysis points, the concentrations of the six determined elements (Ni, Cr, Fe, Mo, Nb, and O) were measured. The data was then superimposed onto the original image as a colour-coded scatter plot for each element. The plots show variations in elemental concentrations as the line traversed from bright to gray to dark areas across the image. It was noted that the coating had a reasonably uniform composition along the line with no major variations in coating composition.

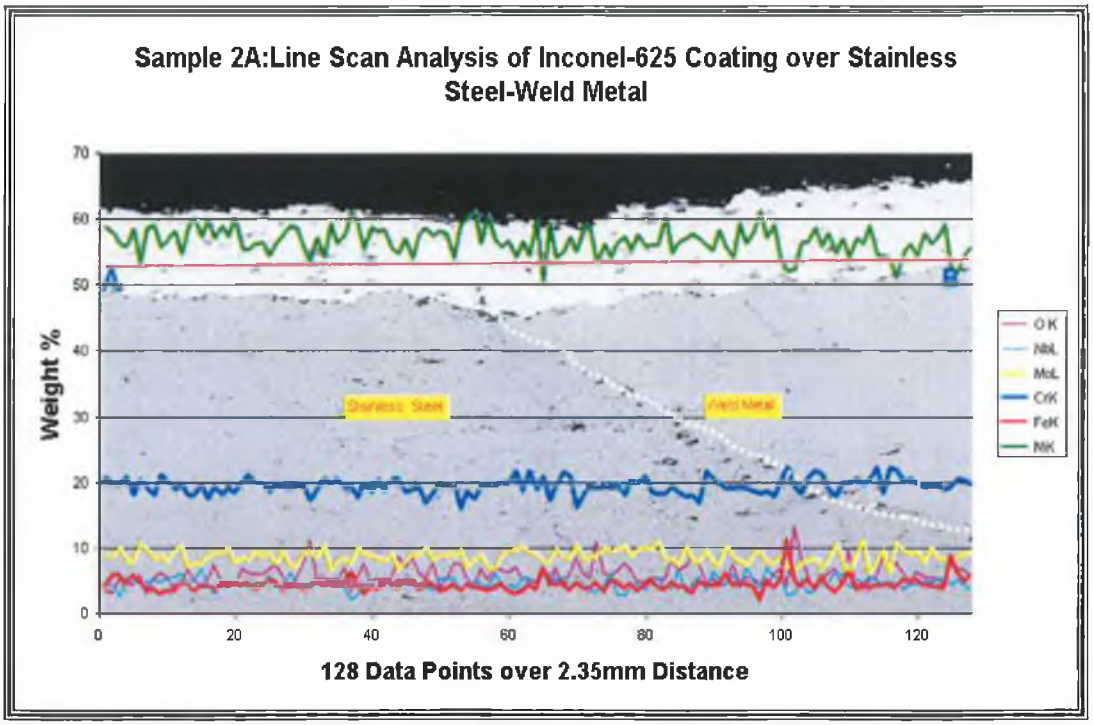

Figure 42 X-Ray line scan analysis of Inconel-625 coating.

X-ray maps showing the distribution of O, Mo, Cr, Fe and Ni across the width of the coating, can be seen in Figure 43. The backscattered electron (BSE) image of the coating is shown in the first box on top left (a) of Figure 43. In this image a sharp interface can be observed between the coating on the left and the Fe-substrate on the right. The intensity of each colour reflects the concentration of the element represented by that colour. For example, high concentrations was represented by bright colours, whereas the absence of that particular element was represented by some electronic noise in a black background. Thus, Ni, Cr, Mo, the main constituents of the coating, show up as bright colours in their respective X-ray maps. In contrast, the low intensity of oxygen (yellow) in the oxygen map suggest that only a minor presence of oxygen existed in the coating (Figure 43 (b)). Also, as expected the Fe (red colour) was low in the coating but it can be readily seen in the Fe-substrate to the right of Figure 43 (e).

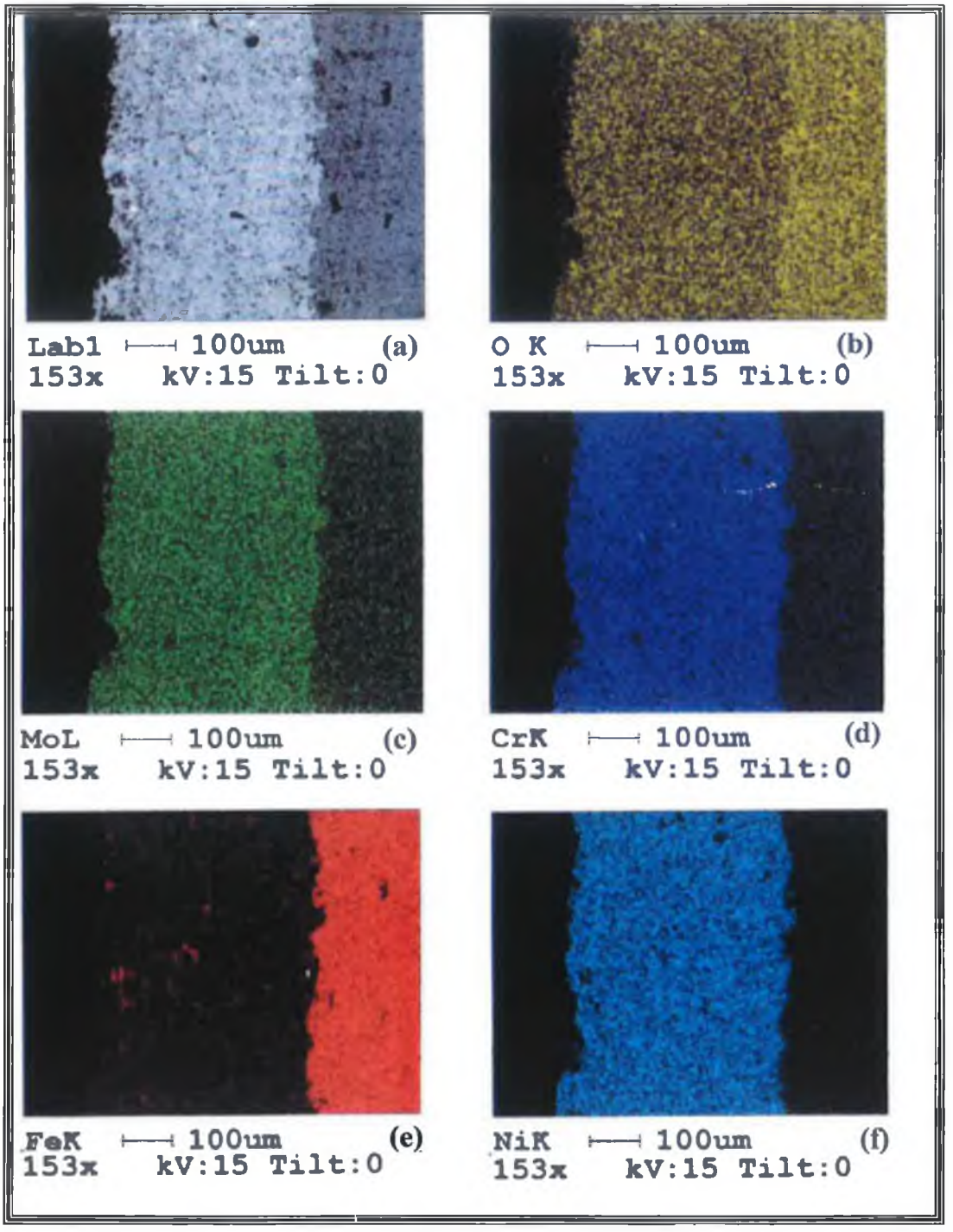

Figure 43 X-ray-maps of Inconel-625 coating over stainless steel surface. (a) sample cross section. (b) Oxygen (O) . (c) Molybdenum (Mo). (d) Chromium (Cr). (e) Iron (Fe). (f) Nickel (Ni).

Figure 44 shows another X-ray linescan of the coating cross section at 2000X magnification. This linescan also represents 128 consecutive analysis points on an arbitrary line A_____B across the composite substrate (stainless steel and weld). At each of the 128 analysis points (3-5μm electron spot) on the line concentrations of seven elements (Fe, Cr, Ni, Mo, Si, Mn and C) were measured. It was observed that the substrate had a change in composition as the line A_____B shifted from stainless steel to the heat affected zone (HAZ) and then to the weld. This variation was due to the fact that both materials are stainless steel but of different types 316, and 309. Figure 45 shows a typical cross-section of the Inconel-625 coating over plain and welded stainless substrate pre testing. The figure shows the uniformity of the coating distribution over both surfaces. The heat effected zone between the weld and the stainless steel (Zone D in Figure 45) is protected by the coating layer to minimize corrosion effect.

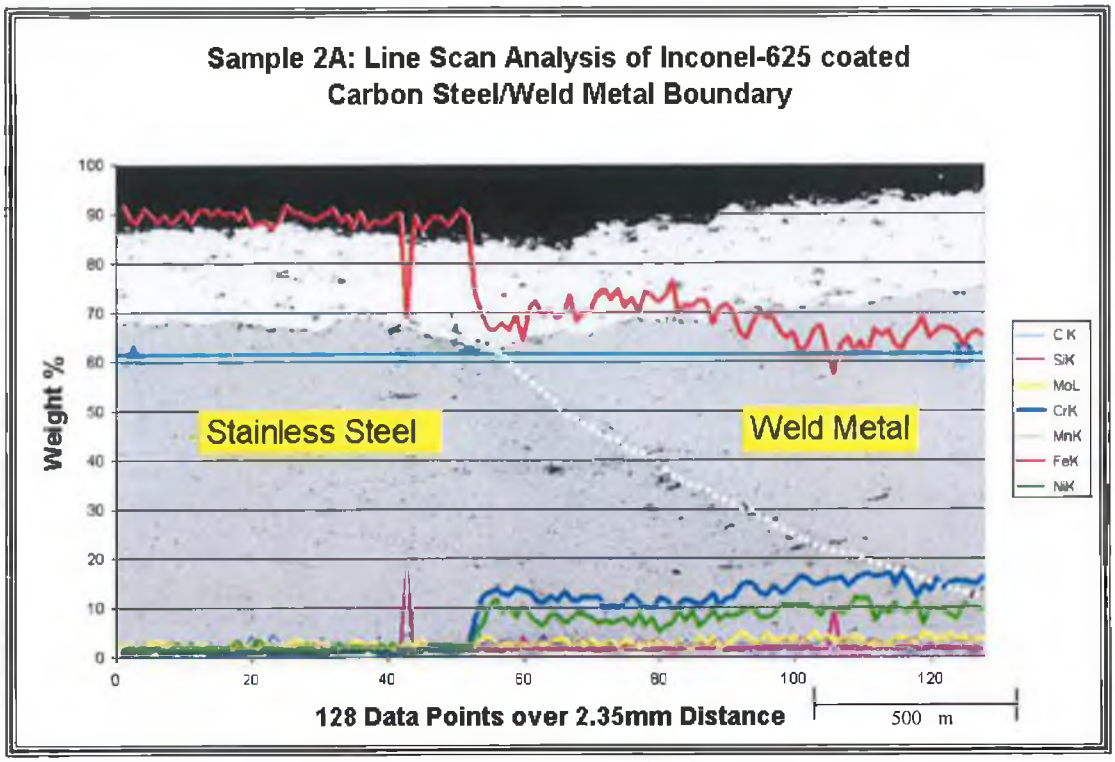

Figure 44 Line scan analysis of stainless steel and weld substarte.

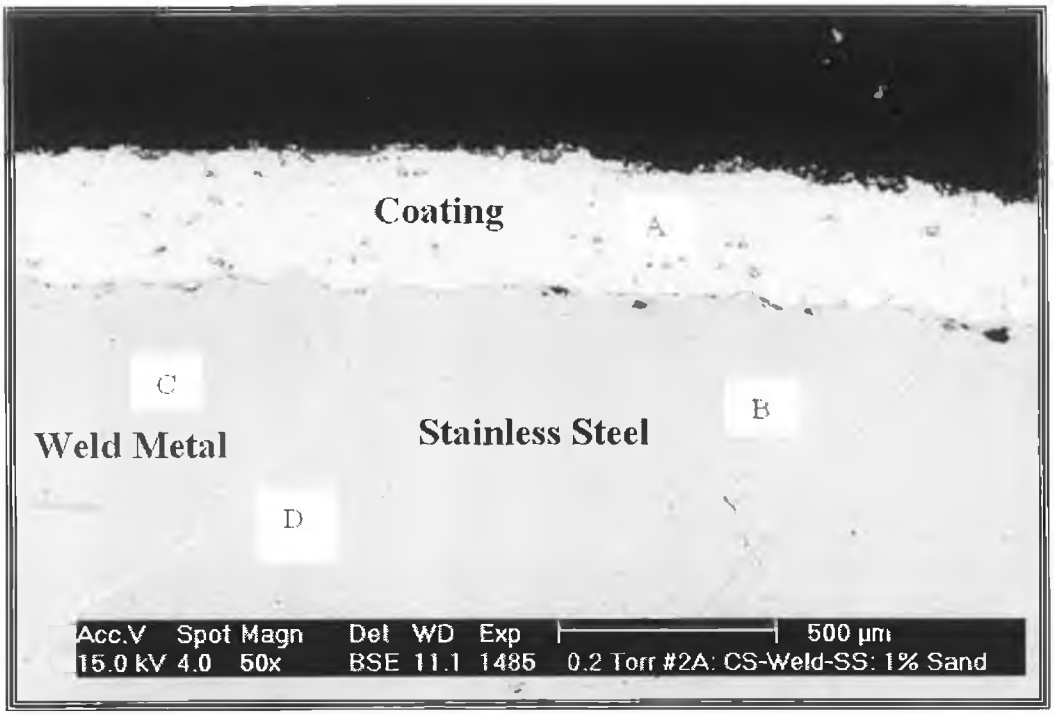

Figure 45 Cross section of sample before test: (A) Inconel-625 coating over stainless steel and weld., (B) Stainless Steel substrate, (C) Weld., (D) The heat affected zone.

4.3 CORROSION BEHAVIOR OF SPRAYED INCONEL-625 APPLIED OVER DIFFERENT METALLIC SURFACE PRIOR TO TESTING

All samples which were subjected to corrosive environment for two or four weeks duration showed a good resistance to static corrosion and no coating failure was observed prior to bending, fatigue, erosion-corrosion and tensile tests. Figure 46 shows a composite sample stainless steel and carbon steel welded sheets together (C-SS-CS) after three point bending test. It should be noted that the sample was subjected to static corrosion in ambient aqueous solution for four weeks duration. It can be observed from the figure that the sample portion of a carbon steel substrate is more susceptible to corrosion as compared to other portion of the sample that has only stainless steel substrate.

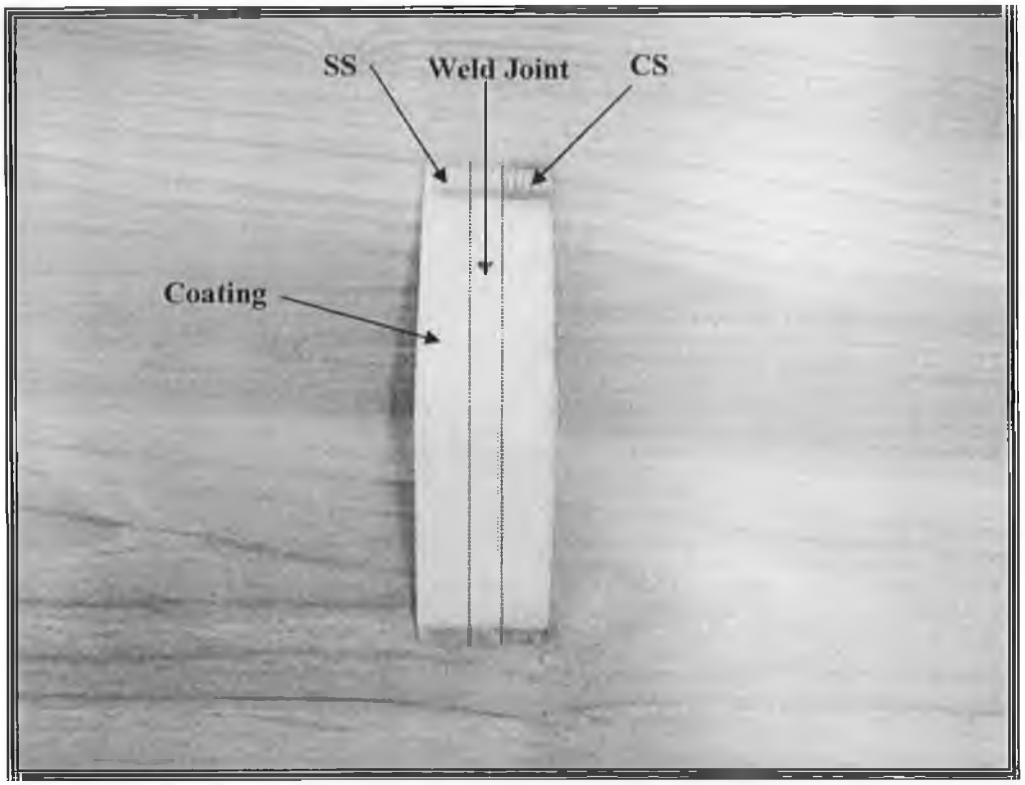

Figure 46 Photograph of composite stainless steel and carbon steel (C-SS-CS) after three point bending test and subjected to corrosion in ambient aqueous solution prior to test.

Figure 47 shows SEM micrograph of coating cross-section before and after the static corrosion tests. In general, the coating presented a lamellar structure, which corresponds to melting of splats before impinging onto the workpiece surface. Moreover, in some regions, partially melted particles corresponding to the microstructure of the stacking of the particles in elliptical or near-spherical shapes are observed. The oxygen content in the splats is found to be low. This can be seen from Table 10, in which the elemental analysis obtained from EDS are given. This indicates that even for well melted particles, oxide formed during in flight was mainly distributed over the surface. It should be noted that the oxidation of the powder in a flame occurs around the particle surface. The oxygen content in the particles increases with time due to oxygen diffusion into the powder. Moreover, after the particles flies off the temperature zone of the flame, oxidation of the particles becomes slower. Also, if the powder particle size becomes large, the oxygen content increases. Small pores unevenly distributed in the coating cross section are observed. No microcrack was observed in the coating cross-section. Moreover, no corrosion products at the coating surface or at interface between coating and base substrate material is observed extensively. However, coating material is corroded locally. This may be because of the inter-corroded pores and splats boundaries, the electrolyte could reach the substrate and it then corrodes the material. It appears that the deterioration of the coating begin along the splat boundaries and corrodes the material nearby.

The cavitations in the interface between the coating and base material accelerate the corrosion of the coating as well as base material, i.e. as a results of the inter-corroded porosity (crevice corrosion), the electrolyte may penetrate the coating and attack the substrate material, even tough the coating is resistant to the corrosive environment. Consequently, the substrate material can be corroded (crevice corrosion) beneath the coating lowering the mechanical properties at the interface.

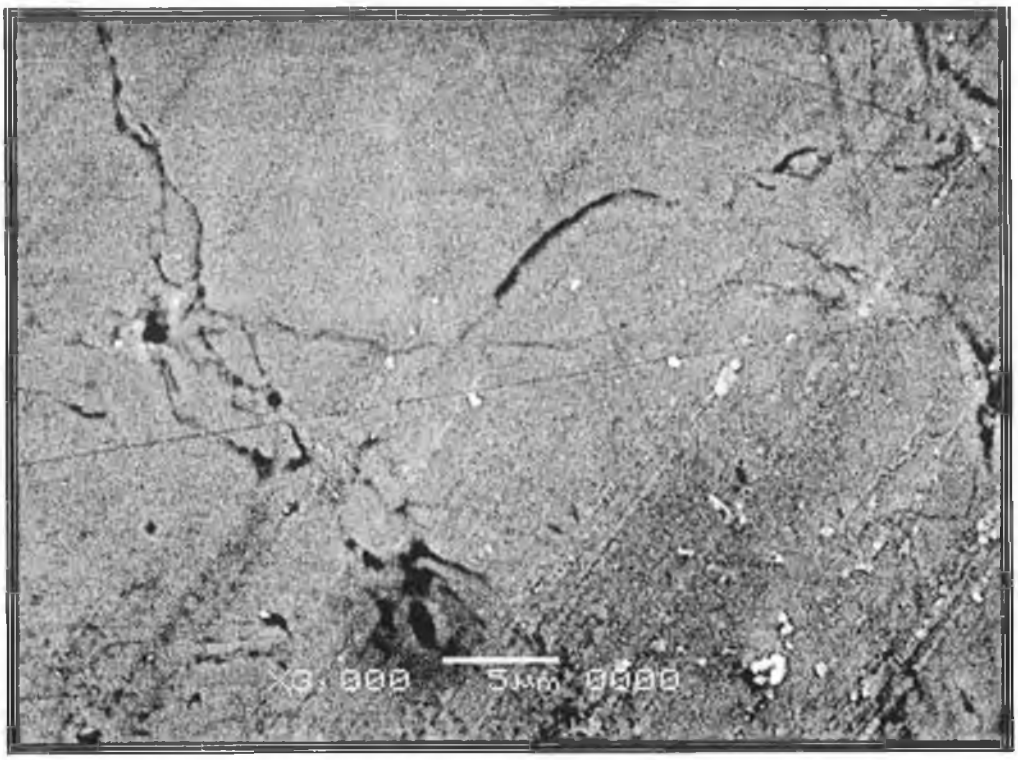

Figure 47 (a) Coating cross-section before the corrosion test.

Figure 47 (b) Coating cross-section after the corrosion test.

It was found that the HAZ corroded easily once the corrosive solution penetrated into the coating (Figure 48). This indicates that Inconel-625 coating prevent corrosion of these different metallic substrates and minimizes the effect of corrosion on joint of two composite materials.

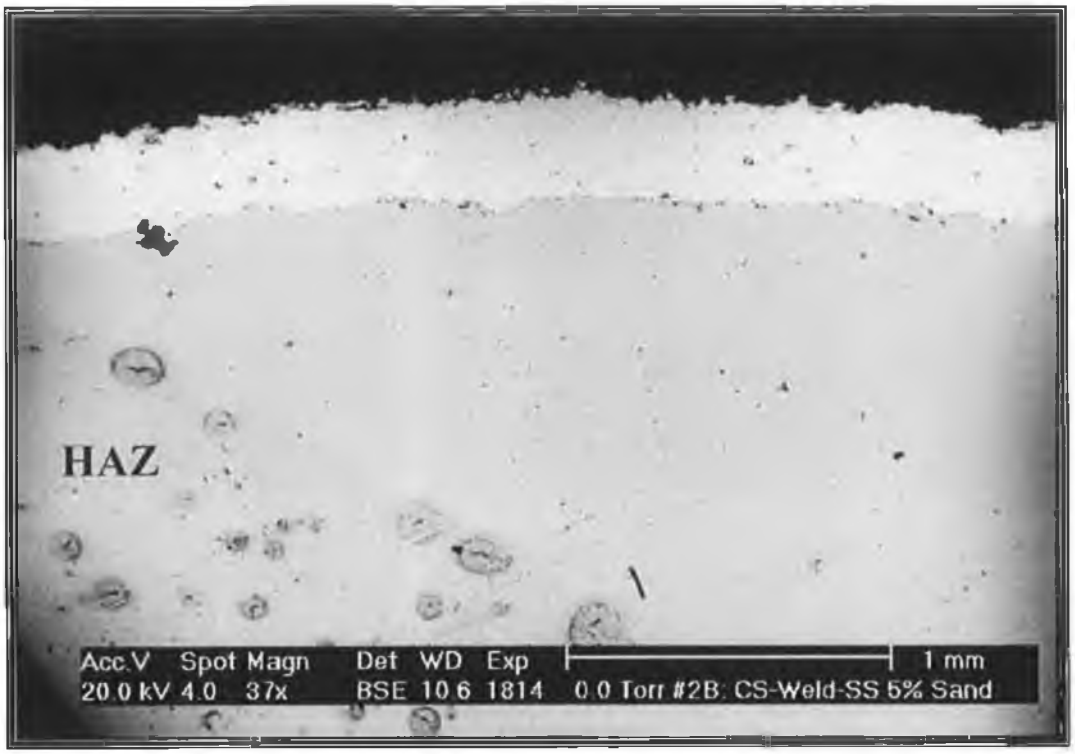

Figure 48 SEM showing close view of the heat affected zone (HAZ).

Table 10 Elemental composition of coating (%wt).

	O	Al	Cr	Fe	Ni	Mo	O
At surface	5.8	1.2	22.1	6.7	58.8	5.3	5.8
At coating cross-section	2.3	1.4	22.5	3.2	64.2	6.3	2.3

4.4 BENDING BEHAVIOUR OF HVOF THERMALLY SPRAYED INCONEL-625 COATINGS ON DIFFERENT METALLIC SURFACES

4.4.1 Effect of Substrate Variation on Coating Performance Due to Bending Testing

(1) Plain Stainless Steel Sample (SS)

Figure 49 shows the stress strain curve obtained from the three-point bending tests for plain stainless steel (SS) substrates tested under four conditions; i) surface un-coated (SS-NC-AR), ii) surface as coated (SS-AR), iii) surface as coated and subjected to aqueous static corrosion test for two weeks (SS-2WK), iv) surface as coated and subjected to aqueous static corrosion test for four weeks (SS-4WK). It should be noted that the three-point bending tests were carried out at constant strain rate and the bending tests were terminated when the coating failed. The elastic behaviour was almost the same for all workpieces, provided that the elastic limit for the un-coated was less than that corresponding to coated workpieces. However, as the bending load increased, all workpieces behave similarly. When the stress strain characteristics for all workpieces were compared, the stress of work pieces with coating was higher than that corresponding to the un-coated workpiece for a known strain, even if where the coating was subjected to abrasive corrosive medium for four weeks. This indicate that Inconel-625 powder coating enhance the corrosion resistance of stainless steel workpiece, and increase the workpiece resistance to bending. However, as the period of exposure to corrosive environment increased, coating resistance to corrosion decreased.

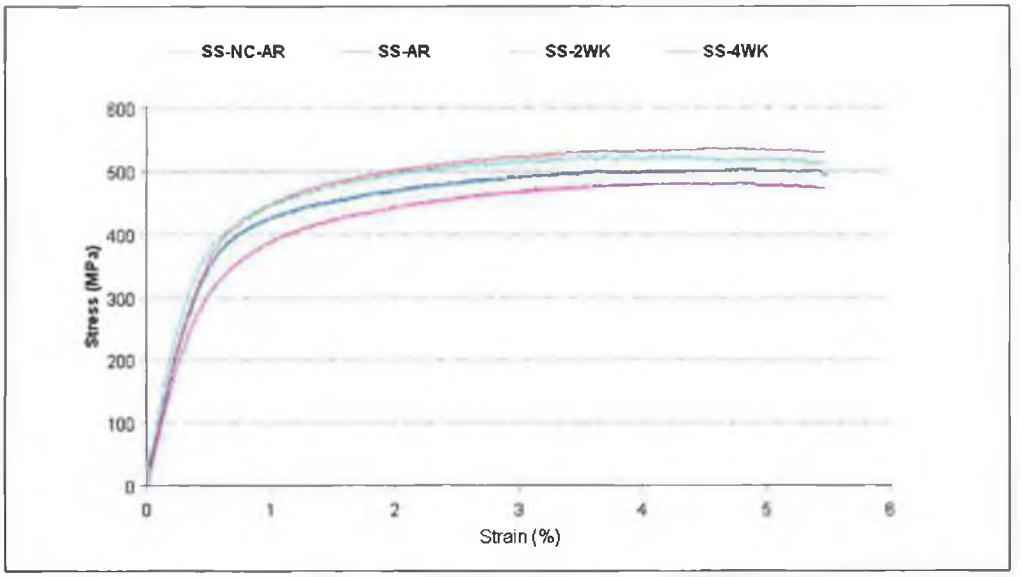

Figure 49 Stress versus strain characteristics of the workpieces during the 3 point bending tests for stainless steel workpiece (SS).

(2) Spot welded Stainless Steel Sample (SW-SS)

It should be noted here that the corrosion resistance of the spot welded stainless steel (SW-SS) coated workpiece significantly decrease compared to the plain stainless steel (SS) ones. The SS ones peaked at 470 → 550 MPa where as the spot welded ones peaked from 525 → 625 MPa. No major variation between the two weeks and the four weeks exposed samples (Figure 50). Obviously, the length of time did not have an effect, it was the corrosion media that reduce the coating capabilities. This is may be due to the presence of weld where the variation in material composition and presence of HAZ decreases corrosion resistance.

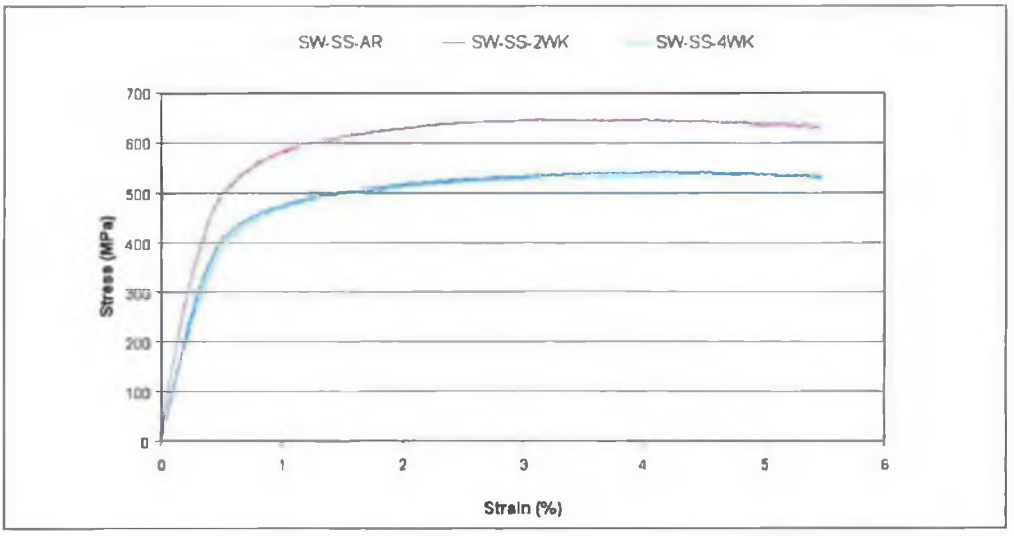

Figure 50 Stress versus strain characteristics of the workpieces during the 3 point bending tests for spot welded stainless steel workpiece (SW-SS).

(3) Composite Carbon Steel and Stainless Steel Sample (C-SS-CS)

Figure 51 shows the stress strain curve characteristics obtained from the three-point bending tests for the composite stainless steel and carbon steel workpiece (C-SS-CS). It was found that the coating enhanced the workpiece resistance to bending by small factor of approximately 20 MPa. However, when the workpiece was subjected to static corrosion, the coated surface exhibited less resistance to bending (reducing by up to 100MPa) , even less than the un-coated surface. The presence of carbon steel in the substrate obviously was effected by the corrosive media, but this media had more of an effect over time on the carbon steel compared to plain steel and spot welded steel.

However, comparing the composite stainless steel subjected to corrosion for four weeks to the same treatment applied to the plain stainless steel sample both were able to sustain the same stress level ≈ 480MPa. However, the deterioration was much higher for the composite substrate (≈ 120MPa)compared to plain (≈ 30MPa) or spot welded samples (≈ 100MPa).

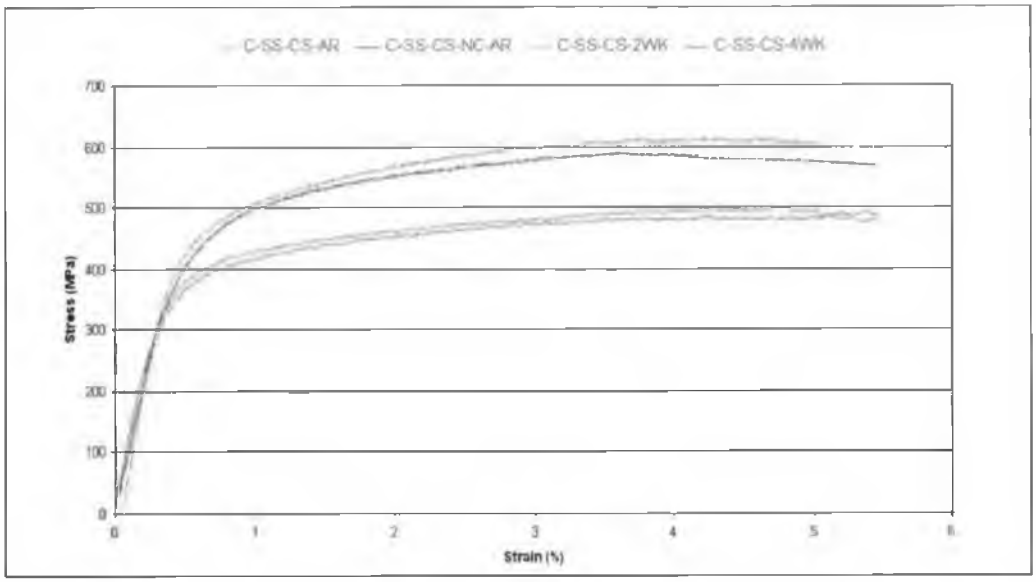

Figure 51 Stress versus strain characteristics of the workpieces during the 3 point bending tests.

4.4.2 Deposit Characterisation Post Bending Testing

Deposit characterisation post corrosion and bending test showed that the brittleness of the coating triggered crack formation in the coating. Since the coating size was about 400 μm, it is possible that the maximum of both normal and shear stresses took place at base metal-coating interface. However, the crack initiation at the interface relieved the stress levels in this region which caused spalling or buckling of the coating. A tensile shear deformation occurs in the coating due to direction of the bending. The crack initiated at the coating surface and propagated through the coating thickness Figure 52 (a).

When the crack surface was examined closely plastic deformation and delamination around the coating edge was observed due to the action of shear stress. Moreover, the internal stresses possibly created local stress concentrations, especially at defect locations around the coating base material interface. Such defects have a marked effect on the failure mechanism of the coating and the stress concentration at these defects are often factors higher than the mean internal stresses [155]. As soon as the local internal stress for crack propagation is reached, the entire coating fails in this region, which can be observed from Figure 52 (b).

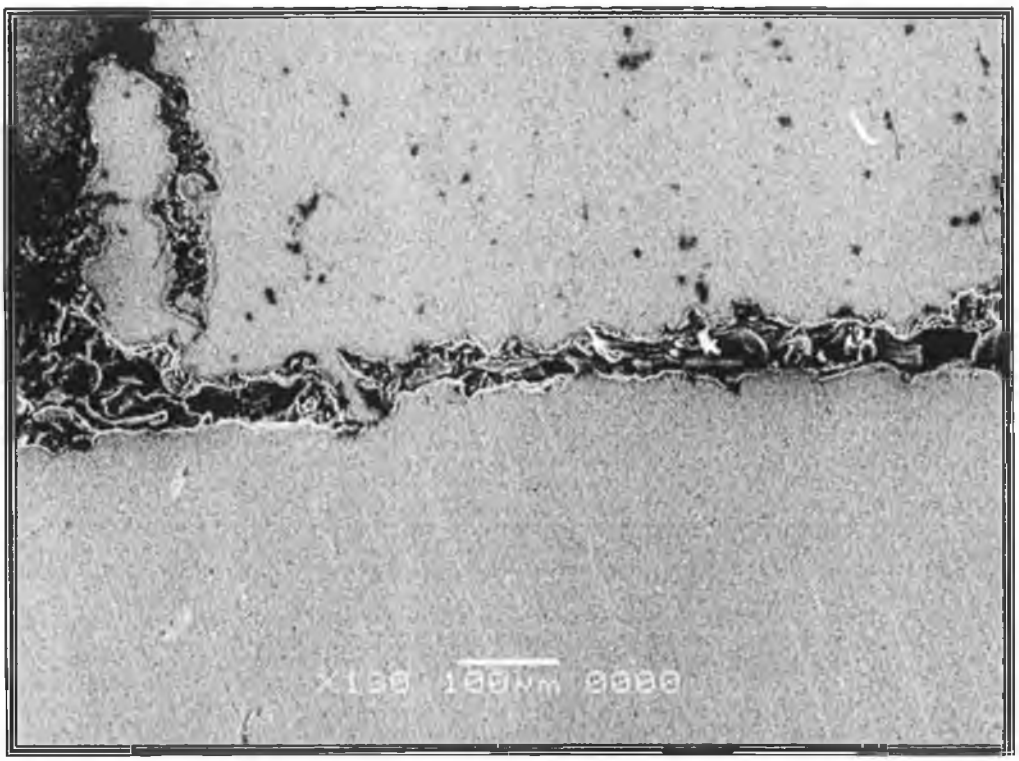

Figure 52 (a) Close view of coating cross-section

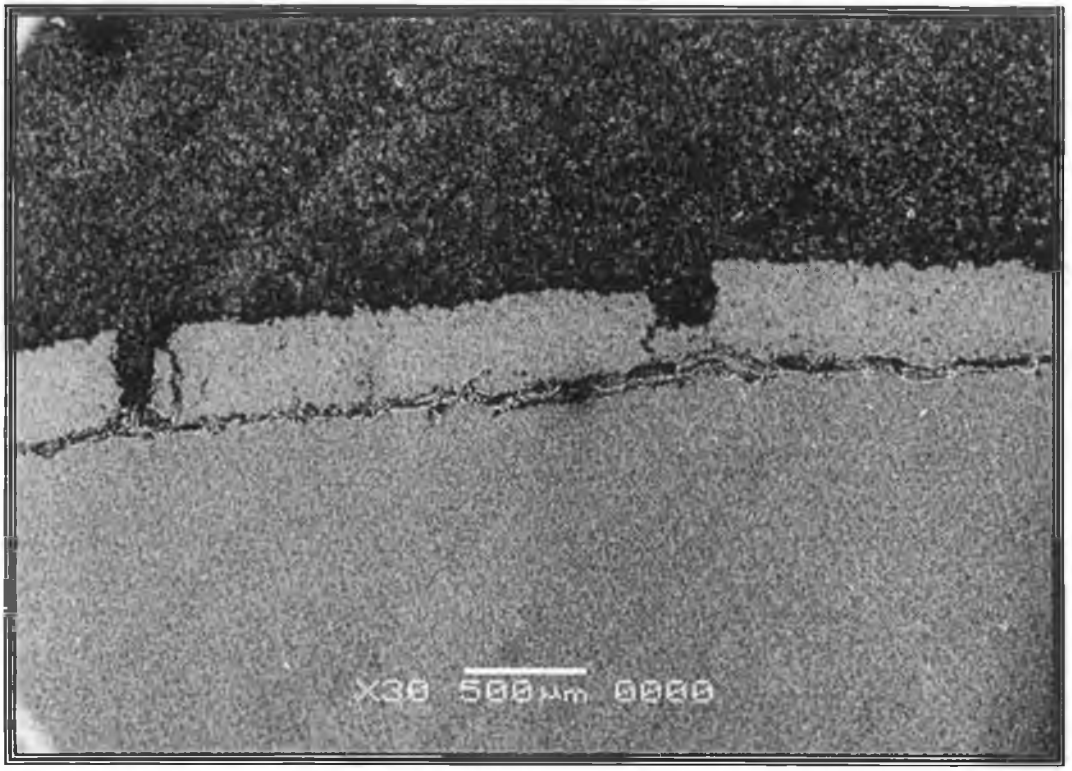

Figure 52 (b), Coating cross-section after the 3-point bending test.

Figure 53 shows SEM micrographs of the coating post the three-point bending tests. The multi cracking of the surface can be observed. The crack extends almost straight along the coating surface. This indicates that the coating does not conform to the plastic deformation occurring in the substrate material as it is a brittle material. The small crack spacing indicates that shear lag separation in the coating took place. In this case, crack regions in the coating dissipate energy through shear deformation. This was particularly true for the workpieces subjected to the corrosive environments.

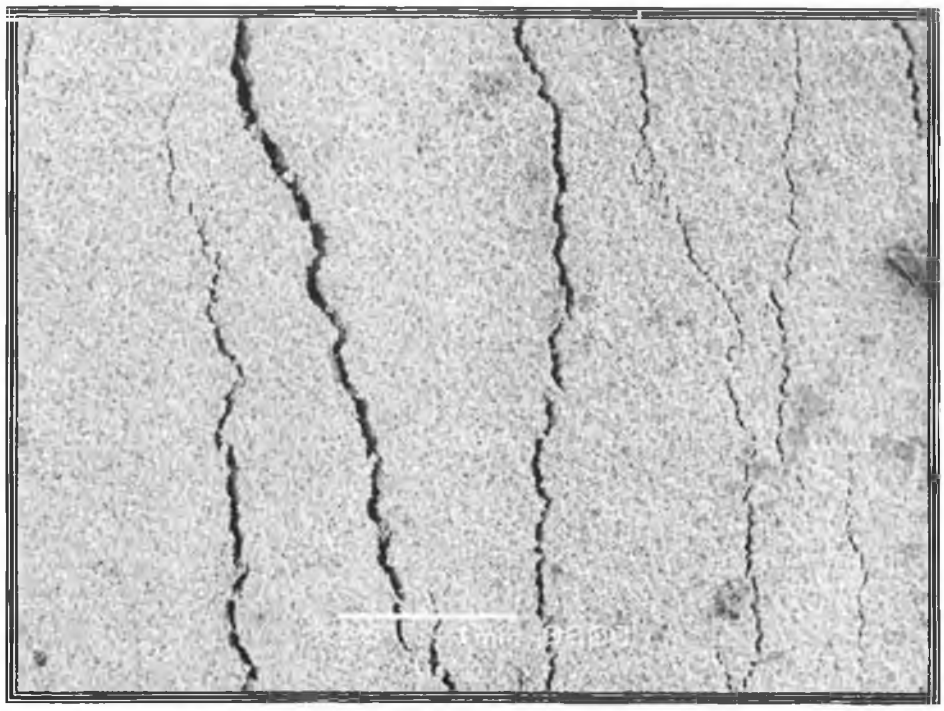

Figure 53 (a) Crack sites in the coating.

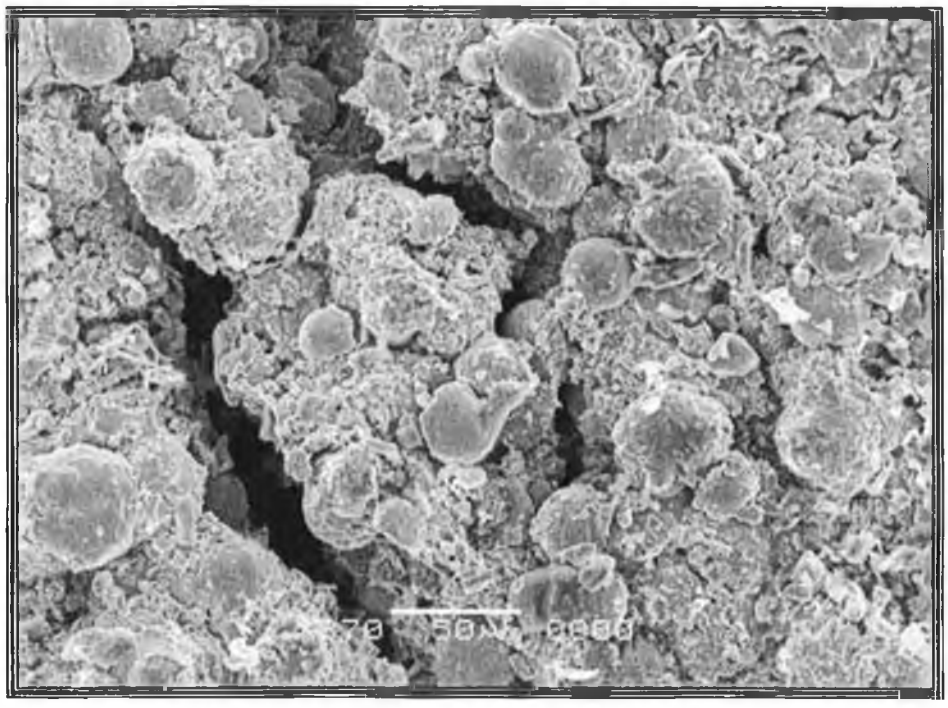

Figure 53 (b) Close view of crack sites on the surface post bending.

4.5 FATIGUE BEHAVIOUR OF HVOF THERMALLY SPRAYED INCONEL-625 COATINGS ON DIFFERENT METALLIC SURFACES

4.5.1 Effect of Substrate Variation on Coating Performance Due to Fatigue Testing

The S-N plot for the axial fatigue tests of the coating over plain, spot- welded and composite surfaces are presented in Figures 54, 55 and 56, respectively. All of the figures illustrate the results obtained at the three different conditions, un-coated, as-coated, as-coated and subjected to two weeks of corrosion, and as-coated and subjected to four weeks of corrosion. Coating the sample did enhance the fatigue behavior of the samples. It was observed in all cases that the fatigue strength decreased as the period of coating exposure to corrosive environment increased and more reduction in fatigue strength took place at samples exposed to the four week corrosion period. In fact after 4 weeks the material behave similar to that of an uncoated samples in all cases. This may be associated with low bonding strength of the coating at high corrosive environments. The spot welded samples behave well compared to the plain samples in terms of fatigues strength. However, for the composite stainless steel and carbon steel surface C-SS-CS, the fatigue strength decreased significantly, by more 60%, when the coating was subjected to the corrosive medium at both periods; two weeks and four weeks. Again the presence of carbon steel in the substrate of the composite caused the composite surface to become more susceptible to corrosion than the plain and spot-welded stainless steel surfaces (Figure 56).

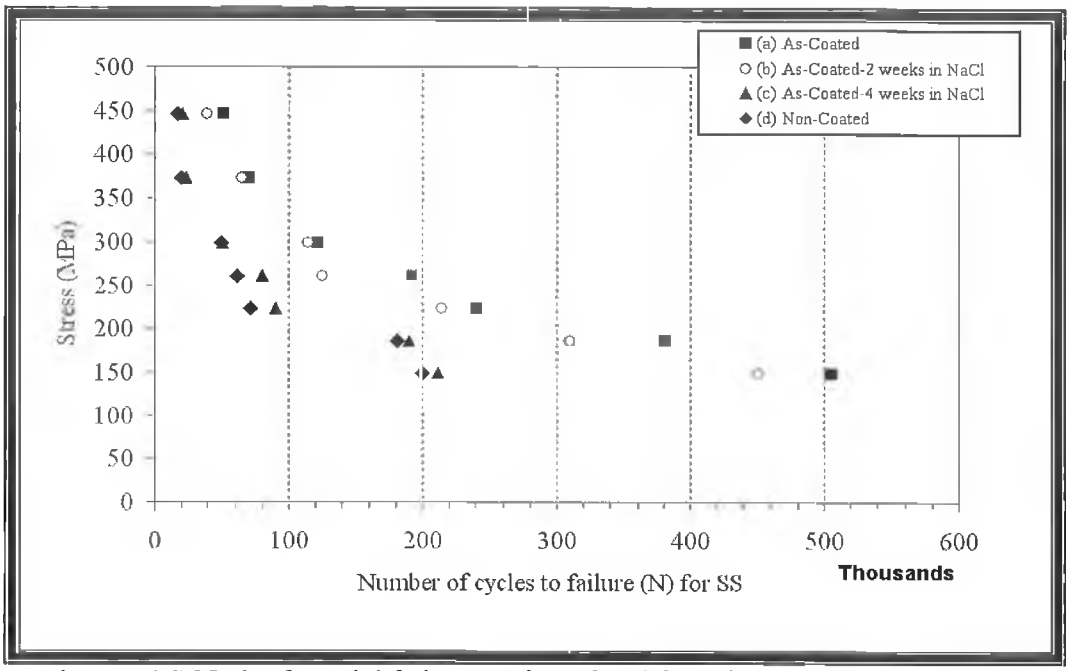

Figure 54 S-N plot for axial fatigue testing of a plain stainless steel (SS) surface coated with Inconel-625.

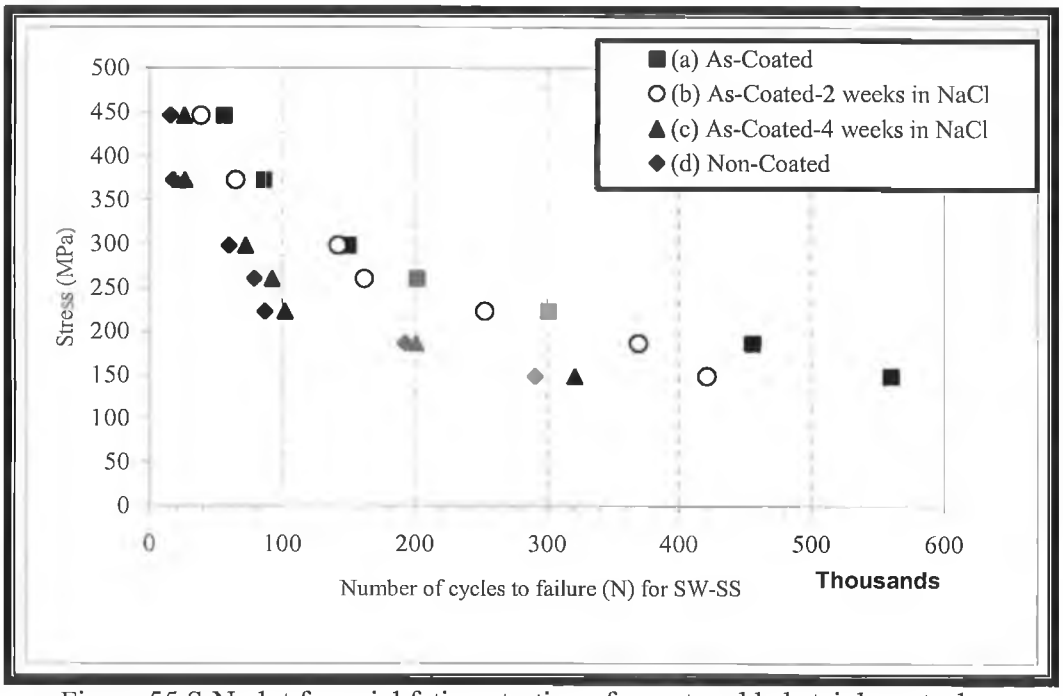

Figure 55 S-N plot for axial fatigue testing of a spot-welded stainless steel (SW-SS) surface coated with Inconel-625.

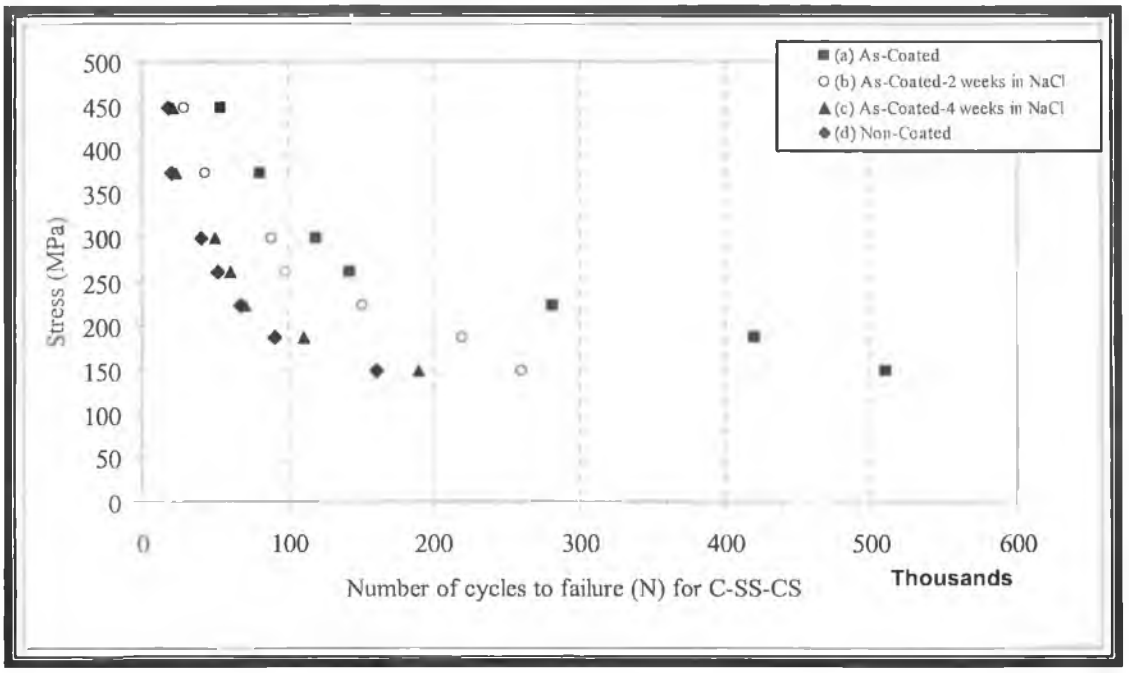

Figure 56 S-N plot for axial fatigue testing of a composite surface (C-SS-CS) coated with Inconel-625.

Figure 57 shows the comparison of coating life cycle over plain and welded surfaces at minimum alternating stresses of 148MPa applied for different durations of corrosive environments. Coating the samples did increase the fatigue strength of each sample. It was noted that both plain and welded surfaces behaved with a similar trend in terms of corrosion fatigue test, when coated by Inconel-625 powder. However, the carbon steel in the composite sample, cased the life cycle to be decreased significantly when the sample was subjected to its corrosive medium. However, after 4 weeks all the samples were reduced to a fatigue strength similar to their uncoated counter parts.

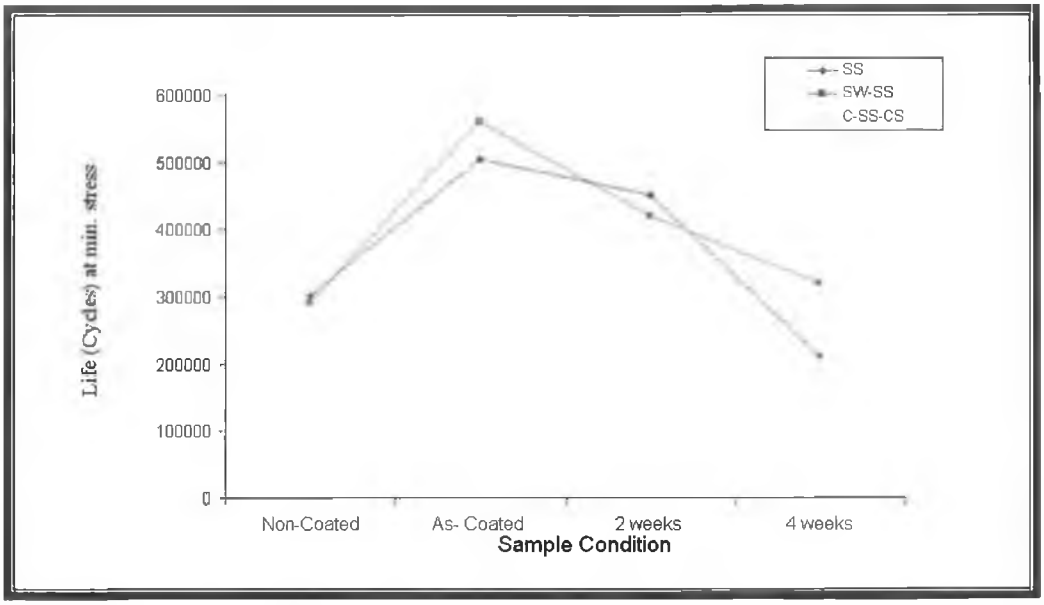

Figure 57 Coating life cycle over plain and welded surfaces at the minimum alternating stress (148 MPa).

4.5.2 Deposit Characterization Post Testing

The Inconel-625 coating surface appeared to have high resistant to corrosion, due to the presence of well stacked partially deformed particles in its microstructure. In this study, pit formation at the surface was not observed. However, the presence of unmelted and alumina particles, in the coating interface possibly caused localised corrosion which took effect after a long period of exposure. As a result of interconnected porosity, corrosion media may have penetrated the coating and attacked the substrate, even though the coating itself was resistant to the particular corrosive environment as shown in Figure 58 and 59.

It should be noted that most of the steel samples were highly susceptible to service corrosion particularly in a chloride containing aqueous media [16]. As a result, the substrates corroded beneath the coatings causing the coating to blister and spall.

Figure 58 shows the cross-section of the coating after the corrosion-fatigue test. It was observed that cracks were formed at both the interface between the coating and substrate, and in the coating itself. Coating crack size was measured as high as 49μm and the interface gap up to 38μm. Although this amount of porosity was small 1 to 3% (using microscopical technique) when comparing to other coating systems, the presence of voids and un-melted particles in the coating would significantly effect its performance when subjected to a highly corrosive environment as shown in Figure 59. The EDS spectrum analysis was measured at both locations of the points B and C (Figure 58), to determine the approximate local chemical composition of both areas. It was observed that the location of point B shows the normal composition of Inconel-625 as a Nickel based alloy. However, the presence of a large Aluminum peak is clearly shown in the location of point C (Table10). Presence of Aluminum in the coating substrate interface resulted from using it as the grit blasting material in the surface preparation process. It is the opinion of the author that these aluminum particles contributed to the rising of the stress concentration at the substrate surface, resulting in the initiation of fatigue cracks which led to specimen fracture and introduce localised residual stresses.

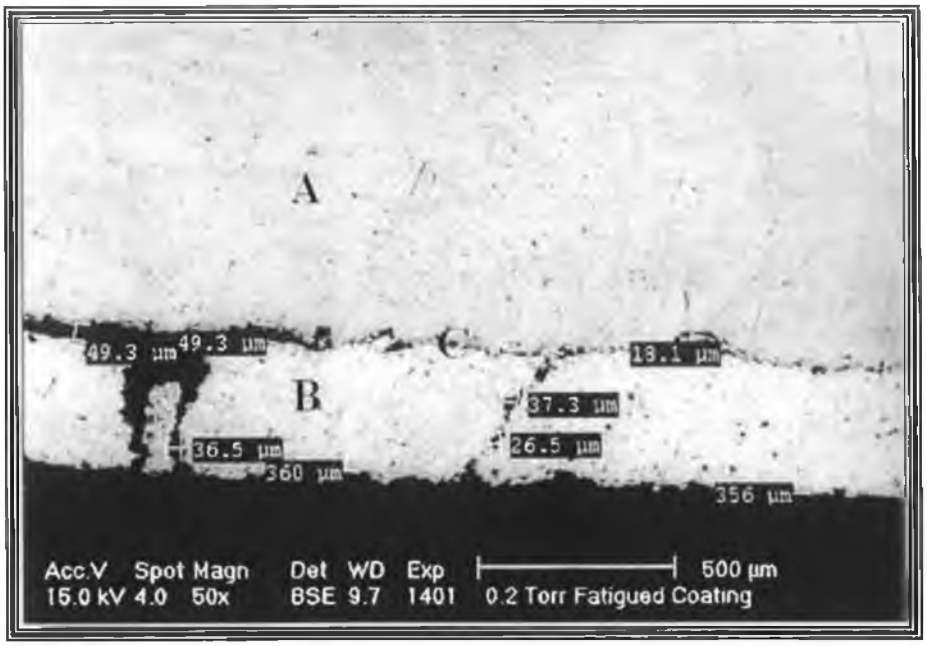

Figure 58 Sample post the corrosion-fatigue test: (A) Stainless Steel substrate. (B) Inconel-625 coating. (C) Interface between coating and Substrate

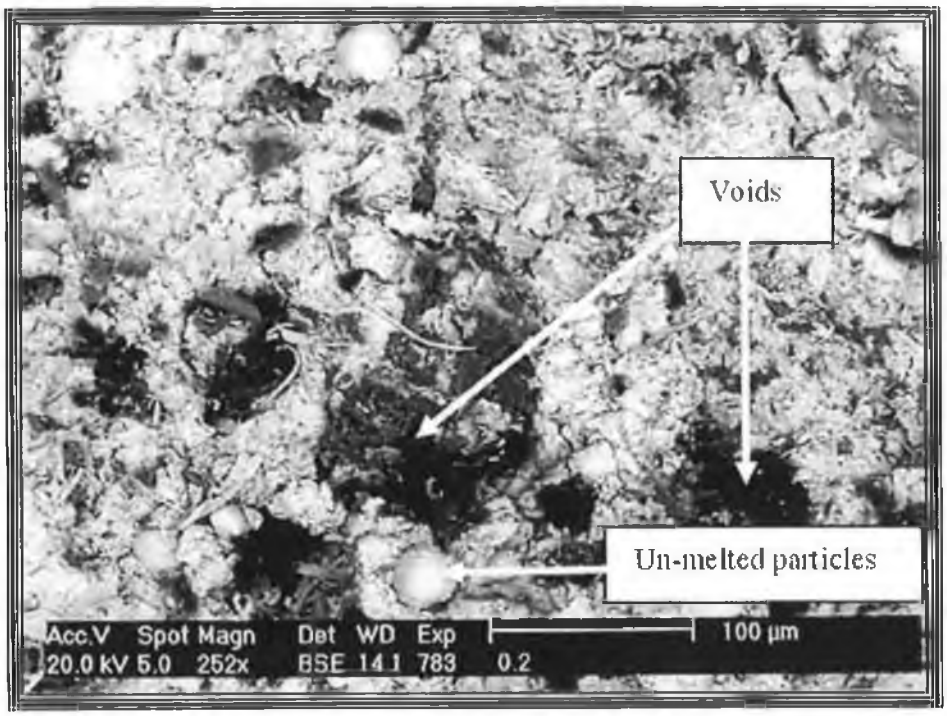

Figure 59 Cross section of Inconel-625 coating post the fatigue test when subjected to four weeks corrosion.

Table 11 Chemical composition of locations B and C as shown in Figure 58.

Location B			**Location C**		
Element	Wt %	At %	Element	Wt %	At %
O	12.03	33.80	O	34.29	37.42
Mo	10.42	4.88	C	27.86	40.50
Cr	18.77	16.22	Al	30.52	19.75
Fe	2.68	2.16	Si	0.25	0.15
Ni	56.10	42.94	Mo	0.29	0.05
			Cr	0.97	0.33
			Fe	4.12	1.29
			Ni	1.49	0.44

4.6 EROSION-CORROSION BEHAVIOUR OF HIGH VELOCITY OXY-FUEL (HVOF) THERMALLY SPRAYED INCONEL-625 COATINGS ON DIFFERENT METALLIC SURFACES

4.6.1 Deposit Characterization (post erosion)

The surface microstructure of the Inconel-625 after 500 hours of slurry jet impingement is shown in Figure 60. It indicates that the metal removal was almost uniform over the tested surface due to the proper setting of the jet impingement nozzle stand-off distance and nozzle size, which controls the jet flow over the whole targeted area. Figure 61 shows the micrograph of the eroded surface at higher magnification. It can be seen that the semi-molten particles were more susceptible to metal removal from the coating surface after the tests. This situation was also observed by Kunioshi et al. [156] for Ni-based alloys where coating damage was more concentrated around unmelted particles.

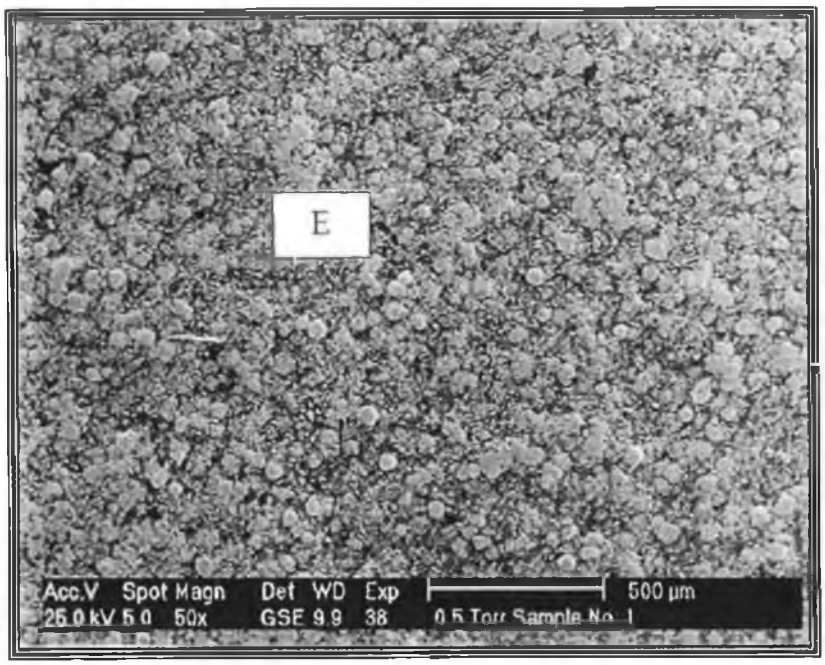

Figure 60 Coating surface after jet impingement testing.

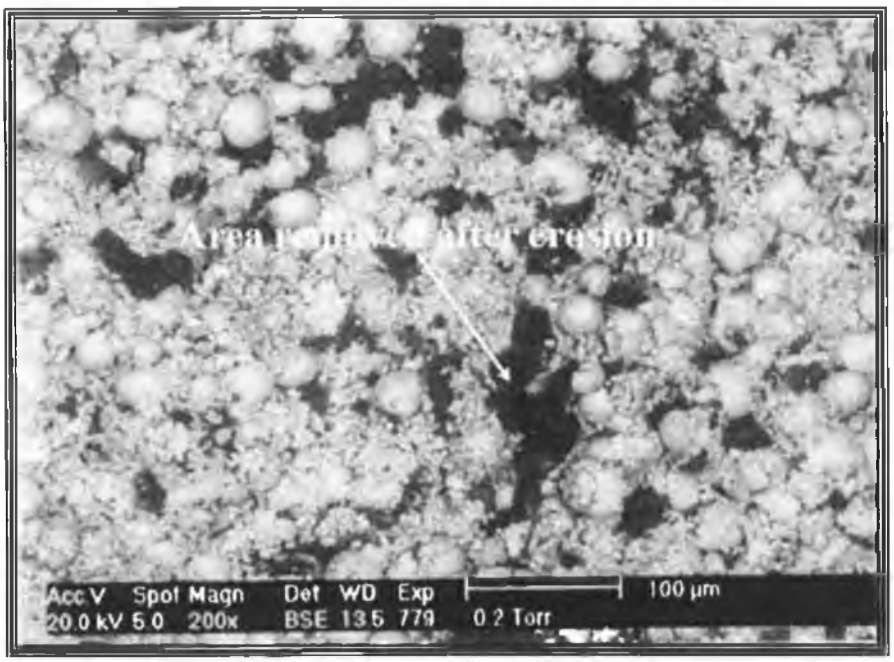

Figure 61 Magnified view of the area depicted as E in Figure 60.

4.6.2 Different Substrate Types (Composite and Welded)

Figure 62 shows a cross section of the Inconel-625 coating applied over various metallic substrates. This reflects the actual use of such a coating in real applications in the oil/gas industries, where the parts are composed of different substrate materials after repair, that is repair through welding, filling, and so on. Thus the substrate has the form of a metal composite. Welding always results in the formation of residual stresses, which are the function of stiffness and the thermal expansion coefficient between the deposit and the substrate material [157]. Consequently, coating over welded substrate raised the stress levels in the deposits causing microcracks or the separation of deposits from the substrate surface [12]. To avoid such an occurrence, the substrates (carbon steel and stainless steel) were preheated prior to welding as preheating improves weldability by reducing the cooling rate and the level of thermal stresses, as well as the shrinkage and possible cracking of the joint [158]. In addition, post-heat treatment and shot peening,

which is another method of stress relief, eliminated the remaining residual stresses in the welded workpiece. Therefore, the welded substrates acted as a uniform composition material during the deposition in the same way as the sample with no welding.

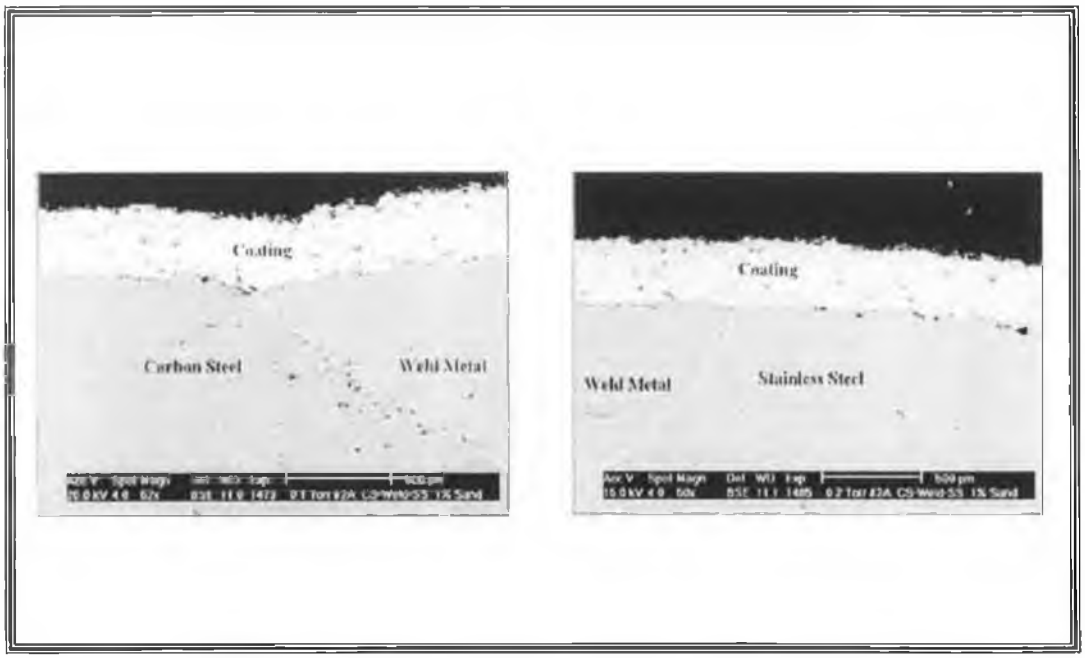

Figure 62 Cross section of the Inconel-625 coating applied over various metallic substrates.

4.6.3 Coating over Spot-Welded Stainless Steel (SW-SS)

Approximately 70% of the samples tested in the present study involved coatings which were applied over welded surfaces, including composite samples (C-CS-SS). It was noted during the coating characterisation of the SW-SS sample that there was no significant change in coating properties, particularly microstructural properties, compared to that applied on the plain stainless steel substrate. This may be due to the fact that the HVOF coating, unlike the welding process, mainly relies on the mechanical interlocking of splats to the substrate surface, regardless of the substrate material type. After the jet impingement tests,

coating over spot-welded stainless steel also showed similar behaviour to that of the coating over plain stainless steel surface. This may be because of the heat treatment of the welded surface prior to coating, following which residual stress levels in the workpiece surface region were minimized.

4.6.4 Coating over Two Dissimilar Metals (C-CS-SS)

Figure 62 illustrates the coating over stainless steel-weld-carbon steel. In terms of coating microstructure, the substrate material and the coating were not affected by the impingement tests. This suggested that the HVOF coating structure was not affected by the inhomogeneity of the substrate material. However, the results of the jet impingement tests showed that greater mass loss occurred over the C-CS-SS region compared to that experienced over the SW-SS and the plain SS coated regions. The mass loss was associated with the vulnerability of carbon steel to corrosion.

4.6.5 Weight Loss

The erosion test results are presented in Table 12, which shows the weight loss and erosion rate per substrate type. Erosion rate results were obtained twice for each case, before and after cleaning. It was observed that in some cases, when the 1% silica sand erosive media were used, the final weight before cleaning resulted in a weight gain rather than weight loss. This was due mainly to the presence of silica sand impinged inside the voids of the eroded surface. The presence of voids in the coating also increased coating loss, particularly when the impinged fluid contained 1% silica sand. The percent weight loss (erosion rate) was higher for carbon steel than for stainless steel.

Table 12, Mass loss results from jet impingement testing during (500 hrs) timing.

Substrate type	Seawater condition	Initial weight (gm)	Final weight (before cleaning) (gm)	Final weight (after cleaning) (gm)	Weig ht loss (gm)	Erosion rate (mg/g)	Average erosion rate (mg/g)
SS	Pure	13.24	12.93	12.92	0.31	2.36E-04	
	Pure	13.35	13.04	13.03	0.32	2.41E-04	2.30E-04
	Pure	13.86	13.57	13.56	0.29	2.14E-04	
	1% Sand	13.21	13.21	12.76	0.45	2.43E-04	
	1% Sand	12.95	12.44	12.44	0.51	2.63E-04	2.51E-04
	1% Sand	13.21	12.79	12.78	0.43	2.47E-04	
SW-SS	Pure	13.65	13.43	13.42	0.23	5.05E-04	
	Pure	13.12	12.78	12.77	0.34	5.05E-04	5.30E-04
	Pure	12.99	12.99	12.67	0.32	5.78E-04	
	1% Sand	13.52	13.02	13.01	0.51	3.41E-04	
	1% Sand	13.25	12.74	12.73	0.52	3.95E-04	3.54E-04
	1% Sand	14.00	13.48	13.46	0.53	3.27E-04	
C-SS-CS	Pure	13.55	12.88	12.87	0.68	3.78E-04	
	Pure	14.06	13.36	13.35	0.71	3.93E-04	3.85E-04
	Pure	13.86	13.07	13.06	0.80	3.83E-04	
	1% Sand	13.23	12.24	12.23	0.99	7.53E-04	
	1% Sand	13.56	12.32	12.31	1.25	9.24E-04	8.68E-04
	1% Sand	14.02	12.73	12.72	1.29	9.26E-04	

4.6.6 Influence of Time

Figure 63 illustrates the variation of weight loss for the different sample conditions with respect to time. In all cases, as the experimental time increased, the weight loss of the coated surface increased. The weight loss of both plain SS and SW-SS exhibited similar behaviour, thus the presence of a weld spot in the substrate had no significant effect on the weight loss of the coating. However, the composite substrate (C-CS-SS) exhibited a much higher degree of weight loss and this significantly increased after 60 hours of testing compared to the other tested conditions. This is mainly because the impinged fluid attacking the substrate material from the sides during testing, that is leaking through the holders, resulted in corrosion that took place in the base material in the region below the coating.

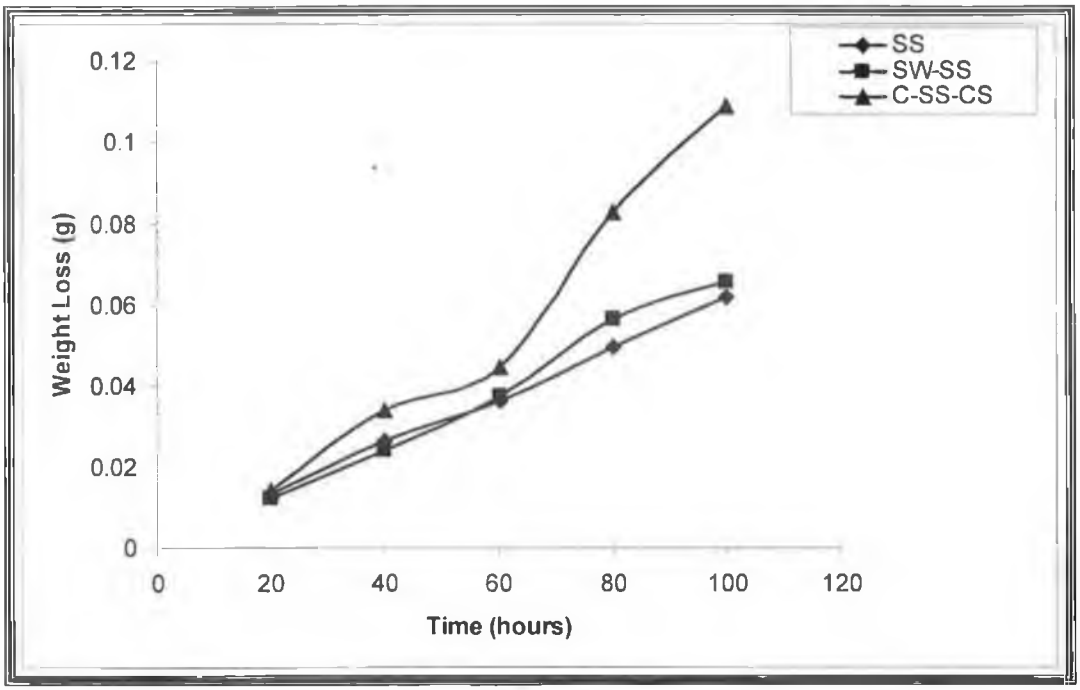

Figure 63 Variation of weight loss with time.

4.6.7 Slurry Effect

Figure 64 shows the variation of weight loss due to fluid condition (pure sea water/ pure sea water containing 1% silica sand) for the three tested substrate types. In all cases, the weight loss increased by approximately 50% when the fluid contained silica sand. Again, both plain SS and SW-SS behaved similarly, presenting no effect of adding weld spots to the substrate with respect to coating resistance. However, the weight loss increased significantly for the C-CS-SS substrate. Both the stainless steel substrate materials (type 306) and weld (type 309) showed excellent resistance to corrosion. However in the case of the 4140 carbon steel substrate, the degree of corrosion was very high, hence the weight loss in the case of the C-CS-SS substrate was not due to weakness in the coating properties, but rather to the corroded area in the carbon steel portion of the tested sample.

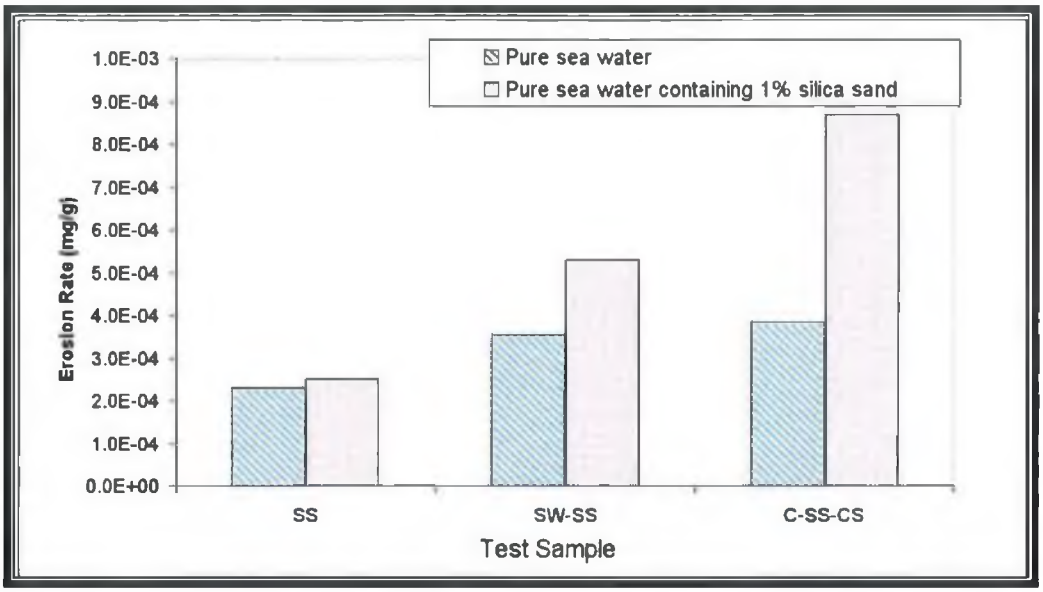

Figure 64 Effect of adding silica sands to the testing fluid.

4.7 TENSILE BEHAVIOUR OF HVOF THERMALLY SPRAYED INCONEL-625 COATINGS ON DIFFERENT METALLIC SURFACES

4.7.1 Effect of Substrate Variation on Coating Performance Due to Tensile Testing

Figure 65 shows the tensile strength behaviour of the plain stainless steel workpiece. It was noted that the coated workpiece exhibited higher tensile strength than the un-coated workpiece, even when the coated workpiece was subjected to a severe corrosive environment. This was similar for the cases of spot-welded stainless steel (SW-SS) and composite stainless steel (C-SS-CS) as shown in Figure 66 and Figure 67, respectively. This indicates that the Inconel-625 coating enhanced the strength behaviour of the stainless steel workpiece (as found in the bending test). It was also found that the corrosion effect on the coated workpiece for both periods two weeks and four weeks was minimal, and they showed a similar behaviour to that of the coated plain stainless steel (SS) workpiece as received. The effect of corrosion became more effective for the SW-SS workpiece, especially when the sample was subjected to aqueous static corrosion for four weeks (Figure 66). This again might be due to the presence of weld in the workpiece which made the workpiece more susceptible to corrosion than when it had no weld.

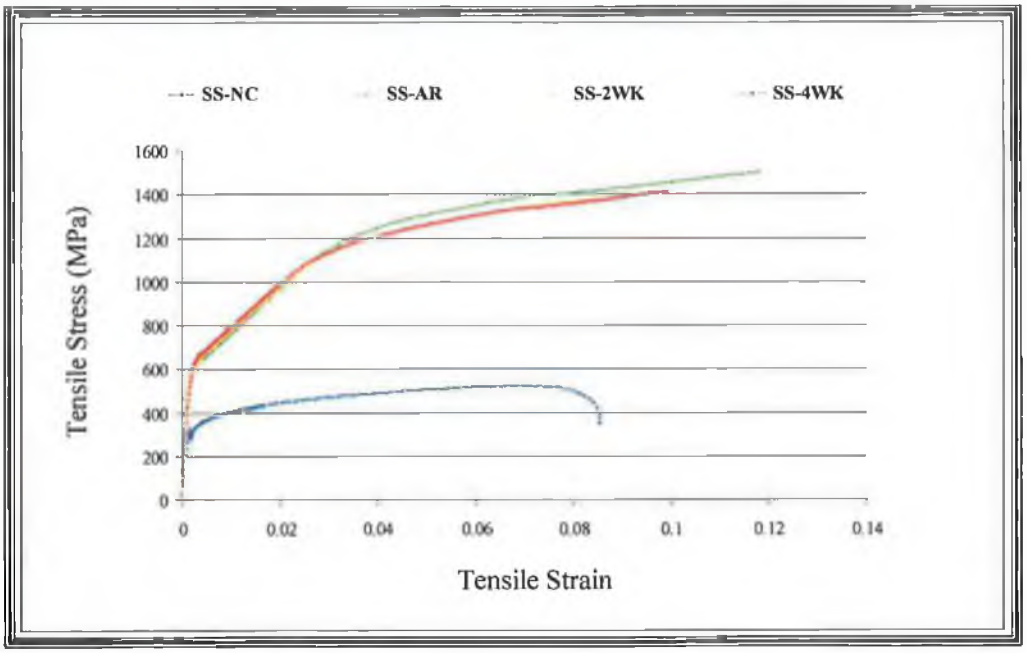

Figure 65 Stress strain curve for plain stainless steel workpiece (SS).

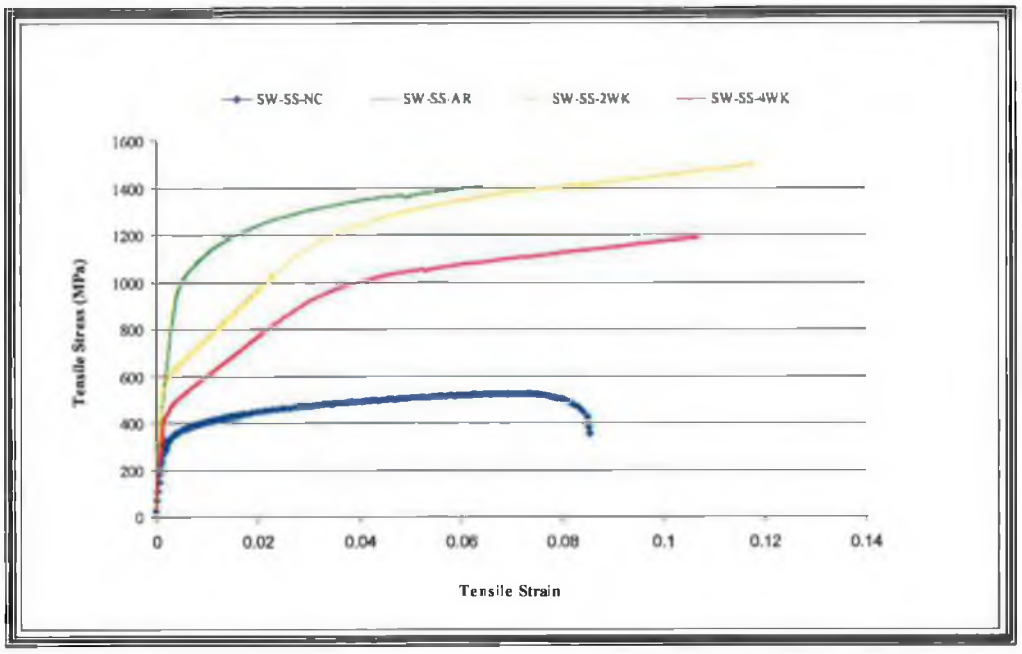

Figure 66 Stress strain curve for spot-welded stainless steel workpiece (SW-SS).

More influence of the corrosion was observed for the (C-SS-CS) workpiece (Figure 67). This might be due to the presence of both the weld and the carbon steel material as a part of the substrate workpiece material.

It is important to note that the yielding limit for the tested samples was changed based on the substrate type and the period of exposure to corrosive media. For instant, the yielding for plain stainless steel sample tested after four weeks of exposure to corrosive media dropped from 600MPa to 420MPa when changing the sample type to spot welded stainless steel SW-SS. Approximately, the same value was obtained when substrate type was changed to composite stainless steel and carbon steel C-SS-CS. It was observed that the presence of weld or composite material enhance the strength of the material. This may be related to the materials properties which modifies after welding. It is important to mention that even if the material strength was enhanced, the corrosion effect behave similarly like all other cases reported from other tests i.e., the coating resistance to the tensile test decreased when the exposure to corrosive environment increased.

4.7.2 Deposit Characterization Post Testing

Figure 68 shows a typical cross section of the Inconel-625 coating over the stainless substrate before corrosion and tensile testing, where the uniformity of coating distribution over substrate surface is observed. Figure 69 shows the sample after tensile test, subjected to aqueous static corrosion for four weeks. It was observed that the coating exhibited a transverse failure through out the sample. This is could be related to the brittleness of the coating. The coating cross-section after the tensile test is shown in Figure 70. It was noted that cracks propegated around the non-melted particles. This is may be due to the availability of surounding voids created during spraying. These voids will also aid in the cracks propagation through aqueous solution towards the coating substrate interface. This is clear from the close view of coating cracks subjected to four weeks aqueous corrosion shown in Figure 71. Figure 72 shows how cracks propagated towards the

weekest points, while some of the cracks intiated and then stopped when they met the tough region.

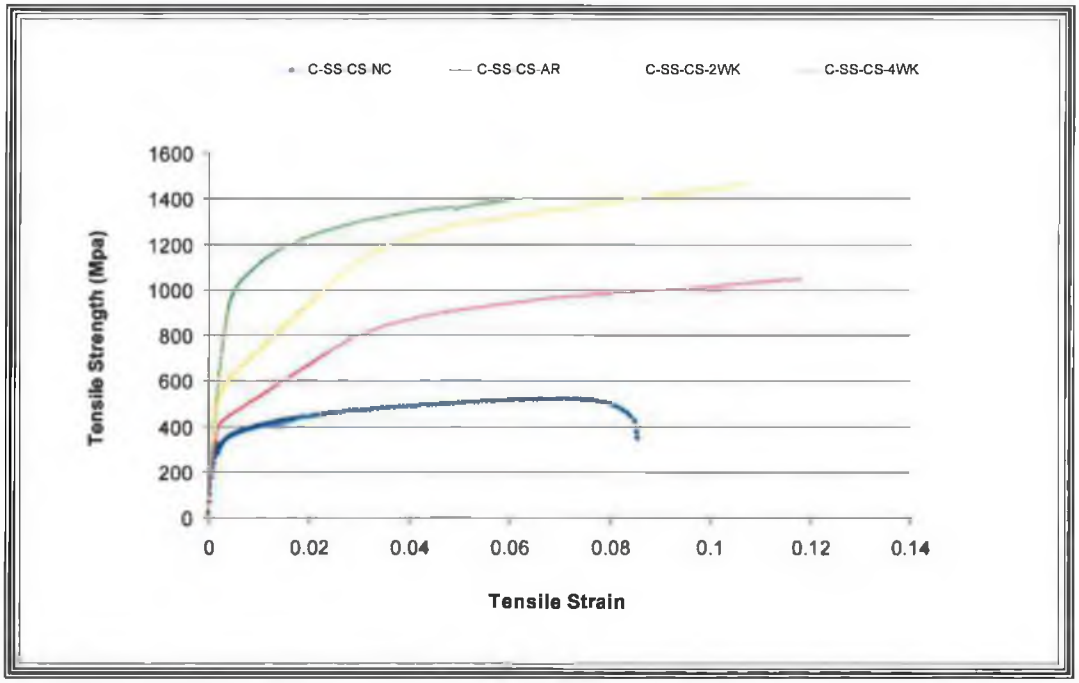

Figure 67 Stress strain curve for composite stainless and carbon steel workpiece (C-SS-CS).

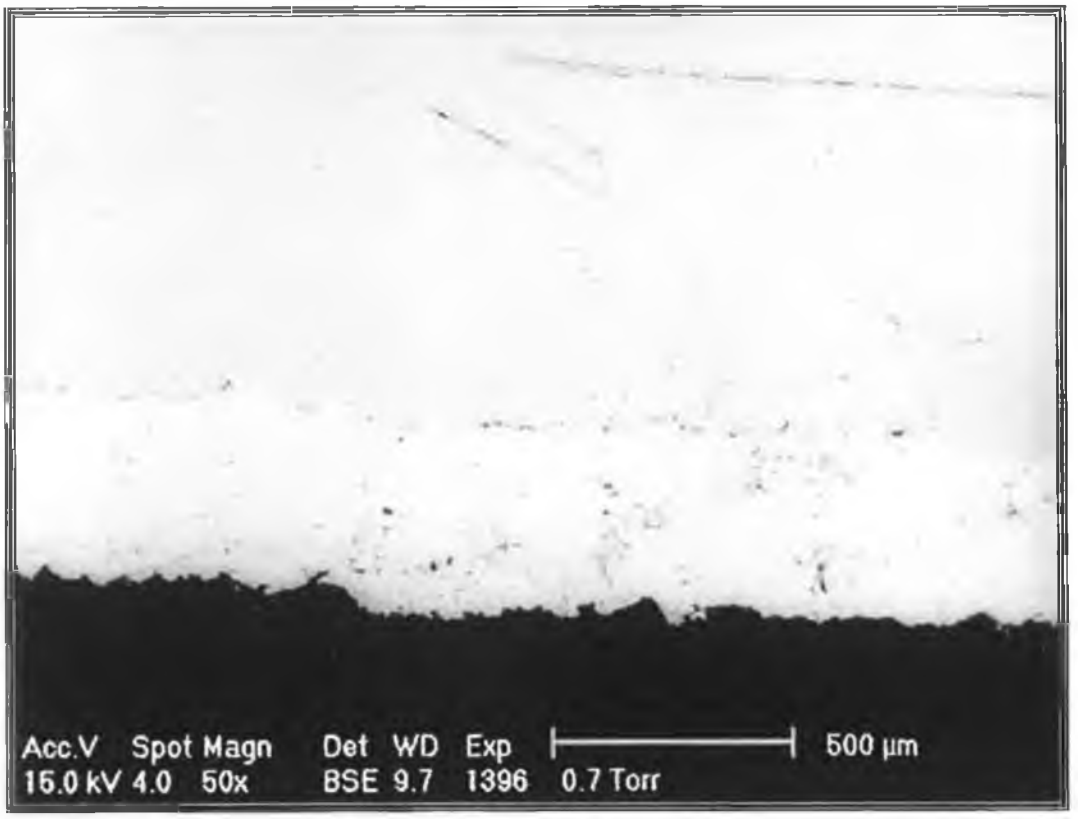

Figure 68 Cross section of tested coating.

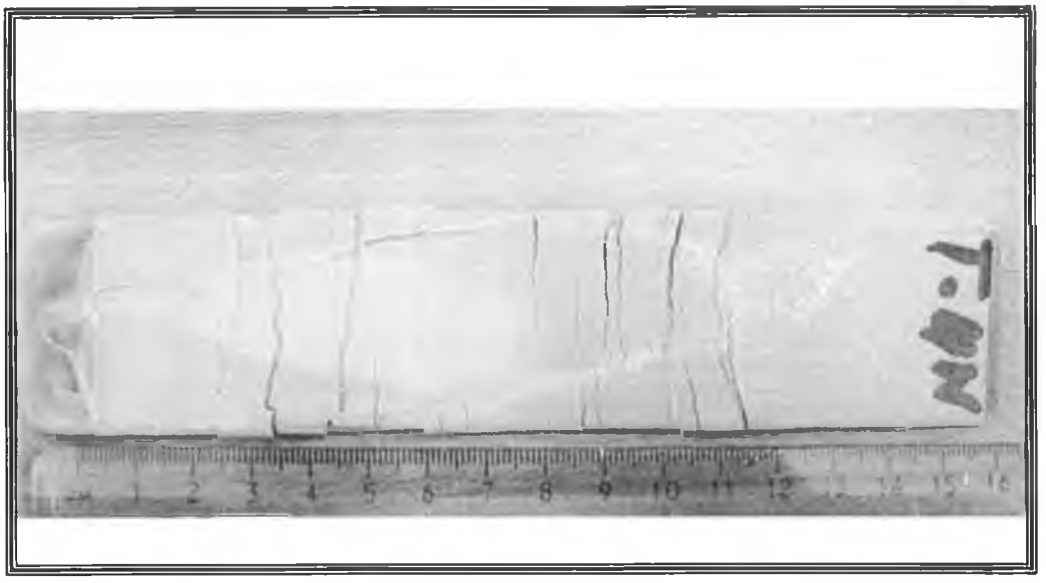

Figure 69 Photograph of plain stainless steel (SS) after tensile test.

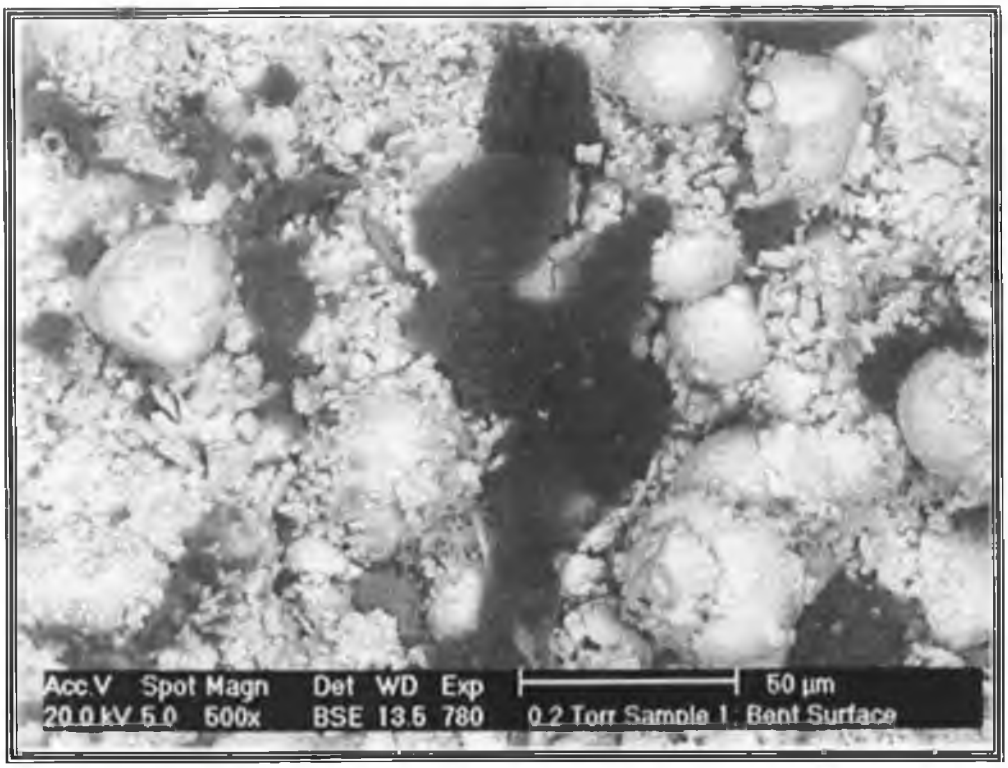

Figure 70 Coating after corrosion-tensile test.

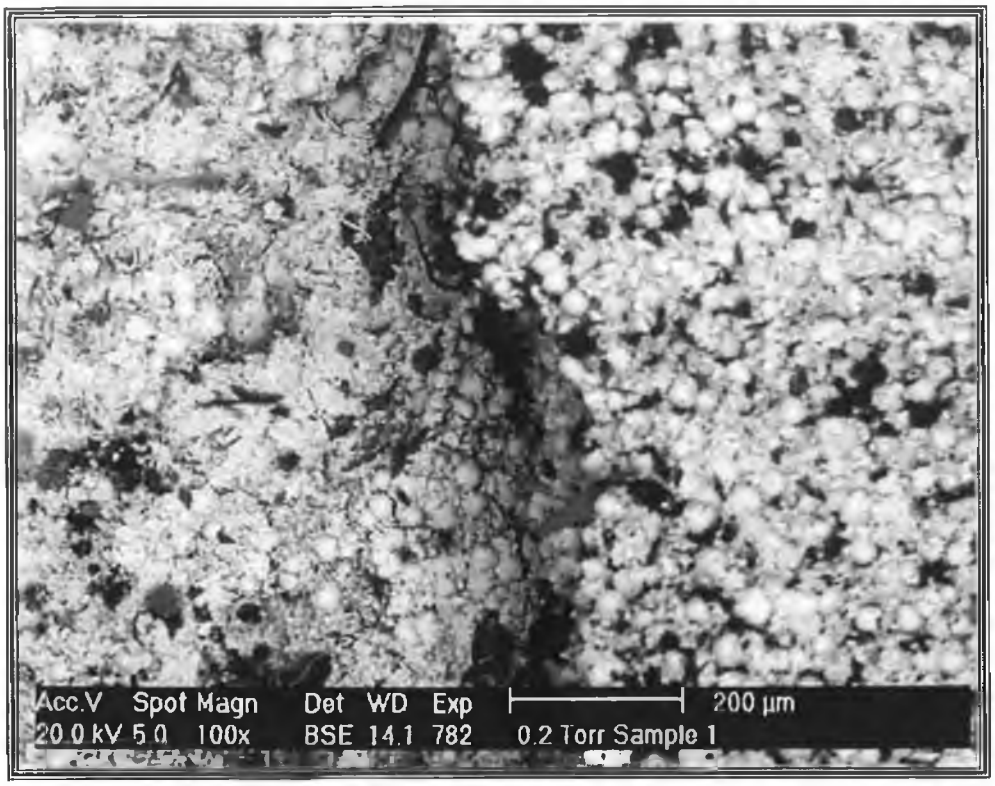

Figure 71 Cross section of tested coating after tensile test.

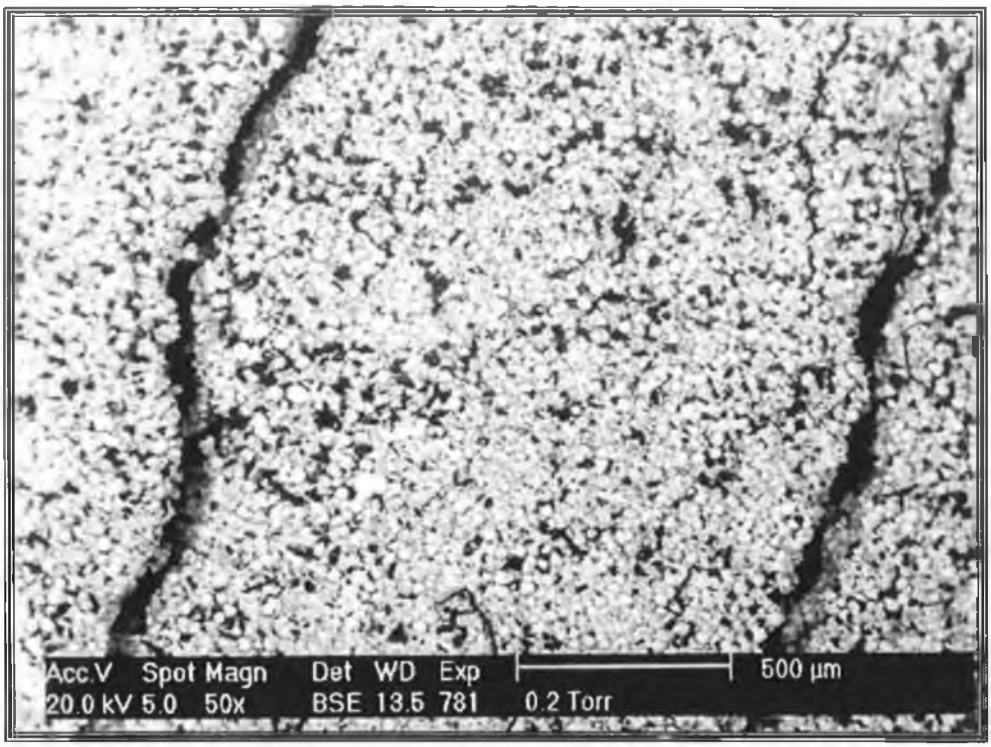

Figure 72 Coating surface after tensile testing.

4.8 MODELLING OF RESIDUAL STRESSES VARIATION WITH SUBSTRATE TYPE

As mentioned in chapter 3, the residual stresses modelling was carried out in two ways; one by subjecting the sample to various temperatures until the resulting deflection equal that found using Clyne's method (Thermal Model). In this case the deflection value obtained at the centre of the sample in the Y-direction, was 0.037 mm (Figure 73). The procedure to calculate the deflection using Clyne's method is shown in [62]. Once the deflection was achieved then the Von Mises stress distribution across the sample was outputted. According to Stokes [62], the important stress results were at the interface of the model for the thermal load analysis.

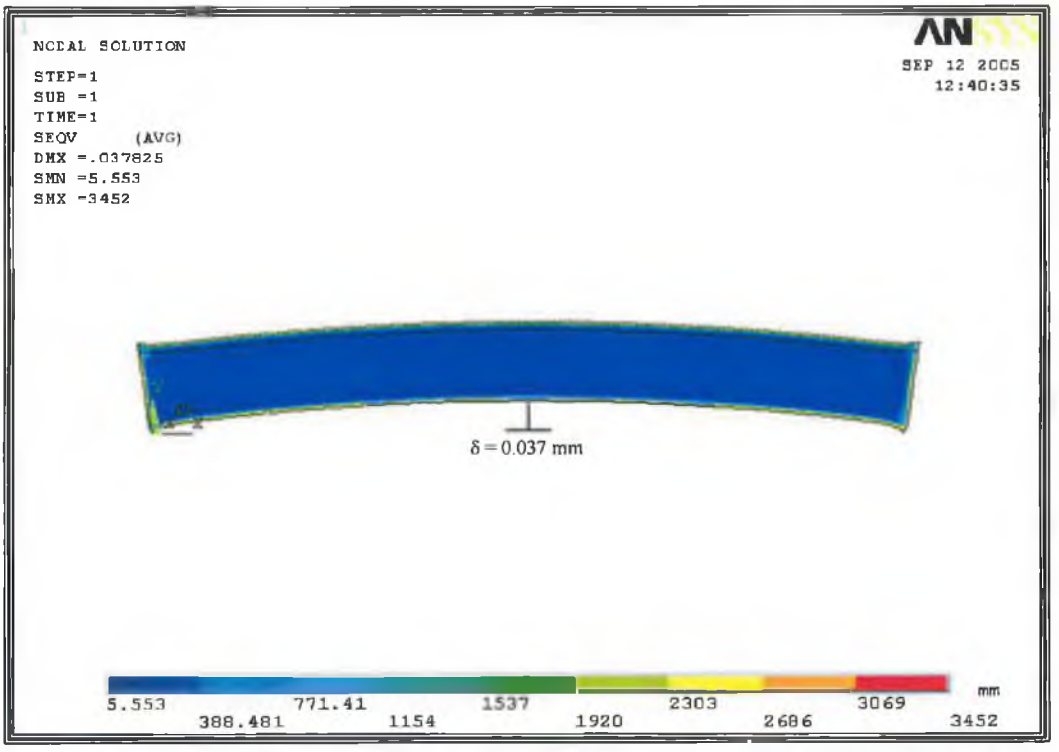

Figure 73 Deflection of plain stainless steel (SS) sample due to thermal load.

The second method involved applying a deflection to the sample in order to generate a moment (Figure 74). Again, according to Stokes [62], the stress distribution at the top of the deposit and at the bottom of the substrate were of interest in determining the stress distribution of the sample. The results were found by carrying out a path plot across the various locations (Top of Coating, Interface and Bottom of Substrate) to get the exact value for stress at each of these locations. The results of each model were then combined to produce an overall stress distribution across the sample (Figure 75).

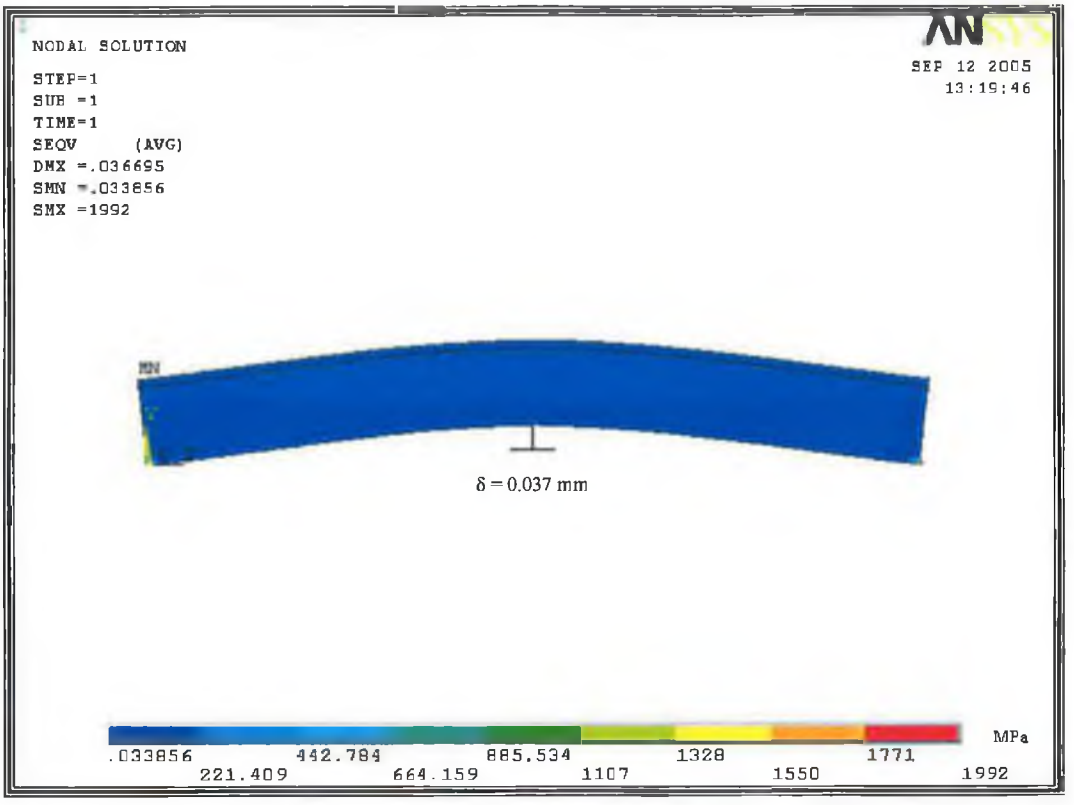

Figure 74 Deflection of plain stainless steel (SS) sample due to moment load.

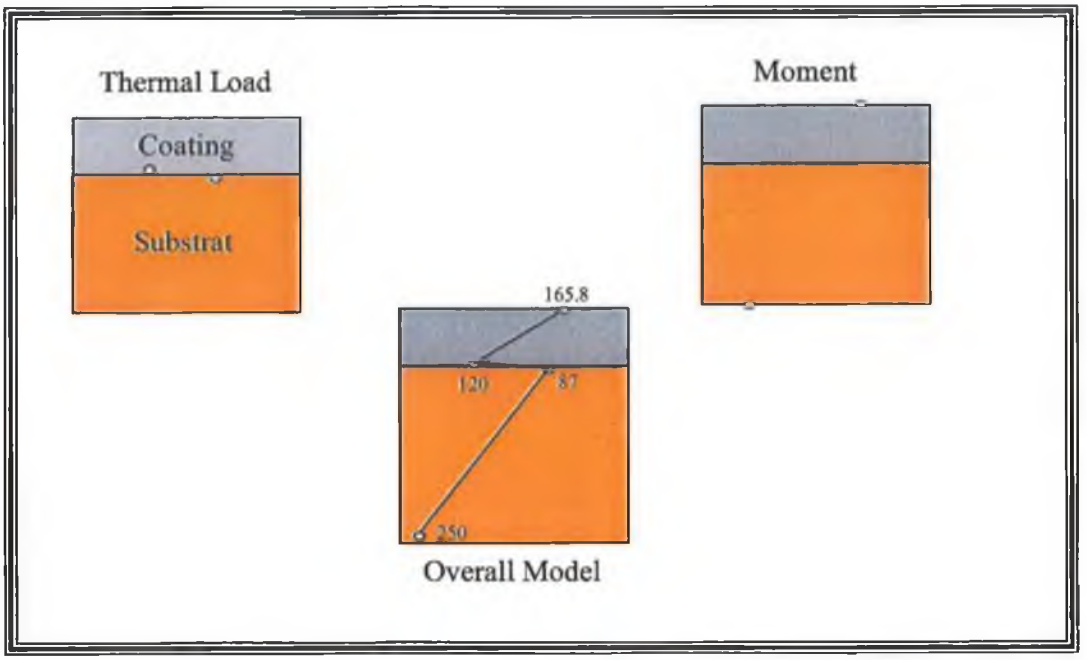

Figure 75 Overall stress distribution across the sample.

4.8.1 Validating the Model

Clyne's method was applied using the same deflection used in the FEA. For instant, the deflection value calculated using Clyne's method for this case was found to be 0.037 mm. It is important to note that this value (0.037 mm) was obtained based on the physical properties of the tested materials and the applied temperature. The same value is then used in the FEA to determine stresses. Stokes [62] used this method and found it to be very effective to determine the residual stresses in WC-Co deposit.

Figure 76 shows a comparison between the combined modelling and the analytical results obtained using Clyne's method. It was observed that the profile of the stress distribution along the coating and substrate was similar with a maximum

variation of approximately 20% at the top of the deposit. As the model and clyne's method are based on numerical and analytical techniques, therefore these results should be validated using experimental data.

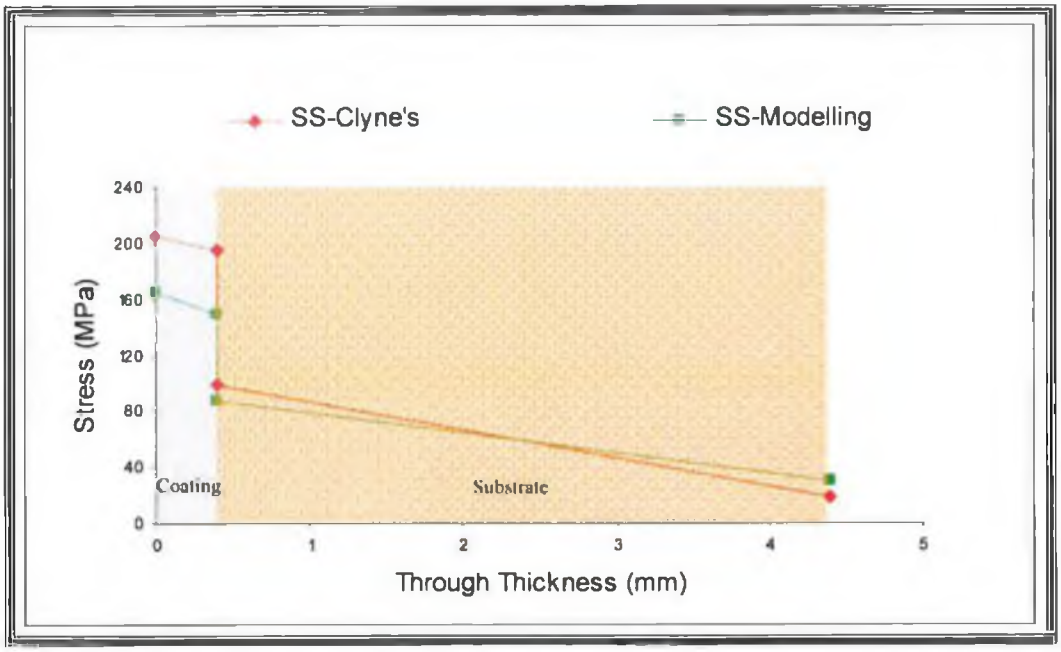

Figure 76 Finite element and analytical stress analysis of Inconel-625 deposit over plain stainless steel substrate (SS).

Stokes [62] validated the proposed model and Clyne's analytical method experimentally (Figure 77). The results of the research showed that the variation found between stresses obtained by Clyne's and the experimental results were negligible. Hence, it becomes appropriate to use Clyne's method in this case to validate the models proposed in this research. The maximum difference between FEA and Clyne's was found to be 23%, 40%, and 37% at the top of the coating, the interface and the bottom of the substrate respectively (Figure 77). However, Clyne's method does not take into account conduction and thermal difference through the sample, hence this would contribute to the error, where as the model did.

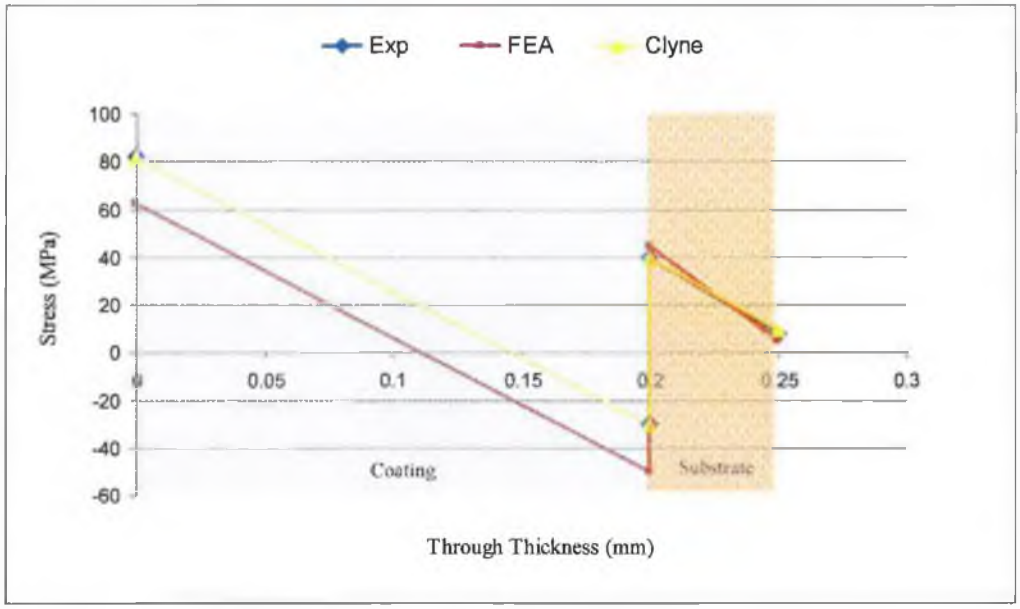

Figure 77 Finite element, experimental and analytical stress analysis of a 0.2mm thick deposit [62].

It is important to note that Clyne's method can be only applied where deposit exist over single material substrates. Therefore this method was implemented to predict the stress distribution in the stainless steel substrates without a weld or joined to other steel material coated with Inconel-625.

For the plain stainless steel substrate (SS), the stress at the top of the deposit was found to be 205 MPa using Clyne's and 165 MPa using FEA. So the model predict an error of 24% which was similar to that found by Stokes [62] for WC-Co deposit. In both methods, the stress decrease across the coating by 4.8% approximately. This small change in stress was associated to the small deposit thickness used (0.4 mm). Stokes [62] found that the stresses changed significantly with increased coating thickness. The model stress at the interface ranged from 150 MPa on the deposit interface side to 87 MPa at the substrate side. Clyne's

distribution at this interface indicated a change from 190 MPa to 92 MPa, so while the model did not match these values, it did predict the same profile.

The change in the stress is due to the difference in the physical properties between coating and substrate (misfit strain) as indicated previously by Clyne's [152]. The stress at the bottom of the substrate was found to decrease by more than 75% compared to the stress at the top of the substrate. This large decrease in the stress was mainly associated with the large substrate thickness (4 mm) used compared to coating (0.4 mm).

4.8.2 Comparison of Each Model Based on Substrate Type

(1) Measurements at the Centre of the Model

Figure 78 shows the distribution of stresses taken from models based on substrate type, plain stainless steel (SS), spot welded stainless steel (SW-SS), and composite stainless steel and carbon steel (C-SS-CS), where the measurements were taken at the centre of the sample. As described in the previous section, Clyne's equations (Equation 4-7) could not be applied to this section when the various coated samples were compared. It was found that the stresses at the top of the deposit were equal to 165 MPa in all cases. This is mainly because the material used for deposition is the same in all cases (Inconel-625) and the substrate type had no influence on stress on the top of the coating. However, a noticeable change was observed at the coating/substrate interface for each substrate type. Using equations 2 and 3 for quenching and cooling, this result can be validated. The stress that affects the deposit mainly occur during spraying, therefore the quenching stress contributes to the stress at this stage according to equation 2. Therefore, substrate type has no influence on the quenching stress (Table 11). Therefore this suggests the results of all three substrates types having the same stress at the top of their respective coatings. For SS, the stress was found to be ranged from 88 to 120MPa, however, for the SW-SS the stress value increased by 17%. The stress

value was increased by 25% when the substrate is change to be (C-SS-CS). This is due to the variation of substrate material properties. Again, looking at equations 2 and 3, the effect of stress at the interface is mainly due to cooling stress and misfit strain (equation 8).

When the substrate type changes more, both stiffness and coefficient of thermal expansion varies between the samples, thus resulting in a change in cooling stress (Table 11). All stresses were found to be quite similar in the range of 78-80 MPa at the bottom of the substrate. As the substrate was quite thick the effect of applying a coating to such a substrate had little effect on stress generated at the bottom of the substrate.

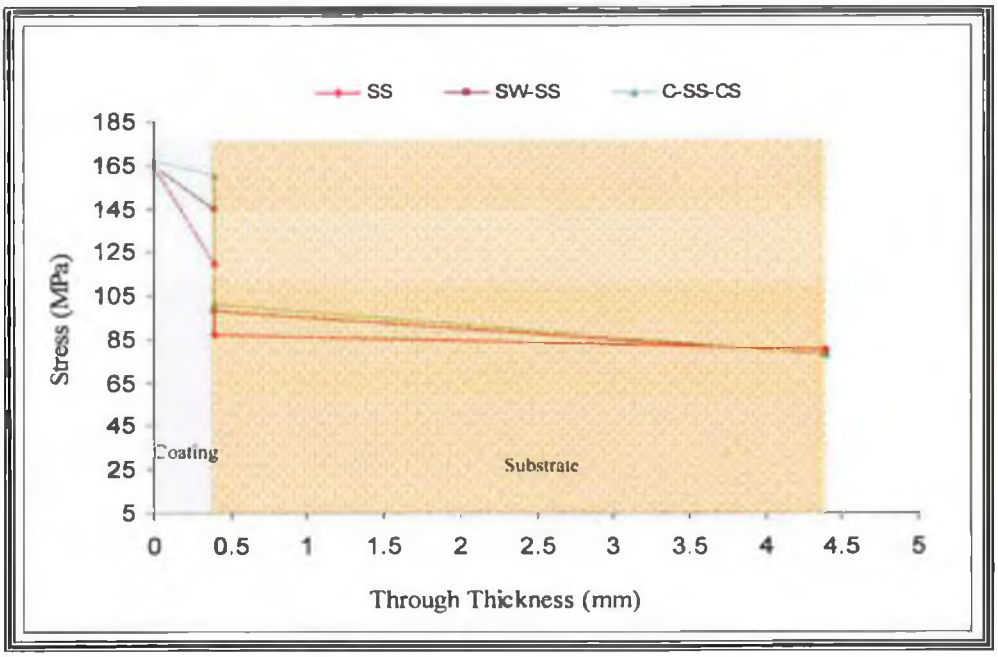

Figure 78 Variation of residual stresses based on substrate type.

(2) Comparison of Stresses at Different Regions in the SW-SS Substrate

Figure 79 shows the stress variation in the spot welded stainless steel (SW-SS) sample. It was found that, at the top of the deposit, the stress at the welded region increased by 27% compared to the non-welded region. This variation is due to the fact that the weld at the centre was subjected to more stress than the stainless steel at the edges. The stress at the interface shows the highest effect. It can be seen that the welded region (I) ranged from 145 MPa (on coating side) to 100 MPa (on substrate side), whereas the un-welded region (II) only experiences a change of 10 MPa. Hence, while the deflection experienced in region (II) was lower than that in region (I), there was also another contribution to this stress change. This can be validated again by cooling stress and misfit strain equations. The change in stiffness and coefficient of thermal expansion across these two regions would have increased the stress in the welded zone (Table 11).

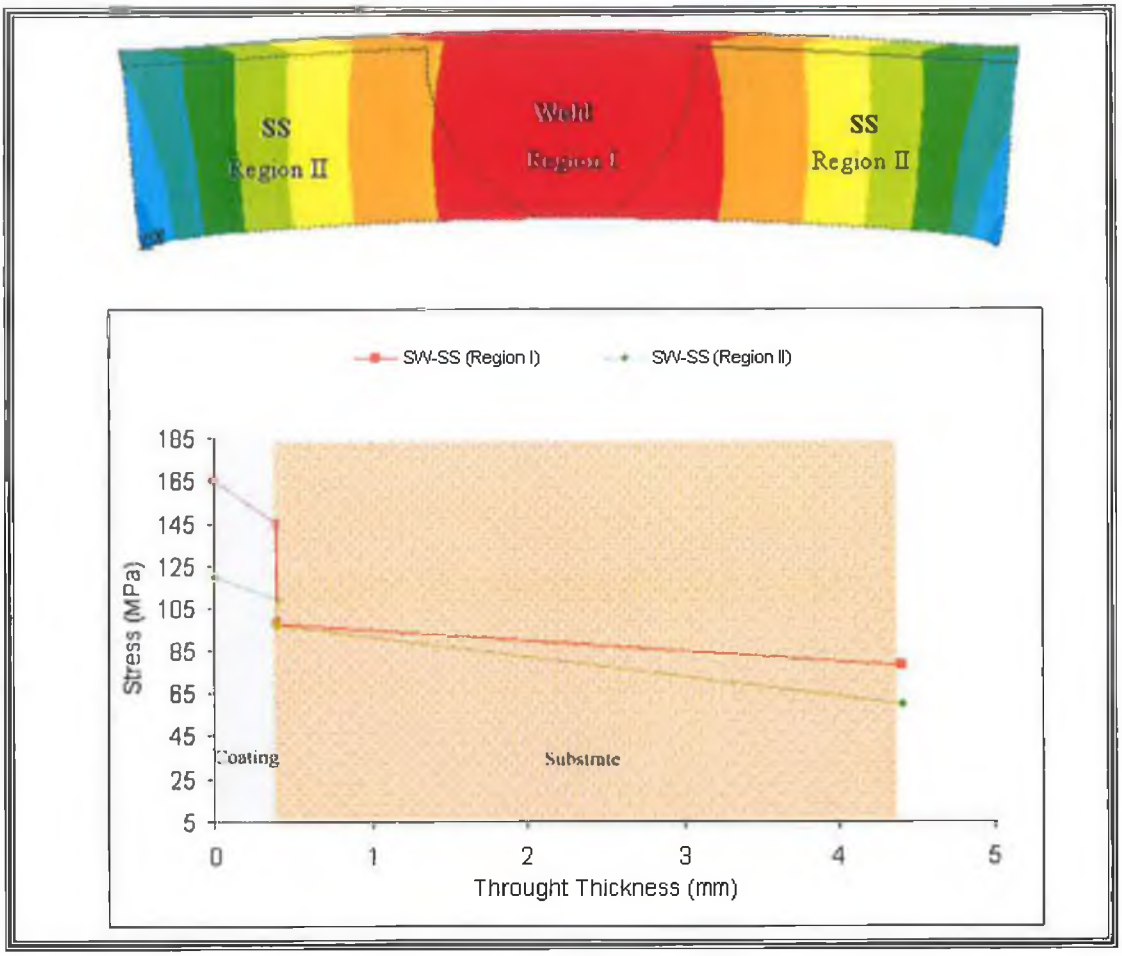

Figure 79 Variation of residual stresses at different regions in (SW-SS).

(3) Comparison of Stresses at Different Regions in the C-SS-CS Substrate

Figure 80 shows the stress variation in the composite stainless steel and carbon steel C-SS-CS sample. It was found that, at the top of the deposit, the stress at the welded region (III) was 28% higher than that of the stress at the carbon steel Region (I) and the plain stainless steel Region (II). This variation was again as a result of the weld at the centre been subjected to more stresses than the carbon steel (CS) and the stainless steel (SS) at the edges. Moreover, the stress ranges at the interface increased dramatically in the welded region by 28% compared to stainless steel region and by 31% compared to carbon steel region due to stresses generated

by presence of weld. Again this is due to the stiffness and coefficient of thermal expansion effects on the misfit strain and cooling mechanisms involved in the stress development in the deposit (Table 9).

Using equations 2 and 3, Fig. 81 shows how overall residual stress changes across the SS 316 to SS 309 (weld) back to SS 316 sample. The weld increases the stress in the deposit by 12 MPa across the welded region. Comparing that to the stress for the Carbon-Steel weld-Stainless Steel substrate, Figure 82 shows that the stress increases from stainless steel to weld by 12 MPa, but from the weld to the Carbon Steel by a further 88MPa. Therefore, welding two different steels together with a weld of another steel has a dramatic effect on residual stress generation during and post deposition. Although these values are low, it must be understood that they are approximate, therefore the realistic effect may not be appreciated in these results.

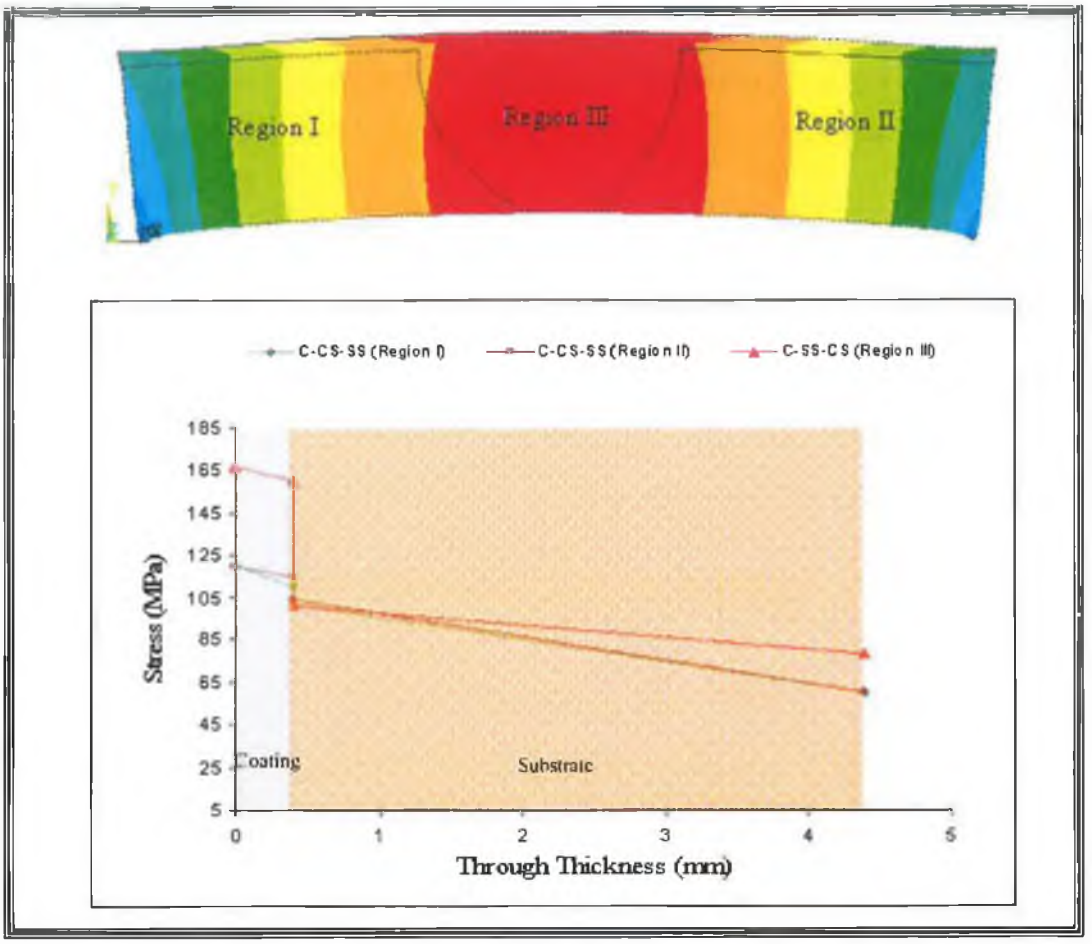

Figure 80 Variation of residual stresses at different regions in (C-SS-CS).

Table 13 Quenching and cooling stresses variation between coating and substrate.

Stress (MPa)	SS	SW-SS	C-CS-SS
*Quenching	265	265	265
**Cooling	-163	-153	-64
Overall Residual Stress	98	112	199

*$\sigma q = Ec \times (Tc-Ts) \times \alpha c$, ** $\sigma c = \dfrac{\left[Ec \times \Delta T(\alpha c - \alpha s)\right]}{\left[1 + 2\dfrac{Ectc}{Ests}\right]}$

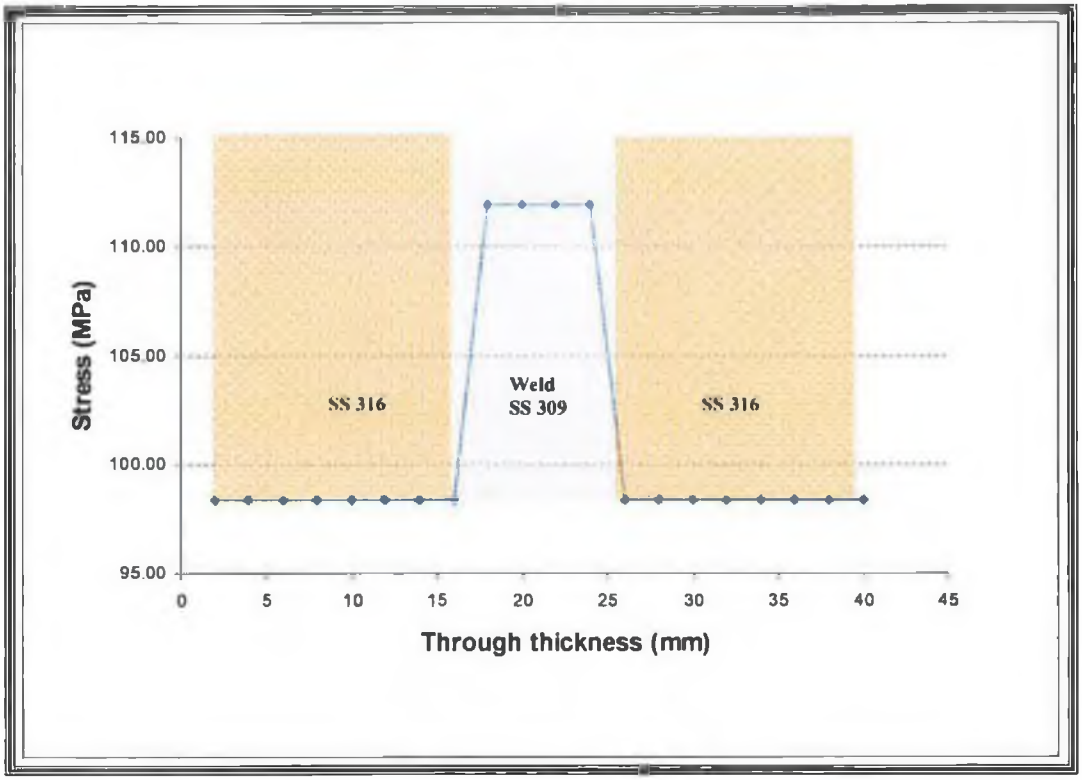

Figure 81 Residual stresses across the SW-SS sample.

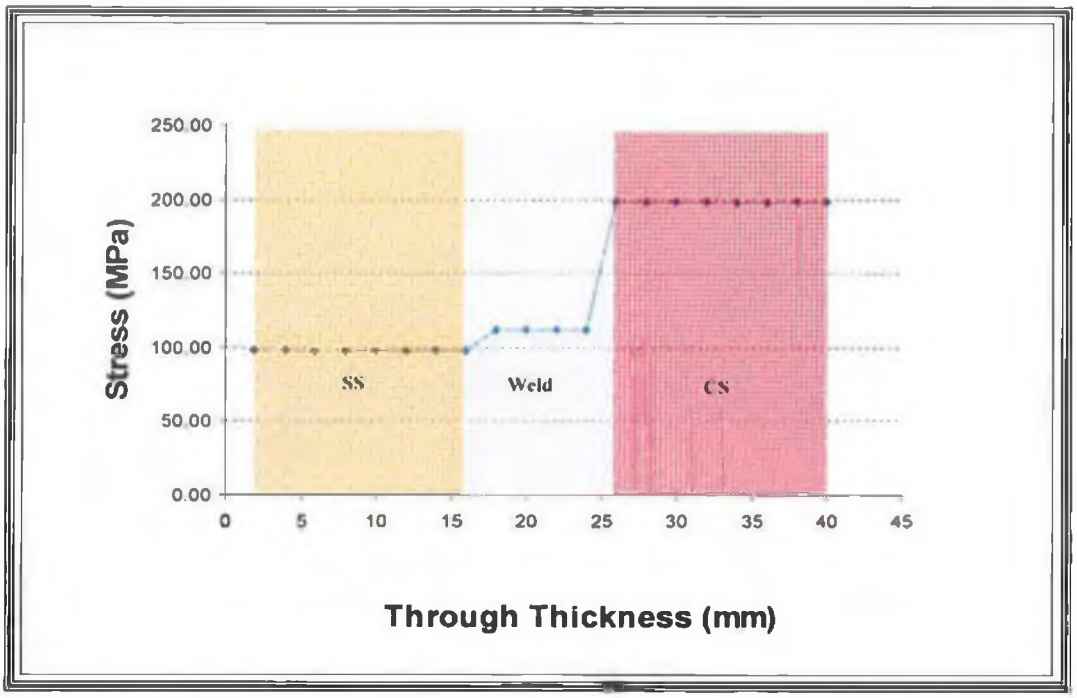

Figure 82 Residual stresses across the C-SS-CS sample.

5

CONCLUSIONS AND RECOMMENDATIONS

5.1 CONCLUSIONS

In the present study, coating charactaristics and mechanical properties of HVOF Inconel-625 coating onto stainless and carbon steel weld joints were examined. The material's resistance to several mechanical tests - including bending, fatigue, erosion-corrosion, and tensile testing, where the coating material was applied over plain, welded and composite substrate materials has been investigated to determine the effect of possible failures of the substrate material when subjected to sever corrosive and erosive environments combined with different mechnical loadings. Furthermore, residual stresses evaluation, using modelling and analytical methods, were used to predict the influence of residual stress when the coating was applied over different metallic substrates. The conclusions resulting from invistigations are summarised as follow:

- The EDS analysis on page 85 showed that the oxide formed in the coating contained mainly the Cr_2O_3 phase. This is mainly due to the high temperature of the deposited particles and presence of air molecules captured in voids between the non-melted or semi-molten particles and the next bonded splats. It was also observed from the EDS analysis that other types of oxides were present at the interface between the coating and the substrate, namely Al_2O_3 and SiO_2. This is because some grit blasting material remained after the surface preparation process where both Al_2O_3 and SiO_2 grits were used in workpiece surface preparation prior to coating.

- The oxygen content in the deposited particles was found to be low and oxide formed in flight was mainly distributed over the surface. The deterioration of the coating occurs along the deposited particles boundaries and corrodes the material nearby as shown by the SEM analysis.

- The cavitations in the interface between the coating and base material seem to have accelerated the corrosion of the coating as well as base material, i.e. as a results of the inter-corroded porosity, the electrolyte could then penetrate the coating and attack the substrate material, even tough the coating was resistant to the corrosive environment. Consequently, the substrate material could be corroded beneath the coating lowering the mechanical properties at the interface.

- Heat Affected Zone (HAZ) corroded easily once the corrosive solution penetrated the coating. This indicates that Inconel-625 coating protected these different metallic substrates against corrosion and minimised the effect of corrosion on two materials attached together.

- Inconel-625 powder coating enhanced the corrosion resistance of stainless steel workpiece, and increased the workpiece resistance to bending. However, as the period of exposure to corrosive environment increased from two weeks to four weeks, coating resistance to corrosion decreased.

- Using bending tests analysis, the corrosion resistance of the spot welded stainless steel (SW-SS) coated workpiece significantly decreased compared to the plain stainless steel (SS) ones. The SS ones peaked at 470 → 550 MPa where as the spot welded ones peaked from 525 → 625 MPa. No major variation between the two week and the four week exposed samples was noted. Also, the length of time, within the tests performed, did not

have an effect, it was the corrosion media that reduced the coating capabilities.

- In the bending test analysis for the composite carbon steel and stainless steel (C-CS-SS), the presence of carbon steel in the substrate obviously was effected by the corrosive media, but this media had more of an effect over time on the carbon steel compared to plain steel and spot welded steel. Comparing the composite stainless steel subjected to corrosion for four weeks to the same treatment applied to the plain stainless steel sample both were able to sustain the same stress level ≈ 480MPa. However, the deterioration was much higher for the composite substrate (≈ 120MPa)compared to plain (≈ 30MPa) or spot welded samples (≈ 100MPa).

- Deposit characterisation post bending test showed that the brittleness of the coating triggered crack formation in the coating layer. Since the coating thickness was about 400 μm, it was possible that the maximum of both normal and shear stresses took place at base metal-coating interface. However, the crack initiation at the interface relieved the stress levels in this region which avoided spalling or buckling of the coating.

- In the bending test analysis, plastic deformation and delamination around the coating edge was observed due to the action of shear stress. Moreover, the internal stresses possibly created local stress concentrations, especially at defect locations around the coating base material interface and as soon as the local internal stress for crack propagation was reached, the entire coating failed in this region.

- For the axial fatigue test, both plain and welded stainless steel surfaces behaved similarly for the three different corrosion durations.

- It was observed that the coating enhanced the fatigue resistance of different metallic substrates. There was a reduction of 300 MPa in the fatigue strength of the coating when subjected to four weeks aqueous corrosion medium in both plain and welded surfaces. The fatigue strength reduced to that of their uncoated counter parts after 4 weeks exposure.

- Microscopic observations of the fracture surfaces of the coated test specimen showed that the fatigue cracks was formed at both the interface between coating and substrate and in the coating itself. Availability of non melted particles and voids in the coating, and the presence of SiO_2 particles in the coating substrate interface contributed to crack initiation in the coating and the coating-substrate interface, respectively.

- Erosion corrosion tests were conducted and SEM investigations of the specimen surfaces showed that the material removal was concentrated more around the unmelted or semi-molten particles rather than any other locations in the coating.

- The coating was found to be highly sensitive to the presence of sand particles in the impinging fluid. As the period of coating exposed to the flow of slurry fluid increased, the weight loss increased significantly. This increment was dependent on the type of substrate material.

- It was found from the tensile tests that Inconel-625 coating enhanced the strength behaviour of the stainless steel workpiece (as found in the bending test). It was also found that the corrosion effect on the coated workpiece for both periods of two weeks and four weeks was minimal, and they showed a similar behaviour to that of the coated plain stainless steel (SS) workpiece as received. This showed that that the Inconel-625 was a good alloy choice for use in industry, especially when corrosion resistance is required.

- Inconel-625 coating enhanced the yielding strength of all samples tested regardless of its substrate type and the period of exposure to corrosive environment.

- Presence of weld in the workpiece made the workpiece more susceptible to corrosion than when it had no weld. More influence of the corrosion was observed for the (C-SS-CS) workpiece. This may be due to the presence of both the weld and the carbon steel material as a part of the substrate workpiece material. Therefore, even if the presence of the weld might not result into the coating failure, it could be highly recomended to avoid it unless there is no choice except having it. In this case, regular inspection of the coating for evidance of corrosion attack would be highly recommended. This was because when the corrosive solution penetrated the coating the weld and the carbon steel area would corrode very fast resulting into a catastrophic failure. This could be de due to electrocell formation between the disimilar metals, leading to electrochemical corrosion.

- For the plain stainless steel substrate (SS), the stress at the top of the deposit was found to be 205 MPa using Clyne's and 165 MPa using FEA. An error between the model and analytical of 24% can be seen. In both methods, the stress decreased across the coating by approximately 4.8%. This small change in stress was associated with small deposit thickness used (0.4 mm).

- The FEA stress model indicate a stress at the interface ranged of 150 MPa on the deposit interface side and 87 MPa at both of the substrate. Clyne's distribution on the other hand, indicated a change from 190 MPa to 92 MPa, so while the model did not match these values, they did predict the same profile. The change in the stress was due to the difference in the physical properties between coating and substrate material (misfit strain).

- The stress at the bottom of the substrate was found to be below the stress at the top by more than 75%. This large difference in the stress was mainly associated with the large substrate thickness (4 mm) used as compared to coating (0.4 mm).

- The numerical study, analytical and expermintal methods showed that the stress at the interface had the highest effect on coating failure. The difference in stiffness and coefficient of thermal expansion between the substrate and the weld and between these and the deposit increased the stress above the welded zone in the deposit. This increase in residual stress makes the sample more susceptible to bending, fatigue, erosion-corrosion, and tensile stresses, therefore it should be avoided in repair.

5.2 RECOMMENDATIONS FOR FUTURE WORK

The results documented in the present research are significant, however further recommendations are as follows:

- Testing Curved Surfaces:

  All tests were performed on plain or round surface such as plates and shafts; however, assessments of coating performance on spherical surfaces could help to improve the practical application of the coating onto valves and spherical joints.

- Comparison and Coating of other Materials:

  The current study was very comprehensive for the Inconel-625 material as a Nickel based alloy; however, in the industry many different types of powders are used. Therefore, it is highly recommended to compare the available tests to other types of powders such as those that contain carbides.

- Experimental Test for Residual Stresses:

  The prediction of residual stresses in this work was done using modeling and analytical methods and the results were validated using experimental work which was conducted on other type of powder WC-Co. Therefore, it is recommended to extend the current work to include experimental test for the residual stresses, which is generated when depositing Inconel-625 powders.

PUBLICATIONS ARISING FROM THIS WORK

Journals

1. **Al-Fadhli, Hussain Y**, J. Stokes, M.S.J. Hashmi, and B.S Yilbas "HVOF Coating of Welded Surfaces: Corrosion-Fatigue Behaviour of Stainless Steel Coated with Inconel-625 Alloy", Surface & Coatings Technology, (2005), Article in Print, (Available Online).

2. **Al-Fadhli, Hussain Y**, J. Stokes, M.S.J. Hashmi, and B.S Yilbas "The Erosion-Corrosion Behaviour Of Inconel-625 Coating Thermally Sprayed Using HVOF Process Applied Over Different Metallic Surfaces", Surface & Coatings Technology, (2005), Article in Print, (Available Online).

Conference Papers

3. **Al-Fadhli, Hussain Y.**, "Influence of HVOF setting parameters on Nickel-Based Alloy Powder (Diamalloy 1005) Coating Properties", Proceeding from the 1st international surface engineering congress and the 13th IFHTSE Congress, (2002), pp. 549-554.

4. **Al-Fadhli, Hussain Y.**, B.S. Yilbas, and M.S.J. Hashmi, "HVOF-Coating of Metallic Surfaces: Coating Response to Corrosion and Bending" Proceeding of the International Thermal Spray Conference, Basel, Switzerland, May 2-4, 2005 - pp. 695-699.

5. **Al-Fadhli, Hussain Y.**, J. Stokes, M.S.J. Hashmi, B.S. Yilbas, I. Taie and S. Mehta "Modelling of HVOF Coating Deposit Applied over Different Metallic Surfaces and Tested in Highly Corrosive Environments". 11th Middle East Corrosion Conference February 26 – March 1, 2006, ***Accepted for Publication***

Poster Papers

6. **Al-Fadhli, Hussain Y.**, J. Stokes, M.S.J. Hashmi, and B.S. Yilbas "Erosion-Corrosion Characteristics of Inconel-625 Coating Sprayed by the HVOF Process and Applied over Different Metallic Surfaces". WOM 2005, San Diego, USA.

7. **Al-Fadhli, Hussain Y.**, J. Stokes, M.S.J. Hashmi, and B.S Yilbas "Tensile Strength Behavior of Plain and Welded Stainless Steel Coated with Inconel-625, Thermally Sprayed Using HVOF Coating", AMPT 2005, Wisla, Poland.

8. **Al-Fadhli, Hussain Y.**, J. Stokes, M.S.J. Hashmi, and B.S. Yilbas "Post Test Analysis of Inconel-625 (HVOF) Coating Using SEM and EDS after Exposure to Erosion-Corrosion Test", M&M 2005, Hawaii, USA.

REFERENCES

1. Scrivani, A., Lanelli, S., Rossi, A., Groppetti, R., Casadei, F., and Rizzi, G, "A Contribution to the Surface Analysis and Characterisation of HVOF Coatings for Petrochemical Application", Journal of Wear, (2001), Vol. 250-251, pp. 107-113.

2. Craft, G.A., "Cost Effective Corrosion Mitigation", Proceedings of the 2nd International Conference on Advances in Underground Pipeline Engineering, Bellevue, WA, (1995), pp. 757-764.

3. Tucker J. R., "Thermal Spray Coatings; Broad and Growing Applications", International Journal of Powder Metallurgy, (2002), Vol. 38 (7), pp. 45-53.

4. Dorfman M. R., "Thermal Spray Applications", Advanced Materials and Process, (2002), Vol. 160 (10), pp. 66-68.

5. Hackett, D and Kopech, H., "Advances in Powder Atomization Capabilities Enable a Range of New Thermal Spray Applications", Advanced Materials and Processes, (2001), Vol. 159 (4), pp. 31-34.

6. Shrestha, S., and Sturgeon, A.J., "Use of Advanced Thermal Spray Processes for Corrosion Protection in Marine Environments", Surface Engineering, (2004), Vol. 20 (4), pp. 237-243.

7. Sahraoui, T., Fenineche, N., Montavon, G., and Coddet, C., "Alternative to Chromium: Characteristics and Wear Behavior of HVOF Coatings for Gas

Turbine Shafts Repair (heavy-duty)", Journal of Materials Processing Technology, (2004), Vol. 152 (1), pp. 43-55.

8. Aidelsztain, L., Picas, J., Kim, G., Bastian, F. Schoenung, J., and Provenzano, V. "Oxidation Behavior of HVOF Sprayed Nanocrystalline NiCrAlY Powder", Materials Science and Engineering, (2002), Vol. 338 (1-2), pp. 33-43.

9. Wang, Y., Chen, W., "Microstructures, Properties and High-temperature Carburization Resistances of HVOF Thermal Sprayed NiAl Intermetallic-Based Alloy Coatings", Surface and Coatings Technology, (2004), Vol. 183 (1), pp. 18-28.

10. Al-Fadhli, H.Y., "Influence of HVOF Setting Parameters on Nickel-Based Alloy Powder (Diamalloy 1005) Coating Properties", International Surface Engineering Congress, Proceedings of the 1st Congress, (2003), pp. 549-554.

11. Al-Fadhli, H, Y. Yilbas, B.S. and Hashmi, M.S.J. "HVOF-Coating of Metallic Surfaces: Coating Response to Corrosion and Bending". Proceeding of the International Thermal Spray Conference, Basel, Switzerland, (2005), pp. 695-699.

12. Al-Fadhli, Hussain Y, J. Stokes, M.S.J. Hashmi, and B.S Yilbas "HVOF Coating of Welded Surfaces: Corrosion-Fatigue Behaviour of Stainless Steel Coated with Inconel-625 Alloy", Surface & Coatings Technology, (2005), Article in Print.

13. Al-Fadhli, Hussain Y, J. Stokes, M.S.J. Hashmi, and B.S Yilbas "The Erosion-Corrosion Behaviour Of Inconel-625 Coating Thermally Sprayed Using HVOF Process Applied Over Different Metallic Surfaces", Surface & Coatings Technology, (2005), Article in Print.

14. Schmid, R.K., Zimmermann, H, McCullough, R, and Warnecke,C., "New HVOF Developments at Sulzer Metco", Sulzer Technical Review, (2004), Vol. 86 (1), pp. 4-7.

15. Dolatabadi, A., Pershin, V., and Mostaghimi, J., "New Attachment for Controlling Gas Flow in the HVOF Process", Journal of Thermal Spray Technology, (2005), Vol. 14 (1), pp. 91-99.

16. Fadhli, H.Y. 2003. Performance Evaluation of (HVOF) Thermal Spray Coating Using Inconel-625 Powder. M.S Thesis. King Fahd University of Petroleum and Minerals.

17. Valentinelli, L., Valente, T., Casadei, F., and Fedrizzi, L., "Mechanical and Tribocorrosion Properties of HVOF Sprayed WC-co Coatings", Corrosion Engineering Science and Technology, (2004), Vol. 39 (4), pp. 301-307.

18. Budinski, K., Overview of Surface Engineering and Wear, ASTM Special Technical Publication, (1996), Vol. 127 (8), pp. 4-21.

19. Brandl, W. Marginean, G. Maghet, D. and Utu, D., "Effects of Specimen Treatment and Surface Preparation on the Isothermal Oxidation Behaviour of the HVOF-Sprayed Mcraly Coatings", Surface and Coatings Technology, (2004), Vol.188-189 (1-3), pp. 20-26.

20. Rodriguez, M. Staia, M. Gil, L. Arenas, F. and Scagni, A., "Effect of Heat Treatment on Properties of Nickel Hard Surface Alloy Deposited by HVOF" , Surface Engineering, (2000), 16 (5), pp. 415-420.

21. Sidhu, T., Agrawal, R., and Prakash, S., "Hot Corrosion of Some Superalloys and Role of High-Velocity Oxy-fuel Spray Coatings", Surface and Coatings Technology, (2005), Vol. 198 (1-3), pp. 441-446.

22. McGrann, R., Kim, J., Shadley, J.R., Rybicki, E, and Ingesten, N., "Characterization of Thermal Spray Coatings Used for Dimensional Restoration", Proceedings of the International Thermal Spray Conference, (2000), pp. 341-349.

23. Bender, D., "Hard Coatings on Tools for Cold Bulk Forming", Wire, (2005), Vol. 55(4), pp. 24-27.

24. Longtin, J., Sampath, S., Tankjewicz, S., Gambino, R., and Greenlaw, R., "Sensors for Harsh Environments by Direct-Write Thermal Spray", IEEE Sensors Journal, (2004), Vol. 4 (1), pp. 118-121.

25. Fukbayashi, H., "Thermal Spray Coatings, Failure and Prevention", International Surface Engineering Congress", Proceedings of the 1st Congress, (2003), pp. 527-53.

26. ASM Handbook Volume 18, Friction, Lubrication, and Wear Technology, First Edition, ASM International.

27. Soon,Y., Seog Y., Won-Sub, C., and Kwang H., "Impact-Wear Behaviors of TiN and Ti–Al–N Coatings on AISI D2 Steel and WC–Co Substrates", Surface and Coatings Technology,(2004), Vol. 177-17(30), pp.645-650.

28. Tan, K. S., Wood, R. J. K., and Stokes K. R., "The Slurry Erosion Behaviour of High Velocity Oxy-Fuel (HVOF) Sprayed Aluminum Bronze Coatings", Wear, (2003), Vol. 255, pp. 195-205.

29. ASTM G 75, Test Method for Determination of Slurry Abrasivity and Slurry Abrasion Response of Material. American Society for Testing and Materials, (1989).

30. ASTM Book of Standards, Metals Test Methods and Analytical Procedures: Wear and Erosion; Metal Corrosion, (2004), Vol. 03.02, ASTM International.

31. Ariely, S., and Khentov, A., "Erosion Corrosion of Pump Impeller of Cyclic Cooling Water System", Engineering Failure Analysis, (2005), In Press, Corrected Proof, Available online.

32. Denny Jones, "Principles and Prevention of Corrosion", 2nd Ed. Prentice-Hall, (1996).

33. Tillis, W., "Corrosion in the Petroleum Industry", Ondeo Nalco Energy Services, Sugar Land, TX, (2003).

34. Asawa, M. Devasenapathi, A. and Fujisawa, M., "Effect of Corrosion Product Layer on SCC Susceptibility of Copper Containing type 304 Stainless Steel in 1 M H_2SO_4Source", Materials Science and Engineering, (2004), Vol. 366 (2), pp. 292-298.

35. Lin, Ch-Ch. Wang, Chi-X., "Correlation between Accelerated Corrosion Tests and Atmospheric Corrosion Tests on Steel", Journal of Applied Electrochemistry, (2005), Vol. 35 (9), pp. 837-843.

36. Kivisakk, U., "A test Method for Dewpoint Corrosion of Stainless Steels in Dilute Hydrochloric Acid", Corrosion Science, (2003), Vol. 45 (3), pp. 485-495.

37. Stack, M.M. and Pungwiwat, N., "Erosion-Corrosion Mapping of Fe in Aqueous Slurries: Some Views on a New Rationale for Defining the Erosion-Corrosion Interaction", Wear, (2004), Vol.256 (5), pp. 565-576.

38. Lopez, D. Sanchez, C. and Toro, Alejandro., "Corrosion-Erosion Behavior of Tin-Coated Stainless Steels in Aqueous Slurries" , Wear, (2005), Vol.258(1-4),pp. 684-692.

39. Shrestha, S. Hodgkiess, T. and Neville, A., "Erosion-Corrosion Behaviour of High-Velocity Oxy-Fuel Ni-Cr-Mo-Si-B Coatings Under High-Velocity Seawater Jet Impingement" , Wear, (2005),. Vol.259 (1-6), pp. 208-218.

40. Lopez, D. Congote, J.P. Cano, J.R. Toro, A. and Tschiptschin, A.P., "Effect of Particle Velocity and Impact Angle on the Corrosion-Erosion of AISI 304 and AISI 420 Stainless Steels" , Wear, (2005), Vol. 259 (1-6), pp. 118-124.

41. Burstein, G.T., and Sasaki, K., "Effect of Impact Angle on the Slurry Erosion-Corrosion of 304L Stainless Steel", Wear, (2000), Vol. 240 (1-2), pp. 80-94.

42. He, D.D., Jiang, X.X., Li, S.Z.; Guan, H.R., "Erosion-Corrosion of Stainless Steels in Aqueous Slurries - a Quantitative Estimation of Synergistic Effects", Corrosion, (2005), Vol. 61(1), pp. 30-36.

43. Brown, J. and Kunnath, S. K., "Low-Cycle Fatigue Failure of Reinforcing Steel Bars" , ACI Materials Journal, (2004), Vol. 101 (6), pp. 457-466.

44. Murakami, Y. Takahashi, K. and Toyama, K., "Mechanism of Crack Path Morphology and Branching from Small Fatigue Cracks Under Mixed Loading" ,Fatigue and Fracture of Engineering Materials and Structures, (2005),Vol. 28 (1-2), pp. 49-60.

45. Das, G. R. Ashok K. Ghosh, S. Das, S. K. and Bhattacharya, D. K., "Fatigue Failure of a Boiler Feed Pump Rotor Shaft" , Engineering Failure Analysis, (2003), Vol. 10 (6), pp. 725-732.

46. Singh, P. Guha, B. and Achar, D.R.G., "Fatigue Life Prediction for Stainless Steel Welded Plate CCT Geometry Based on Lawrence"s Local-Stress Approach" , Engineering Failure Analysis, (2003), Vol. 10 (6), pp. 655-665.

47. Bris, J. Maury, H. Pacheco, A. Torres, J. and Wilches, J., "High Temperature Corrosion Fatigue of Duplex Stainless Steel Shaft", International Journal of Fatigue, (2003), Vol. 25 (9-11), pp. 1195-1201.

48. Kang, J. Hadfield, M. and Ahmed, R., "The Effects of Materials Combination and Surface Roughness in Lubricated Silicon Nitride/Steel Rolling Fatigue", Materials and Design, (2003), Vol. 24 (1) p1.

49. Davis, J.R., Handbook of Thermal Spray Technology ASM International, (2004).

50. Pawlowski, L., "The Science and Engineering of Thermal Spray Coatings", London: Wiley and Sons, (1995).

51. Krepski, R. "Thermal Spray Coating Applications in the Chemical Process Industries", Houston: NACE Intl, (1993).

52. Berget. J., 1998. Influence of Powder and Spray Parameters on Erosion and Corrosion Properties of HVOF Sprayed WC-Co-Cr coatings. Ph.D. Thesis, Norwegian University of Science and Technology, Engineering Material Science, Norway.

53. Edris, H., McCartney, D.G., and Sturgeon, A.J., "Microstructural Characterization of High Velocity Oxy-Fuel Sprayed Coatings of Inconel-625", Journal of Materials Science, (1997), Vol. 32 (4), pp. 863-872

54. Lih, Wei-Cheng Y., S.H.; Su, C.Y.; Huang, S.C.; Hsu, I.C.; Leu, M.S., "Effects of Process Parameters on Molten Particle Speed and Surface Temperature and the Properties of HVOF CrC/NiCr Coatings" , Surface and Coatings Technology, (2000), pp. 54-60

55. Totemeier, T.C., "Wright, R.N. and Swank, W.D. Residual Stresses in High-Velocity Oxy-Fuel Metallic Coatings", Metallurgical and Materials

Transactions A: Physical Metallurgy and Materials Science, (2004), Vol. 35 A (6), pp.1807-1814.

56. Oksa, M., Turunen, E., and Vans, T., "Sealing of Thermally Sprayed HVOF Coatings for Boiler Applications", Proceedings of the International Thermal Spray Conference, Proceedings of the International Thermal Spray Conference, (2004), pp. 120-124.

57. Arya, V. and Mann, B.S., "HVOF Coating and Surface Treatment for Enhancing Droplet Erosion Resistance of Steam Turbine Blades", Wear, (2003), Vol. 254 (7-8), pp. 652-667.

58. Kawakita, J. Kuroda, S. and Kodama, T., "Evaluation of Through-Porosity of HVOF Sprayed Coating", Surface and Coatings Technology, (2003), Vol. 166 (1), pp. 17-23.

59. Sobolev, V.V. and Guilemany, J.M., "Investigation of Coating Porosity Formation during High Velocity Oxy-Fuel (HVOF) Spraying", Materials Letters, (1994), Vol. 18 (5-6), pp. 304-308.

60. Hanson, T.C. Settles, G.S., "Particle Temperature and Velocity Effects on the Porosity and Oxidation of an HVOF Corrosion-Control Coating. Source" Journal of Thermal Spray Technology, (2003), Vol. 12 (3), pp. 403-415.

61. Modi, S.C., and Calla, E., "Structure and Properties of HVOF Sprayed NiCrBSi Coatings", Proceedings of the International Thermal Spray Conference, (2001), pp. 281-284.

62. Stokes. J. 2003. Production of Coated and Free-Standing Engineering Components Using the HVOF (High Velocity oxy-Fuel) Process. Ph.D. Thesis, School of Mechanical and Manufacturing Engineering, Dublin City University, Ireland.

63. Reisel, G. Wielage, B. Steinhauser, S. Morgenthal, I. and Scholl, R.., "High Temperature Oxidation Behavior of HVOF-Sprayed Unreinforced and Reinforced Molybdenum Disilicide Powders", Surface and Coatings Technology, (2001), Vol. 146-147, pp. 19-26.

64. Brandl, W., Toma, D., Krueger, J., Grabke, H.J., and Matthaeus, G., "Oxidation Behaviour of HVOF Thermal-Sprayed MCrAlY Coatings", Surface and Coatings Technology, (1997), Vol. 94-95 (1-3), pp. 21-26.

65. Planche, M.P. Normand, B. Liao, H.; Rannou, G. and Coddet, C., "Influence of HVOF Spraying Parameters on in-Flight Characteristics of Inconel 718 Particles and Correlation with the Electrochemical Behaviour of the Coating", Surface and Coatings Technology, (2002), Vol. 157 (2-3), pp. 247-256.

66. Remesh, K. Ng, H.W. and Yu, S.C.M., "Influence of Process Parameters on the Deposition Footprint in Plasma-Spray Coating", Journal of Thermal Spray Technology, (2003), Vol. 12(3), pp.377-392.

67. Korpiola, K. Hirvonen, J.P. Laas, L. and Rossi, F., "Influence of Nozzle Design on HVOF Exit Gas Velocity and Coating Microstructure" , Journal of Thermal Spray Technology, (1997), Vol. 6 (4), pp. 469-474.

68. Hanson, T.C. Hackett, C.M. and Settles, G.S., "Independent Control of HVOF Particle Velocity and Temperature" , Journal of Thermal Spray Technology, (2002), Vol. 11 (1), pp.75-85.

69. Mahbub, H. 2004. Production of Functionally Graded Coatings Using HVOF Thermal Spraying Process. PhD. Thesis, School of Mechanical and Manufacturing Engineering, Dublin City University, Ireland.

70. Smith, C.W. and Naisbitt, G., "Application and Experience of HVOF Coatings in the Repair and Overhaul of Industrial Gas Turbines" , American Society of Mechanical Engineers, (1994), pp.1-6.

71. He, J., Ice, M., and Lavernia, E., "Particle Melting Behavior During High-Velocity Oxygen Fuel Thermal Spraying" , Journal of Thermal Spray Technology, (2001), Vol. 10 (1), pp. 83-93.

72. Yilbas, B.S., Arif, A.F.M., and Gondal, M.A., "HVOF Coating and Laser Treatment: Three-Point Bending Tests", Journal of Materials Processing Technology, (2005), Vol. 164-165,pp. 954-957.

73. Hornhede A. Nylund A., "Adhesion Testing of Thermally Sprayed and Laser Deposited Coatings", Surface and Coating Technology, (2003), Vol. 184, pp. 208-218.

74. Jokinen, P., Korpiola, K., and Mahiout, A., "Duplex Coating of Electroless Nickel and HVOF (High-Velocity Oxygen Fuel) Sprayed", Journal of Thermal Spray Technology, (2000), Vol. 9, (2), pp. 241-244.

75. Kumar, Ashok, Boy, J., Zatorski, Ray, and Stephenson, Larry D., "Thermal Spray and Weld Repair Alloys for The Repair of Cavitation Damage in Turbines and Pumps: a Technical Note", Journal of Thermal Spray Technology, (2005), Vol. 14 (2), pp. 177-182.

76. Menini, R., Salah, N., Nciri, R., "Stripping Methods Studies for HVOF WC-10Co-4Cr Coating Removal", Journal of Materials Engineering and Performance, (2004), Vol. 13 (20), pp. 185-194.

77. Kawakita, Jin, Kuroda, Seiji, Fukushima, Takeshi, Kodama, and Toshiaki, "Corrosion Resistance of HVOF Sprayed Hastelloy C Nickel Base Alloy in Seawater", Corrosion Science, (2003), Vol. 45 (12), pp. 2819-2835.

78. Al-Fadhli, Hussain Y,J. Stokes, M.S.J. Hashmi, B.S Yilbas, I. Taie and S. Mehta "Modelling of HVOF Coating Deposit Applied Over Different Metallic

Surfaces and Tested In Highly Corrosive Environments" ,11th Middle East Corrosion Conference, (2006).

79. Okane, Masaki, Shiozawa, Kazuaki, Hiki, Masaharu, and Suzuki, Kazutaka, "Fretting Fatigue Properties of WC-Co Thermal Sprayed Nicrmo Steel", ASTM Special Technical Publication, Vol.142 (5), (2002), pp. 385-399.

80. Ogawa, T. K. Tokaji, T. Ejimat, Y. Kobayashi, and Y. Harada, "Evaluation of Fatigue Strength of WC Cermet-and 13 Cr Steel-Sprayed Materials and Their Coatings", Proceeding of the 15th International Thermal Spray Conference, 25-29 Nice, France, (1998), pp. 635-640.

81. L. Hernandez, F, J.A. Berrios, C. Villalobos, A, Pertuz, E.S. Pushi Cabrera, "Fatigue Properties of a 4340 Steel Coated with a Colmonoy 88 Deposit Applied by High-Velocity Oxygen Fuel", Surface and Coatings Technology, (2000), Vol.133-134, pp. 68-77.

82. F. Oliveira, L. Hernandez, F, J.A. Berrios, C. Villalobos, A, Pertuz, E.S. Pushi Cabrera, "Corrosion-Fatigue Properties of a 4340 Steel Coated with Colmonoy 88 Alloy, Applied by HVOF Thermal Spray" , Surface and Coatings Technology, (2001), Vol. 140 (2), pp. 128-135.

83. V. Hidalgo, J. Varela, A. Menendez, and S. Martinez, "Effect of Thermal Spray Procedure and Thermal Fatigue on Microstructure and Properties of NiCrAlMoFe Coating", Surface Engineering, (2001), Vol. 17 (6), pp. 512-517.

84. E.S. Pushi Cabera, E.S. Berrios, J.A, Da-Salva, and J.Nunes , "Fatigue Behaviour of A 4140 Steel Coated with a Colmonoy 88 Alloy Applied by HVOF", Surface and Coatings Technology, (2003), Vol. 172 (2-3), pp. 128-138.

85. A. Ibrahim, C.C Berndt, "The Effect of HFPD Thermally Sprayed WC-Co Coatings on the Fatigue Behavior and Deformation of Al 2024-T4",

Proceedings of the International Thermal Spray Conference, (2000), pp. 1297-1301.

86. R. Nieminen, P. Vuoristo, K. Niemi, T. Mantyle, and G, Barbezat, "Rolling Contact Fatigue Failure Mechanisms In Plasma and HVOF Sprayed WC-Co Coatings", Wear, (1997), Vol. 212 (1), pp. 66-77.

87. R. Ahmed, "Contact Fatigue Failure Modes of HVOF Coatings", Wear, (2002), Vol. 253 (3-4), pp. 473-487.

88. K. Padilla, A. Valasquez, A. J.A Berrios, E.S Pushi Cabrea, "Fatigue Behaviour of A 4140 Steel Coated with a Nimoal Deposit Applied by HVOF Thermal Spray", Surface and Coatings Technology, (2002), Vol. 150 (2), pp.151-162.

89. M.P Nascimento, R.C Souza, W.L Pigatin, H.J.C Voorwald, "Effects of Surface Treatments on the Fatigue Strength of AISI 4340 Aeronautical Steel", International Journal of Fatigue, (2001),Vol. 23 (7), pp.607-618.

90. Brandt, O.C. "Mechanical Properties of HVOF Coatings", Journal of Thermal Spray Technology, (1995), Vol. 4 (2), pp. 147-152.

91. Ahmed, R. Hadfield, M. and Tobe, S., "Variation In Residual Stress Field During Fatigue Failure of Thermal Spray Coating" Proceeding of The International Thermal Spray Conference, (2000), pp. 399-406.

92. R. Ahmed, and M. Hadfield., "Mechanism of Fatigue Failure in Thermal Spray Coating", Journal of Thermal Spray Technology, (2002), Vol.11 (3), pp.333-349.

93. J. Stokes and L. Looney, "HVOF System Definition to Maximise the Thickness of Formed Components", Surface and Coatings Technology, (2001), Vol. 148, pp.18-24.

94. Watanabe, S., Tajiri, T., Sakoda, N., Amano, J., "Fatigue Cracks in HVOF Thermally Sprayed WC-Co Coatings", Journal of Thermal Spray Technology, (1998), Vol. 7 (1), pp. 93-96.

95. McGrann, R.T.R., Greving, D.J., Shadley, J.R., Rybicki, E.F., Bodger, B.E., Somerville, D.A., "Effect of Residual Stress in HVOF Tungsten Carbide Coatings on the Fatigue Life in Bending of Thermal Spray Coated Aluminum", Journal of Thermal Spray Technology, (1998),Vol. 7 (4),pp.546-552.

96. Lima C., Nin, J., and Guilemany J., "Evaluation of Residual Stresses of Thermal Barrier Coatings with HVOF Thermally Sprayed Bond Coats Using the Modified Layer Removal Method (MLRM)", Surface And Coatings Technology,(2005), In Press, Corrected Proof, Available online.

97. Guilemany, J. Fernández, J. Delgado, A. V., "Benedetti And F. Climent "Effects of Thickness Coating on the Electrochemical Behaviour of Thermal Spray Cr_3C_2–Nicr Coatings", Surface and Coatings Technology, (2002), Vol. 153 (2-3), pp. 107-113.

98. Wood, R.J.K., "Challenges of Living with Erosion-Corrosion", Imeche Event Publications, Second International Symposium on Advanced Materials for Fluid Machinery, (2004), pp. 113-132.

99. Arsenault, B., Immarigeon, J., Parameswaran, V., Hawthorne, H., and Legoux, J., "Slurry and Dry Erosion of High Velocity Oxy-Fuel Thermal Sprayed Coatings", Proceedings of The International Thermal Spray Conference, (1998), Vol.1, pp. 231-236.

100. Higuera, V. Belzunce, F. Carriles, A. and Poveda, S., "Influence of the Thermal Spray Procedure on the Properties of a Nickel-Chromium Coating", Journal of Material Science, (2002), Vol. 37, pp. 649-654.

101. Gil, L. and Staia, M., "Effect of HVOF Parameters on Adhesion and Microstructure of Thermal Sprayed Niwccrbsi Coatings", Surface Engineering, (2002), Vol.18 (4), pp. 309-315.

102. Zhang, D. Harris, S. and McCartney, D., "Microstructure Formation and Corrosion Behaviour in HVOF-Sprayed Inconel-625 Coatings", Material Science and Engineering, (2003), Vol. 344 (1-2), pp. 45-56.

103. Yilbas, B., Khalid, M. and Abdul-Aleem, B., "Corrosion Behaviour of HVOF Coated Sheets. Journal of Thermal Spray Technology, (2003), Vol. 12, pp. 572-575.

104. Shrestha, S., Hodgkies, T. and Neville, A., "The Effect of Post-Treatment of a High-Velocity Oxy-Fuel Ni-Cr-Mo-Si-B Coating-Part 2: Erosion Corrosion", Thermal Spray Technology, (2001), Vol.10 (4), pp. 656-665.

105. Kenichi, S. Nakahama, S. Hattori, S. and Nakano, K., "Slurry Wear and Cavitation Erosion of Thermal-Sprayed Cermets", Wear, (2005), Vol.258, pp.768-775.

106. Wang, B. and Luer, K., "Erosion-Oxidation Behaviour of HVOF Cr_3C_2-Nicr Cermet Coating", Wear (1994), Vol.174 (1-2), pp.177-185.

107. Hawthorne, H. Arsenault, B. Immarigeon, J. Legoux, J. and Parameswaran, V.,"Comparison of Slurry and Dry Erosion Behaviour of Some HVOF Thermal Sprayed Coatings", Wear,(1999), Vol.225-229 (2), pp. 825-834.

108. Ak, N.F. Celik, E. Cetinel, H. Tekmen, C. and Soykan, H., "Corrosive Wear Behaviors of HVOF-Sprayed Nicr Coatings on Stainless Steel Substrates", Engineering Materials, (2004). Vol.264-268(1), pp. 529-532.

109. Uusitalo, M. Vuoristo, P. and Mantyla, T., "Elevated Temperature Erosion-Corrosion of Thermal Sprayed Coatings in Chlorine Containing Environments", Wear, (2002), Vol.252 (7-8), pp. 586-594.

110. Wang, Buqian, and Lee, Seong W., "Erosion-Corrosion Behaviour of HVOF Nial-Al_2O_3 Intermetallic-Ceramic Coating", Wear, (2000), Vol. 239 (1), pp. 83-90.

111. Al-Fadhli, Hussain Y, J. Stokes, M.S.J. Hashmi, and B.S Yilbas, "Erosion-Corrosion Characteristics of Inconel-625 Coating Sprayed By the HVOF Process Applied Over Different Metallic Surfaces", WOM, (2005), San Diego, USA.

112. Gourlaouen, V., Verna, E., Kho, K., and Quek, P.S.T., "Role of Some Fuel Gases on Properties of HVOF Metallic Coatings" Proceedings of the International Thermal Spray Conference, (2001), pp. 519-525.

113. Gourlaouen, V., Verna, E., and Beaubien, P., "Influence of Flame Parameters on Stainless Steel Coatings Properties", Proceedings of the International Thermal Spray Conference, (2000), pp. 487-493.

114. Li, Chang-Jiu, Wang, Yu-Yue, "Effect of Particle State on the Adhesive Strength of HVOF Sprayed Metallic Coating", Journal of Thermal Spray Technology, (2002), Vol. 11(4), pp. 523-529.

115. Sundararajan, T., Kuroda, S. Abe, F. Sodeoka, S., "Effect of Thermal Cycling on The Adhesive Strength of Ni-Cr Coatings", Surface and Coatings Technology, (2005), Vol. 194 (2-3), pp. 290-299.

116. Wang, Y.-Y. , Li, C.-J. and Ohmori, A., "Influence of Substrate Roughness on the Bonding Mechanisms of High Velocity Oxy-Fuel Sprayed Coatings", Thin Solid Films, (2005), Vol. 485 (1-2), pp. 141-147.

117. Lu, S.P., Guo, Y., and Chen, L.S., "Preparation and its Wear Resistance of WC-Co/Nicrbsi Metallurgical Bonded Composite Coating", Acta Metallurgica Sinica (English Letters), (2000), Vol. 13 (3), pp. 857-861.

118. Lu, Shan-Ping, Kwon, Oh-Yang, Guo, Yi, "Wear Behavior of Brazed WC/NiCrBSi(Co) Composite Coatings", Wear, (2003), Vol. 254 (5-6), pp. 421-428.

119. Li, C.J. , and Li, H., "Effect Of WC-Co Addition on The Adhesion of HVOF Ni-Based Coatings", Proceedings of the International Thermal Spray Conference, Vol. 1, (1998),pp. 723-728.

120. Yunfei Qiao, Traugott E. Fischer and Andrew Dent, "The Effects of Fuel Chemistry and Feedstock Powder Structure on the Mechanical and Tribological Properties of HVOF Thermal-Sprayed WC–Co Coatings with Very Fine Structures", Surface and Coatings Technology, (2003), Vol. 172, pp. 24-41.

121. J. Koutsky, "High Velocity Oxy-Fuel Spraying", Journal of Materials Processing Technology, (2004), Vol. (157-158), pp. 557-560.

122. Wang, Zhiping, Dong, Zujue; Huo, Shubin; Wen, Jinlin, "Dynamic Analysis of Particle Temperature in HVOF Spray", China Welding (English Edition), (2000), Vol. (1), pp. 15-19.

123. Kuroda, S., Fukushima, T.; Kodama, T.; Sasaki, M., "Microstructure and Corrosion Resistance of HVOF Sprayed 316L Stainless Steel and Ni Base Alloy Coatings", Proceedings of the International Thermal Spray Conference, (2000), pp.455-462.

124. ASTM C 633: "Adhesion or Cohesive Strength of Flame-Sprayed Coatings," Annual Book of ASTM Standards.

125. Buchmann, Michael, Gadow, Rainer, Lopez, Daniel, and Wenzelburger, Martin, "Process Dodeling and Simulation of Plasma and HVOF Sprayed Cylinder Liner Coatings", Ceramic Engineering and Science Proceedings, (2003), Vol. 24 (4), pp. 309-316.

126. Ghafouri-Azar, R., Mostaghimi, J., and Chandra, S., "Modeling Development of Residual Stresses in Thermal Cpray Coatings", Computational Materials Science, (2006), Vol. 35 (1), pp. 13-26.

127. M. Wenzelburger, M. Escribano and R. Gadow, "Modeling of Thermally Sprayed Coatings on Light Metal Substrates: Layer Growth and Residual Stress Formation", Surface and Coatings Technology, (2004), Vol. 180-181 (1), pp. 429-435.

128. Harvey, D., "The Ultimate Coating-Thermal Spraying at Abington", TWI, Bulletinm, (1994), pp. 456.

129. Tuominen, J., Vuoristo, P., Mantyla, T., Latokartano, J., Vihinen, J., and Andersson, P.H., "Microstructure and corrosion behavior of high power diode laser deposited Inconel 626 coatings", Journal of Laser Applications, (2003), Vol. 15 (1), pp. 55-61.

130. Margadant, Nikolaus , Siegmann, Stephan, Patscheider, J., Keller, Thomas, Wagner, Werner, Ilavsky, Jan, Pisacka, Jan, Barbezat, Gerard, Fiala, Petr, "Microstructure - Property Relationships and Cross-Property-Correlations of Thermal Sprayed Ni-Alloy Coatings", Proceedings of the International Thermal Spray Conference, (2001), pp. 643-652.

131. Kharlanova, E., Lafreniere, S., Kim, G.E., and Brzezinski, T.A., "Development of Tailored Metallographic Preparation Techniques for Thermally

Sprayed Coatings", Proceedings of the International Thermal Spray Conference, (2000), pp. 967-970.

132. Buchmann, M., and Gadow, R., "Mechanical and Tribological Characterization of APS and HVOF Sprayed TiO_2 Coatings on Light Metals", Proceedings of the International Thermal Spray Conference, (2001), pp. 1003-1008.

133. Xu, H., and Neville, A., "Using SEM for post-test analysis of HVOF-sprayed WC-Cr-Ni and WC/CrC coatings after erosion-corrosion in concentrated slurries", Proceedings of the Institute of Physics Electron Microscopy and Analysis Group Conference, (2004), pp. 425-428.

134. Hollerith, C., Wernicke, D., Buhler, M.; Feilitzsch, F.V., Huber, M., Hohne, J., Hertrich, T., Jochum, J., Phelan, K., Stark, M., Simmnacher, B., Weiland, W., and Westphal, W., "Energy dispersive X-ray spectroscopy with microcalorimeters". Nuclear Instruments and Methods in Physics Research, Section A: Accelerators, Spectrometers, Detectors and Associated Equipment, (2004), Vol. 520 (1-3), pp. 606-609.

135. Simmnacher, B., Weiland, R., Langer, E., Buhler, M., Hohne, J., Hollerith, C., "Microcalorimeter Energy Dispersive X-Ray Spectroscopy in Routine Semiconductor Failure Analysis", Conference Proceedings from the International Symposium for Testing and Failure Analysis, (2002), pp. 87-92.

136. Mustapha, Z., Chan, Siu-Wai, Lam, A., and Gerhardt, R., "Accuracy of energy dispersive X-ray composition analysis of YBCO films on yttrium-containing substrates as compared to Rutherford backscattering spectroscopy", Journal of Materials Science, (2000), Vol. 35 (2), pp. 443-448.

137. Boettinger, W.J., Vaudin, M.D., Williams, M.E., and Bendersky, L.A.,and Wagner, W.R., "Electron backscattered diffraction and energy dispersive X-ray

spectroscopy study of the phase $NiSn_4$", Journal of Electronic Materials, Vol. 32 (6), pp. 511-515.

138. ASTM D 790, "Standard Test Methods for Flexural Properties of Unreinforced and Reinforced Plastics and Electrical Insulating Materials", American Society for Testing and Material Standards, Philadelphia, (2003).

139. ASTM E 739, "Standard Practice for Statistical Analysis of Linear or Linearized Stress-Life (S-N) and Strain-Life (e-N) Fatigue Data", American Society for Testing and Material Standards, Philadelphia, (1991).

140. ASTM G 73, "Standard Practice for Liquid Impingement Erosion Testing", American Society for Testing and Material Standards, Philadelphia, (2004).

141. ASTM E8, "Standard Method of Tension Testing of Metallic Materials", American Society for Testing and Material Standards, Philadelphia, (2004).

142. Pejryd, Lars, Wigren, Jan, "Engine Test Experience with HVOF WC-Co Coated Fan Blade Dampers", American Society of Mechanical Engineers (Paper), (1996), 96-GT-435, 6pp.

143. Richard, C.S., Beranger, G., Lu, J., Flavenot, J.F., and Gregoire, T. "Four-Point Bending Tests of Thermally Produced WC-Co Coatings", Surface & Coatings Technology, (1996), Vol. 78 (1-3), pp. 284-294.

144. Gibmeier, Jens, Nobre, Joao Paulo, and Scholtes, Berthold, "Residual Stress Determination by the Hole Drilling Method in the Case of Highly Stressed Surface Layers", Materials Science Research International, (2004), Vol. 10 (1), pp. 21-25.

145. Lachmann, C., Nitschke-Pagel, T., and Wohlfahrt, H., "Characterization of Residual Stress Relaxation in Fatigue Loaded Welded Joints by X-ray

Diffraction and Barkhausen Noise Method", Materials Science Forum, (2000), Vol. 347, pp. 374-379.

146. Kang, Yilan , Qiu, Yu, Lei, Zhenkun, and Hu, Ming, "An Application of Raman Spectroscopy on the Measurement of Residual Stress in Porous Silicon", Optics and Lasers in Engineering, (2005), Vol. 43 (8), pp. 847-855.

147. Koo, J., Valgur, J., "Layer Growing/Removing Method for the Determination of Residual Stresses in Thin Inhomogeneous Discs", Materials Science Forum, (2000), Vol. 347, pp. 89-94.

148. Fontanari, V., Frendo, F., Bortolamedi, Th., and Scardi, P., "Comparison of the Hole-Drilling and X-ray Diffraction Methods for Measuring the Residual Stresses in Shot-Peened aAuminium Alloys", Journal of Strain Analysis for Engineering Design, (2005), Vol. 40(2),pp. 199-209.

149. Clyne, T.W. & Gill, S.C., "Residual Stresses in Thermal Spray Coatings and Their Effect on Interfacial Adhesion: A Review of Recent Work", Journal of Thermal Spray Technology, (1996), Vol. 5 (4), pp. 401-418.

150. Stokes, J. and Looney, L., "Residual Stress in HVOF Thermally Sprayed Thick Deposits", Surface and Coating Technology, (2004), Vol. 177-178, pp18-23.

151. Clyne, T.W., "Residual Stresses in Surface Coatings and Their Effects on Interfacial Debonding", Key Engineering Materials, (1996), Vol. 116-117, pp. 307-330.

152. Tsui, Y.C., and Clyne, T.W, "Analytical Model for Predicting Residual Stresses in Progressively Deposited Coatings. Part 1: Planar Geometry", Thin Solid Films, (1997), Vol. 306 (1), pp. 23-33.

153. Clyne, T.W, "Residual Stresses in Thick and Thin Surface Coatings" Encyclopedia of Materials: Science and Technology, 4.1.3b - "composites: MMC, CMC, PMC", A. Mortensen (ed.), Elsevier, (2001).

154. Kalpakjian, S. and Schmid, S. R., "Manufacturing Engineering and Technology". Prentice-Hall Inc. (2001).

155. Lima, M.M., Godoy, C., Avelar-Batista, J.C., and Modenesi, P.J., "Toughness Evaluation of HVOF WC-Co Coatings Using Non-linear Regression Analysis", Materials Science and Engineering A, (2003), Vol. 357 (1-2), pp. 337-345.

156. Kunioshi, Clarice Terui, Correa, Olandir Vercino, Ramanathan, Lalgudi Venkataraman, "Erosion-Oxidation Behavior of Thermal Sprayed Ni20Cr Alloy and WC and Cr_3C_2 Cermet Coatings", Materials Research, (2005), Vol. (2), pp 125-129.

157. Han, J., Han, S., Shin, B., and Kim, J., "Evaluation of Fatigue Life Based on a Modified Notch Strain Approach Considering Welding Residual Stress Relaxation", Proceedings of the Fourteenth (2004) International Offshore and Polar Engineering Conference, (2004), pp. 89-94.

158. Rodriguez, M.A., Gil, L., and Staia, M.H., "Post-Heat Treatment Microstructural Changes in Nickel Based HVOF Coating", Surface Engineering, (2002), Vol. 18 (5), pp 358-362.